



# The long noncoding RNA H19 controls endothelial cell functions by STAT3 repression

Dissertation

zur Erlangung des Doktorgrades

der Naturwissenschaften

Vorgelegt beim Fachbereich Biowissenschaften (FB15)

der Johann Wolfgang Goethe-Universität

in Frankfurt am Main

von

Patrick Hofmann

aus Weinheim (Bergstraße)

Frankfurt 2017

(D 30)

Vom Fachbereich Biowissenschaften (FB 15) der

Johann Wolfgang Goethe-Universität als Dissertation angenommen

Dekan: Prof. Dr. Meike Piepenbring

Gutachter: Prof. Dr. Stefanie Dimmeler

Prof. Dr. Amparo Acker-Palmer

Datum der Disputation:

## Table of contents

1.	Introduction.....	1
1.1	The mammalian cardiovascular system .....	1
1.1.1	The circulatory system of mammals.....	1
1.1.2	Angiogenesis.....	3
1.1.3	Shear Stress .....	5
1.1.4	Atherosclerosis .....	6
1.2	Aging.....	9
1.2.1	Systemic Aging.....	9
1.2.2	Senescence .....	10
1.2.3	Aging of the Cardiovascular System .....	12
1.2.4	IL-6/JAK2/STAT3 Signaling .....	14
1.3	Noncoding RNAs.....	17
1.3.1	Noncoding RNAs.....	17
1.3.2	MicroRNAs.....	17
1.3.3	Long Noncoding RNAs .....	20
1.3.4	The Long Noncoding RNA H19 .....	24
2.	Objective.....	31
3.	Materials and Methods .....	32
3.1	Materials.....	32
3.2	Methods .....	40
3.2.1	Cell culture.....	40
3.2.2	<i>In vitro</i> assays .....	42
3.2.3	Molecular Biology.....	44
3.2.4	Animal Experiments.....	48
3.2.5	Statistics.....	49
4.	Results .....	50
4.1	H19 is repressed by aging and induced by KLF2.....	50
4.2	H19 can be pharmacologically inhibited with siRNAs and LNA GapmeRs and overexpressed with lentivirus.....	52
4.3	H19 does not function <i>via</i> known mechanisms in endothelial cells .....	53
4.4	Depletion of H19 delays proliferation and promotes senescence in endothelial cells.....	57
4.5	H19 does not influence migration <i>in vitro</i> .....	64
4.6	H19 depletion impairs endothelial cell function <i>ex vivo</i> and <i>in vivo</i> .....	65
4.7	H19 induces inflammatory signaling <i>in vitro</i> .....	71

4.8	H19 exerts its function mainly through inhibition of STAT3 activation .....	73
5.	Discussion .....	77
5.1	Expression of H19 is tightly regulated .....	77
5.2	Loss of H19 promotes senescence and counteracts proliferation .....	77
5.3	H19 is required for proper endothelial cell function <i>ex vivo</i> and <i>in vivo</i> .....	81
5.4	Loss of H19 promotes inflammatory activation of endothelial cells.....	84
5.5	H19 does not regulate endothelial cell function <i>via</i> previously described mechanisms .....	84
5.6	H19 mainly exerts its functions <i>via</i> regulation of STAT3 activation.....	86
5.7	H19 overexpression partially confirms loss-of-function studies .....	89
5.8	Therapeutic perspectives of H19.....	90
5.9	Conclusion .....	90
6.	Summary.....	92
7.	Zusammenfassung.....	95
8.	References.....	101
	Abbreviations .....	125
	Eidesstattliche Erklärung.....	128
	Acknowledgements .....	129
	Curriculum Vitae.....	130

# **1. Introduction**

## **1.1 The mammalian cardiovascular system**

### **1.1.1 The circulatory system of mammals**

In the mammalian organism, two vascular systems provide oxygen, liquids, and nutrients to all of its cells. The cardiovascular system forms a closed network, while the lymphatic vasculature is a blind end network of vessels. The lymphatic system maintains fluid homeostasis and transports immune cells<sup>1,2</sup>. The cardiovascular system comprises the heart and all blood vessels. Muscular contraction of the left heart ventricle pumps oxygenized blood into the aorta and through branching arteries into capillaries, in which oxygen ( $O_2$ ), carbon dioxide ( $CO_2$ ), and nutrient exchange with the surrounding tissue takes place along the gradient<sup>3</sup>. Blood with low oxygen content is then transported back to the heart through veins and pumped by the right ventricle into the pulmonary circulation, where  $CO_2$  diffuses from the blood into the lung alveoli and  $O_2$  diffuses into the blood. The oxygenized blood then enters the body circulation through the left ventricle again (Fig. 1).

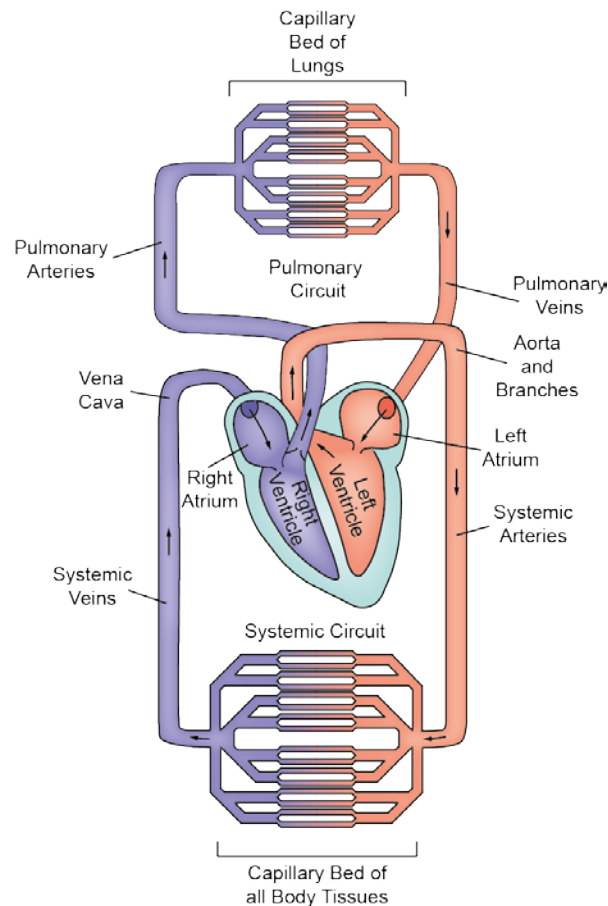


**Figure 1: The human circulatory system. Blood is oxygenized in the capillary bed of the lungs, enters the heart through the left atrium and is pumped into the aorta and all body tissues by the left ventricle. Oxygen and nutrient exchange happens in the capillary bed of all body tissues and CO<sub>2</sub>-rich blood flows back to the heart through the systemic veins and the finally the *vena cava* into the right atrium. The right ventricle pumps the blood into the pulmonary circuit, where it is oxygenized again. Modified from Guyton and Hall 2016, Textbook of Medical Physiology, Philadelphia, USA, Elsevier.**

Arteries are the most complex blood vessels in the human body; they consist of the *tunica intima* as the most inner and thinnest layer, which comprises a single layer of endothelial cells surrounded by subendothelial connective tissue interlaced with the internal elastic membrane and the basement membrane. The *tunica media* mainly consists of smooth muscle cells and elastic tissue and is the thickest layer in arteries. Smooth muscle cells control the diameter of the vessel and therefore play an important role in the regulation of blood pressure. The *tunica adventitia* consists of connective tissue and contains nerves, as well as capillaries in larger arteries. Arteries divide into arterioles that branch into capillaries. Arterioles are covered with one or two layers of smooth muscle cells and are the primary sites of vascular resistance. Nutrient exchange takes place in capillaries, which form a tight network in the whole body. Capillaries consist of a single layer of endothelial cells, supporting basement membrane and are covered by pericytes. Three different types of capillaries exist: Continuous, fenestrated, and sinusoid capillaries, which manage different tasks, from supply of surrounding tissue with small molecules, water, and lipid-soluble molecules (continuous), to

additional supply with larger molecules and limited amounts of proteins (fenestrated) to exchange of blood cells (sinusoid). Oxygen and nutrient deprived blood gathers in venules and from there flows into veins. Veins usually contain up to 75% of the blood of the body and consist of a single layer of endothelial cells, a supporting basement membrane, a thin layer of smooth muscle cells and the adventitia, which is the thickest layer of veins. In contrast to arteries, veins possess valves to prevent blood from flowing backwards.

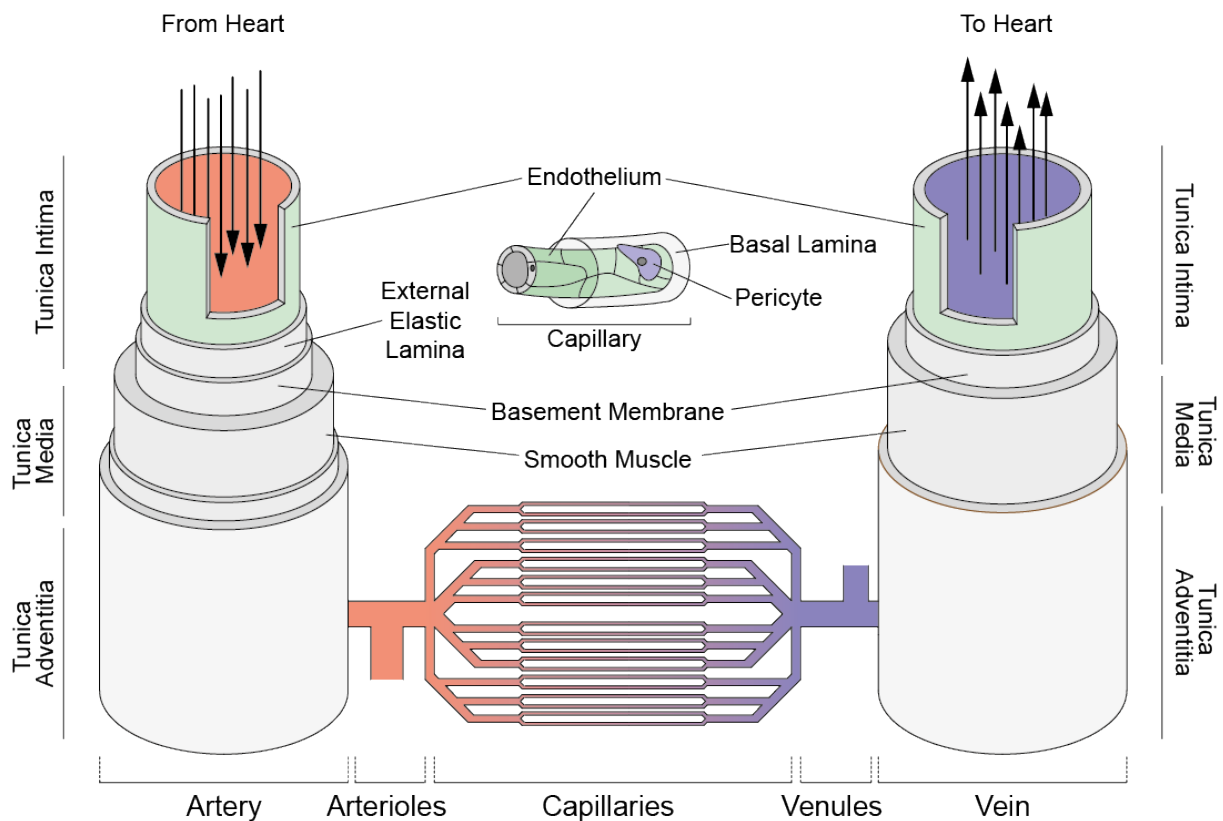


**Figure 2: Overview of different types of blood vessels in the human body. Oxygenized blood leaves the heart through complex blood vessels called arteries. Arteries branch into arterioles and arterioles branch into capillaries where oxygen exchange takes place. Capillaries consist of the endothelial monolayer, pericytes, and the surrounding basal lamina, allowing exchange of gases and nutrients. Oxygen-poor blood gathers in venules and veins leading back to the heart. Modified from Guyton and Hall 2016, Textbook of Medical Physiology, Philadelphia, USA, Elsevier.**

### 1.1.2 Angiogenesis

Angiogenesis is the process through which new blood vessels are formed from pre-existing vessels. In contrast, vasculogenesis denotes the process of the *de novo* formation of endothelial cells from endothelial precursors and arteriogenesis refers to the widening and remodeling of existing arteries. Angiogenesis mainly takes place during embryonal development, where a primitive vasculature is formed through vasculogenesis, after which angiogenesis is responsible for most of the blood vessel growth<sup>4-6</sup>. In the adult organism, angiogenesis only takes place during the female menstrual cycle

and during wound healing, while under pathological conditions, angiogenesis is involved in tumor development, diabetic retinopathy, ischemic heart disease and many more <sup>7</sup>. Under physiological conditions, endothelial cells form a quiescent unilayer, lining the luminal side of all blood vessels. This quiescent state is defined by low proliferative and migratory capacity, as well as by reduced metabolic activity <sup>8,9</sup>. Upon hypoxia, cells secrete angiogenic factors and VEGF-A is the most important factor for inducing angiogenesis <sup>8,10</sup>. Upon VEGF-A binding to endothelial VEGF receptor 2 (VEGFR2), ECs secrete Angiopoietin-2 (Ang-2), which triggers pericyte detachment from blood vessels <sup>10</sup>. Matrix metalloproteases degrade the basement membrane, allowing EC proliferation and migration <sup>10</sup>. VEGFR2 signaling induces tip-cell behavior at the forefront of the vessel sprout during the angiogenic switch <sup>4</sup>. 6-phosphofructo-2-kinase/fructose-2,6-biphosphatase 3 (PFKFB3)-driven glycolysis further contributes to the tip-cell phenotype <sup>11</sup>. In the elongating sprout, Delta-like 4-mediated activation of Notch signaling promotes proliferation of stalk cells that elongate the vascular sprout <sup>8</sup>. The tip- stalk-cell decision is tightly regulated and tip cells show a distinct phenotype with actin-rich filopodia containing VEGFR2 to sense VEGF-A <sup>8</sup>. Tip cells have a high migratory capacity while showing reduced proliferative capacity, whereas stalk cells are highly proliferative <sup>8</sup>. The tip cell leads the forming sprout along the VEGF-A gradient towards increasing VEGF-A concentration and stalk cells release soluble VEGFR1 to inhibit VEGF signaling in other stalk cells <sup>8</sup>. Stalk cells establish a lumen in the newly formed vessel through different mechanisms, depending on the vascular bed. A newly formed vessel is completed when the tip cell of one sprout meets the tip cell of another sprout and the sprouts fuse <sup>8</sup>. The maturation of the newly formed vessels requires formation of EC-EC junctions, deposition of extracellular matrix, and the recruitment of mural cells <sup>5,6</sup>. A main driver for vessel maturation is laminar blood flow, which induces expression of the transcription factor Krüppel-like factor 2 (KLF2) in ECs <sup>12</sup>. Expression of KLF2 promotes vessel quiescence and remodeling by increasing endothelial nitric oxide synthase (eNOS) expression and reduction of VEGFR2 expression <sup>13-16</sup>. Another main step in vessel maturation is the recruitment of pericytes. During angiogenesis, the tip cell releases platelet derived growth factor- $\beta$  (PDGF- $\beta$ ) <sup>17</sup>. Binding of PDGF- $\beta$  to PDGF receptor- $\beta$  (PDGFR- $\beta$ ) induces pericyte migration and proliferation and recruits pericytes to the newly formed blood vessel <sup>17</sup>.



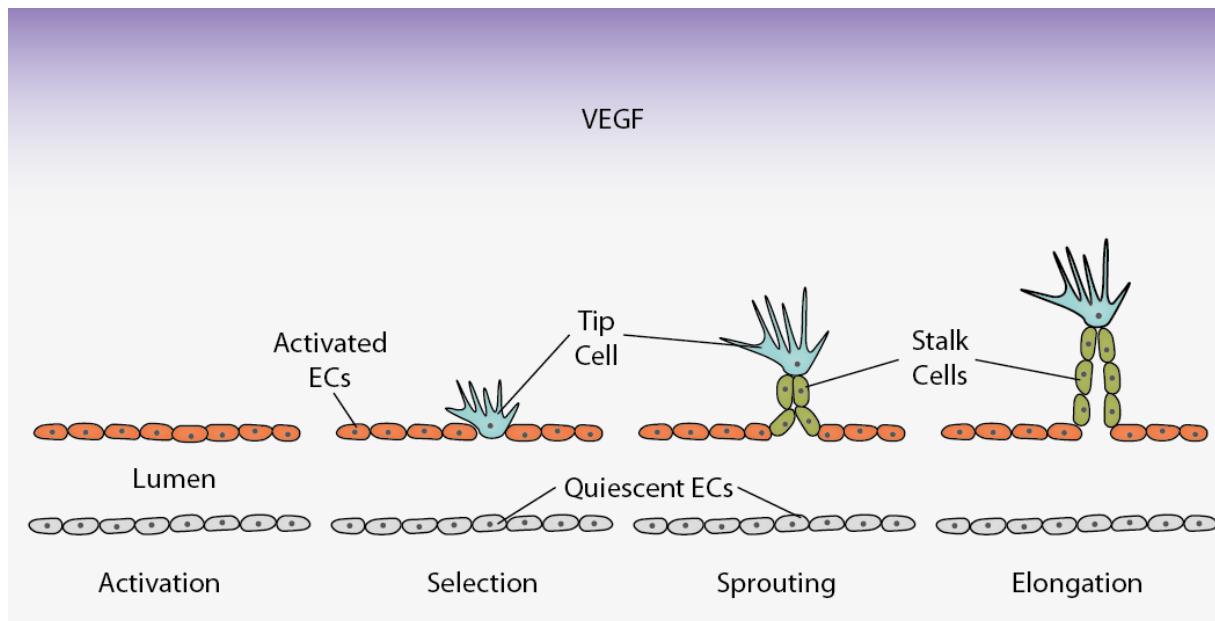


**Figure 3: Schematic representation of angiogenesis.** Upon VEGF sensing, otherwise quiescent endothelial cells get activated and start to proliferate. Activated ECs differentiate into tip- and stalk-cells with the highly migratory tip cell leading the newly forming sprout towards the highest VEGF concentration. Highly proliferative stalk cells form the new blood vessel. Modified from <sup>18</sup>.

### 1.1.3 Shear Stress

Endothelial cells are the only cells that are in contact with blood and blood flow constantly applies hemodynamic forces to ECs. The major mechanical forces exerted on the endothelial layer are shear stress (parallel to vessel wall), circumferential stretch (pressure leading to a cyclic stretch of the wall), and hydrostatic pressure (perpendicular to vessel wall) <sup>19</sup>. Shear Stress differs between different types of blood vessels. The shear stress in veins is usually in the range between 1 and 6 dyn/cm<sup>2</sup>, while it is higher with 10 to 70 dyn/cm<sup>2</sup> in arteries <sup>20</sup>. Mechanosensors sense blood flow and this activates intracellular signaling and translates hemodynamic forces to biochemical signals. VE-Cadherin and PECAM-1 have been described to sense shear stress and activate PI3K/Akt pathway and tyrosine kinase receptors such as VEGFR2 were also shown to activate PI3K/Akt in a shear stress dependent manner <sup>21</sup>. G-proteins and G-protein receptors were furthermore shown to sense shear stress and to promote cytoskeleton rearrangement *via* activation of Rho GTPases <sup>21</sup>. Different kinds of shear stress have different effects on the endothelial monolayer. Prolonged unidirectional laminar shear stress of  $\geq 12$  dyn/cm<sup>2</sup> was shown to possess an atheroprotective function <sup>20</sup>. *In vitro*, ECs react to unidirectional laminar shear stress with reorganization of the cytoskeleton, elongation, and alignment in the direction of flow, whereas ECs exposed to turbulent flow do not align. Disturbed flow is associated with vascular inflammation and focal distribution of atherosclerotic lesions, while steady unidirectional shear stress is anti-inflammatory and atheroprotective <sup>22</sup>. Unidirectional shear

stress induces the expression of the transcription factor KLF2 *in vivo* and *in vitro*<sup>23</sup>. Upon shear stress exposure, nuclear factors bind to the promoter region of KLF2 in ECs and promote expression<sup>24</sup>. Furthermore, MAP kinases and the MEK5/ERK5/MEF2 cascade are also involved in KLF2 transcription activation upon shear stress exposure<sup>25</sup>. KLF2 is known to possess an atheroprotective function and KLF2 overexpression induces EC quiescence similar to shear stress. KLF2 regulates almost 70% of the gene sets regulated by shear stress<sup>23</sup>. KLF2 regulates the flow-mediated expression of eNOS and suppresses thrombin adhesion<sup>26–28</sup>. KLF2 suppresses inflammatory activation of ECs by inhibiting NFκB transcriptional activity and inhibition of TNF-α and IL-1β induced expression of adhesion molecules<sup>15</sup>.

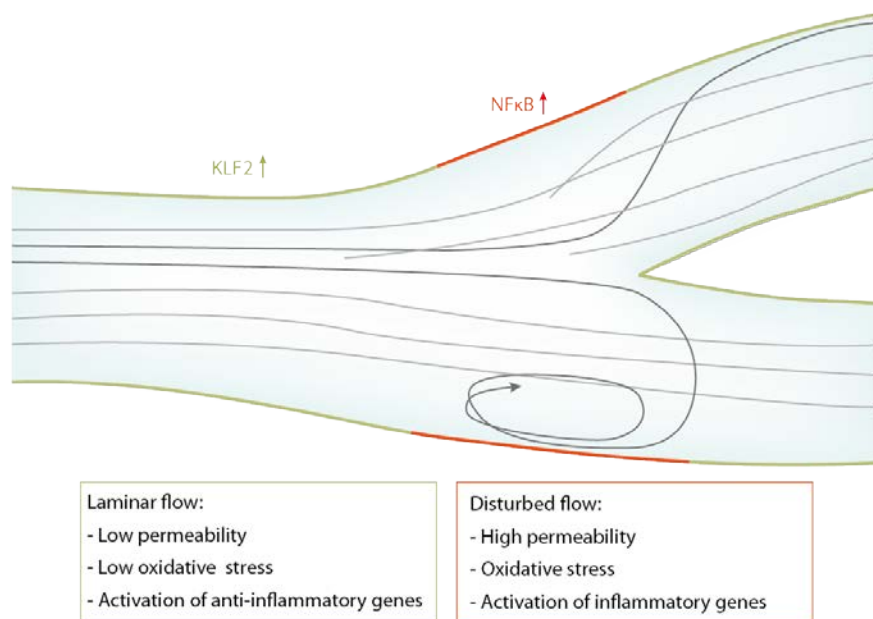


**Figure 4: Schematic representation of blood flow in arteries. Blood flow constantly applies a physical force to endothelial cells called shear stress. Laminar unidirectional flow has atheroprotective effects and upregulates, among others, the transcription factor KLF2. Regions with disturbed or low flow are prone to inflammatory activation and disturbed flow induces the expression of NFκB. Adapted from<sup>29</sup>.**

### 1.1.4 Atherosclerosis

Atherosclerosis is an inflammatory disease<sup>30</sup>. During the process of atherosclerotic lesion formation the artery wall thickens due to infiltration of leukocytes and proliferation of smooth muscle cells, which leads to a narrowing of the blood vessel and to impaired blood supply to downstream tissue. Atherosclerotic lesion formation usually starts at regions with low or disturbed shear stress like bifurcations of arteries<sup>31</sup>. The underlying pathology is characterized by endothelial dysfunction and structural alterations, including the absence of a confluent luminal elastin layer and the exposure of proteoglycans, which permit subendothelial accumulation of low-density lipoprotein (LDL)<sup>32,33</sup>. Early

atherosclerotic lesions are made up almost entirely of monocyte derived macrophages<sup>34</sup>. The recruitment of these inflammatory cells begins with attachment to activated endothelial cells using cellular adhesion molecules such as ICAM-1 and VCAM-1<sup>35</sup>. Adhesion molecules are expressed in response to various inflammatory cytokines on the surface of endothelial cells and permit adhesion and transmigration of circulating leukocytes<sup>35</sup>. The inhibition of monocyte adhesion through reduced expression of VCAM-1 was associated with a 40% reduction in atherosclerotic lesions in mice<sup>36</sup>. Levels of soluble ICAM-1 positively correlated with the risk for developing myocardial infarction in previously healthy men<sup>37</sup>. In humans, baseline ICAM-1 and VCAM-1 levels in patients with angiographically documented coronary artery disease were elevated in those who died from cardiovascular causes<sup>38</sup>. An increase in the expression of ICAM-1 and VCAM-1 therefore plays important roles in atherogenesis. In the progression of lesion formation, apolipoprotein B100 (ApoB100)-containing LDL binds to negatively charged extracellular matrix proteoglycans, which leads to retention of LDL particles in the intima, where they are susceptible to oxidative modification by reactive oxygen species<sup>33</sup>. Elevated levels of circulating ApoB100 bound LDL were shown to promote atherosclerosis and cardiovascular disease<sup>39</sup>. Oxidized lipids and LDL further trigger the expression of adhesion molecules and the secretion of chemokines by endothelial cells, which, together with the deposition of platelet-derived chemokines, further drive infiltration of immune cells into the intima<sup>33</sup>. Transmigrating leukocytes differentiate into macrophages that ingest oxidized LDL particles, forming specialized foam cells. Monocyte chemoattractant protein-1 (MCP-1) is a chemokine, essential in the recruitment of monocytes and its knockout in LDL receptor-deficient mice resulted in an 83% reduction in lipid-filled macrophages in the artery wall upon high fat diet<sup>40</sup>.

If the recruitment of fat-removing high-density lipoprotein (HDL) particles is insufficient, foam cells eventually rupture and apoptotic cells, debris, and cholesterol crystals accumulate in the plaque. This necrotic core formation again attracts leukocytes, which further contributes to plaque growth. T-cells, mast cells and other inflammatory cells are recruited to the intima and T-cells secrete various cytokines which stimulate smooth muscle cells and endothelial cells<sup>40,41</sup>. Mast cells release various cytokines that promote the expression of matrix-degrading proteases<sup>42</sup>. This promotes the replication of smooth muscle cells and remodeling of the extracellular matrix and leads to plaque growth<sup>30</sup>. Plaques are covered by a fibrous cap consisting of smooth muscle cells which get replaced by macrophages in later stages of atherosclerosis progression<sup>33</sup>. Elevated local matrix metalloprotease production degrades the fibrous cap and further contributes to lesion rupture (Figure 5). Growing evidence supports the theory that, besides plaque rupture, plaque erosion might actually also play an important role in arterial thrombosis<sup>43</sup>. Animal studies showed that therapy with blood lipid lowering statins can reinforce the fibrous cap, decreased the lipid pool, and reduced inflammation<sup>44</sup>. Imaging studies in humans indicated that statin therapy reduces the lipid content of

plaques and reduces the proportion of the plaque composed of fibrous tissue, which is associated with resistance to rupture<sup>45,46</sup>. All these characteristics are features of plaque erosion and highlight the role of this pathophysiology to ischemic diseases<sup>43</sup>.

Reasons and risk factors for atherosclerosis initiation and progression are numerous. Age is the predominant risk factor for atherosclerosis progression, followed by sedentary lifestyle with hypercholesterolemia. A recent study found that age-related somatic mutations of TET2 in hematopoietic cells promote clonal expansion of mutant blood cells and play a causal role in atherosclerosis<sup>47</sup>. Advancing age goes along with increased systemic inflammation and this is especially true for the vasculature<sup>48</sup>. Prolonged low level inflammation, determined by hsCRP levels, is associated with increased risk for CVD, despite an association of CRP with CVD is under discussion<sup>49</sup>. Interleukin-6 (IL-6) is an inflammatory cytokine that plays a central role in propagating the downstream inflammatory response responsible for atherosclerosis<sup>35</sup>.

Disturbed flow increased, whereas laminar unidirectional flow inhibited YAP/TAZ activity and endothelial YAP/TAZ inhibition was recently shown to suppress inflammation and to retard atherogenesis<sup>50</sup>.

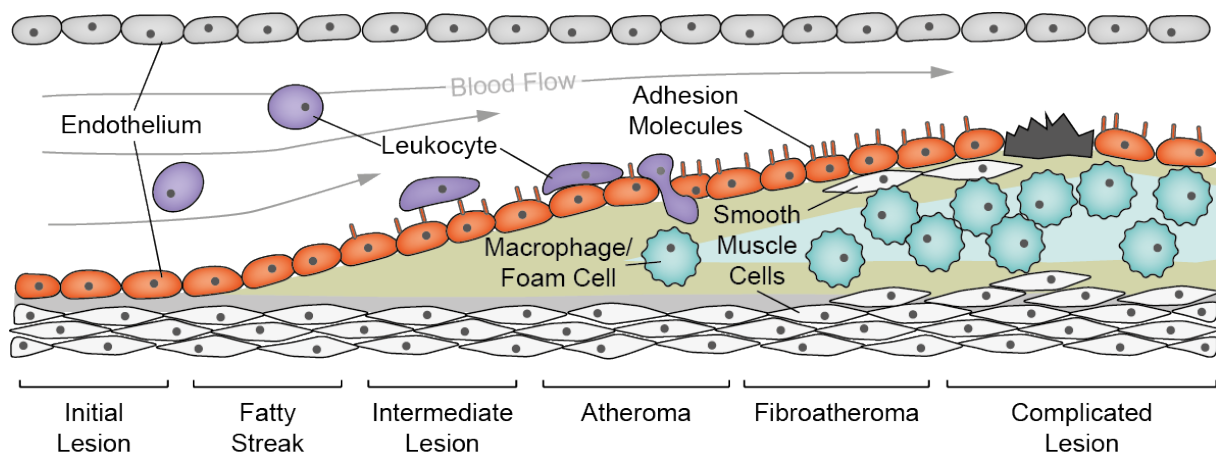


**Figure 5: Atherogenesis in human arteries. The endothelial monolayer gets activated by various stimuli and expresses and presents adhesion molecules on its cell surface. Circulating leukocytes attach to adhesion molecules, transmigrate through the endothelial monolayer and differentiate into macrophages. Different mechanisms lead to subendothelial accumulation of low density lipoproteins (LDL). Macrophages ingest LDL and form specialized, lipid rich foam cells. Foam cell apoptosis further promotes inflammatory activation of the tissue, leading to more leukocyte infiltration, smooth muscle cell proliferation, and progression of lesion formation. Modified from<sup>51</sup>.**

## 1.2 Aging

### 1.2.1 Systemic Aging

Aging in general refers to an organism's decline in the capability to react and cope with external stress stimuli and, to a general decline in fitness. Aging is among the greatest known risk factors for most human diseases<sup>52</sup>. During an organism's lifespan, the exposure to damaging agents is inevitable. Damaging agents can either derive from external or internal sources. External physical agents (e.g. UV exposure) or biological agents (viruses, bacteria, parasites) and internal damaging agents (e.g. inescapable products of metabolic processes, like reactive oxygen species) challenge an organism to different degrees. The mammalian body is equipped with a panel of mechanisms to cope with such stress factors. At the molecular level, DNA damage repair pathways can counteract DNA damage. At the cellular level, damaged cells can remove themselves from the organism by apoptosis or autophagy or enter senescence. Cells can be replaced by progenitors derived from stem cells. Nevertheless, repair mechanisms are always prone to errors, leading to an accumulation of damage over time and to reduced capacity of the organism to react to new stress. Cells respond to DNA damage by reversible growth arrest to repair damage before genome replication. Telomeres shorten with each cell division and critically short telomeres are recognized as DNA double strand breaks that are non-repairable. If the DNA is damaged extensively, cells can either undergo apoptosis or enter a permanent growth arrest called senescence. It has previously been suggested that chronic low level inflammation contributes to acceleration of biological aging<sup>53</sup>. In contrast to characteristics of acute inflammation, where the immune response is reduced within days, chronic inflammation is characterized by elevated levels of proinflammatory cytokines in response to physiological and environmental stressors that essentially arrest the immune system in a state of low-level activation<sup>54</sup>. Interestingly, isolated peripheral blood mononuclear cells from elderly donors showed higher production of proinflammatory cytokines compared to young donors<sup>55</sup>. This relation between inflammation and aging was termed inflammaging<sup>56</sup>. Immunosenescence of the acquired system contributes to inflammaging and can be seen as a result of cellular 'exhaustion' and this includes reduction of naïve T-cells, accumulation of memory and effector T-cells and reduction of T-cell repertoire<sup>57</sup>. Immunosenescence contributes to chronic inflammation by the reduced ability to clear novel pathogens, thus prolonging infect duration and by an increase in functionally distinct T-cell populations, which have an amplified proinflammatory phenotype<sup>55</sup>.

## 1.2.2 Senescence

In 1961, Hayflick and Moorhead showed that cultured cells have a limited capacity for replication<sup>58</sup>. The authors cultivated 25 different strains of diploid human fibroblasts and all strains stopped to proliferate after approximately 50 subcultivations and entered a permanent cell cycle arrest, which was termed replicative or cellular senescence<sup>58</sup>. Senescent cells do not divide anymore, but remain metabolically and transcriptionally active. Telomere erosion was the first stimulus identified that promotes senescence and subsequently telomeres were termed as molecular clocks that determine the number of cell divisions<sup>59</sup>. With each cell division, fragments of telomeres are lost and when telomeres become critically short and lose their protective function on the genome, DNA damage response is activated that upregulates cell cycle inhibitors<sup>60</sup>. Upon telomere shortening or other stresses, damage sensor proteins such as ataxia telangiectasia mutated (ATM) activated the master regulator p53 that activated p21 and facilitated cell cycle arrest at G1 phase<sup>61</sup>. Besides telomere erosion, exposure to oxidants, UVB-light,  $\gamma$ -irradiation and other DNA damaging stimuli can lead to senescence as well. Expression of oncogenes like BRAF<sup>V600E</sup> and loss of tumor suppressors like PTEN promotes senescence, suggesting a role of senescence in tumor suppression<sup>62,63</sup>. This theory is further supported by the finding that mice lacking p19<sup>Arf</sup> or p16<sup>ink4A</sup> are predisposed to cancer<sup>64,65</sup>.

Senescence is established by two pathways with the p53-p21 axis being the main one and p16<sup>ink4A</sup>-pRB being the secondary pathway in most cases. Most stimuli that induce DNA damage induce upregulation or stabilization of p53. p53 is stabilized by p19<sup>Arf</sup> that targets HDM2, which in turn targets p53 for degradation. p21 is a cyclin-dependent kinase inhibitor and is one of the most important targets of p53 in senescent cells<sup>66</sup>. p21 inhibits the activity of each member of the cyclin/CDK family<sup>67</sup>. p21-mediated cell cycle arrest prevents S-phase entry under unfavorable conditions for DNA replication<sup>68</sup>. Upregulation of p21 is sufficient for the cell cycle arrest, but prolonged arrest leads to upregulation of p16<sup>ink4A</sup> and this might be essential for the senescent-cell cycle arrest<sup>69</sup>. p16<sup>ink4A</sup> activation inhibits the kinases CDK4 and CDK6, which phosphorylate the retinoblastoma protein (pRB)<sup>66</sup>. Unphosphorylated pRB binds and inhibits E2F transcription factors, leading to cell cycle arrest in G1<sup>70,71</sup>.

Common features of senescent cells are upregulation of p16<sup>ink4A</sup>, p21 and p53, downregulation of cell cycle markers like KI67, slow BrdU incorporation and senescence-associated  $\beta$ -Galactosidase (SA- $\beta$ -gal) activity. The distinct SA- $\beta$ -gal activity is detected when cells are incubated with the chromogenic substrate 5-bromo-4-chloro-3-indolyl- $\beta$ -D-galactopyranoside (X-Gal) at pH6.0 and is a manifestation of the increase in lysosomal mass in the senescent cells<sup>72</sup>. Senescent cells were shown to have a unique secretome, the so called senescence-associated secretory phenotype<sup>73,74</sup>. SASP activation is

mainly mediated by the transcription factors NF $\kappa$ B and C/EBP $\beta$ <sup>75-77</sup>. The SASP differs along different cell types, but upregulation of inflammatory cytokines like IL-6 and IL-8 is highly conserved and plays a major role in maintaining the SASP<sup>75-77</sup>. The SASP was first described *in vitro*, but it is also thought to play a role *in vivo* during wound healing, development, and aging<sup>78</sup>. For example, activated fibroblasts were shown to undergo senescence, which terminates their tissue remodeling response and avoids excessive extracellular matrix deposition<sup>79-81</sup>. This theory is supported by the finding that mice, that lack p16<sup>ink4A</sup> or p53 suffer from increased fibrosis upon liver injury or cutaneous wounds<sup>81</sup>.

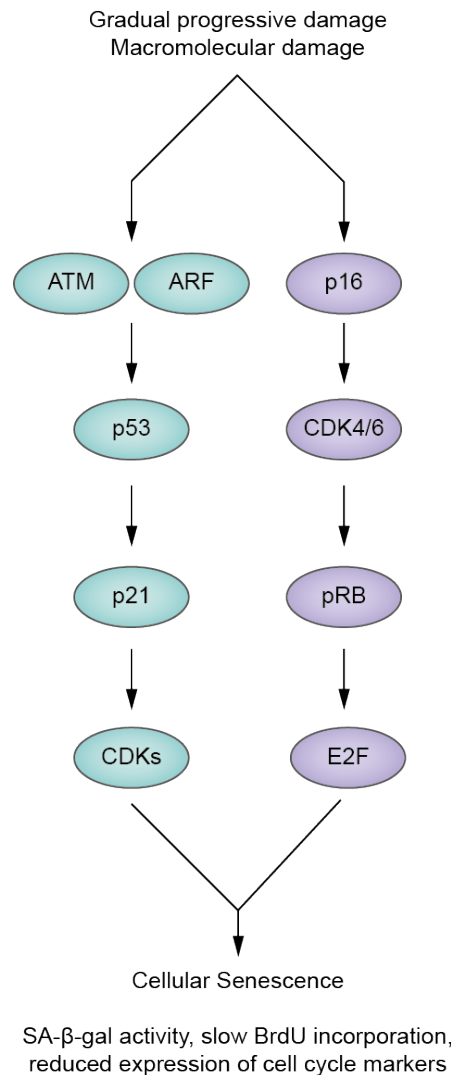


**Figure 6: Senescence is established by two pathways. Upon different stimuli, cells express damage sensors like ataxia telangiectasia mutated (ATM) that induce p53 expression. ARF stabilizes p53 protein and p21 is one of the most important transcriptional targets for p53. P21 inhibits cyclin-dependent kinases and arrests the cell cycle in G1 phase. Prolonged arrest and other stimuli lead to upregulation of p16<sup>ink4A</sup>, which inhibits CDK4 and CDK6. Both kinases phosphorylate retinoblastoma protein (pRB) and unphosphorylated pRB binds E2F transcription factors, also leading to cell cycle arrest. Modified from<sup>51</sup>.**

Senescence has been implicated in many normal and pathological age-related degenerative phenotypes<sup>82</sup>. Senescent pulmonary artery smooth muscle cells (PA-SMCs) were shown to promote the proliferation of normal PA-SMCs, leading to pulmonary hypertension, mainly *via* secretion of

inflammatory cytokines<sup>83</sup>. Morphological changes, that resemble the phenotype of senescent endothelial cells *in vitro*, were found in endothelial cells covering regions of aortic, carotid, and coronary atherosclerotic lesions<sup>84,85</sup>. Furthermore, similar morphological changes were found in senescence-associated  $\beta$ -galactosidase positive endothelial cells covering atherosclerotic plaques<sup>86</sup>. Senescent cells can be found in advanced atherosclerotic plaques and vascular smooth muscle cell senescence was shown to promote plaque formation<sup>86-89</sup>. On the other hand, mice lacking core components of senescence pathways such as p53, p21, or p19<sup>Arf</sup> show accelerated atherosclerosis, implying a protective role for senescence<sup>90-94</sup>. Senescent cells were present in atherosclerotic lesions of LDL receptor-deficient mice upon high fat diet and clearance of p16<sup>ink4A</sup>-positive cells led to lesion regression in early stages of atherogenesis and repressed plaque growth and remodeling in later stages<sup>90</sup>. The role of senescence in atherogenesis is thus not clear and might have different effects in different cell types.

### **1.2.3 Aging of the Cardiovascular System**

Cardiovascular disease (CVD) is the leading cause of death worldwide<sup>95</sup>. In 2014, 39% of all deaths in Germany were due to diseases of the vasculature and the heart (Fig. 7A). Besides alterable risk factors for CVD like lipid levels, diabetes, and sedentary lifestyle, advanced age is one of the major independent and important risk factors for CVD. CVD includes several diseases, like coronary artery disease, hypertension, congestive heart failure, cardiomyopathy, aneurysms and stroke. In general, diseases, which involve the heart and blood vessels. The risk for death by CVD rises with advanced age. Figure 6B shows the percentage of deaths by CVD of total deaths by age in the American population in 2013. At 85 years or older, more than 40% of all deaths are due to CVD (Fig. 7B).



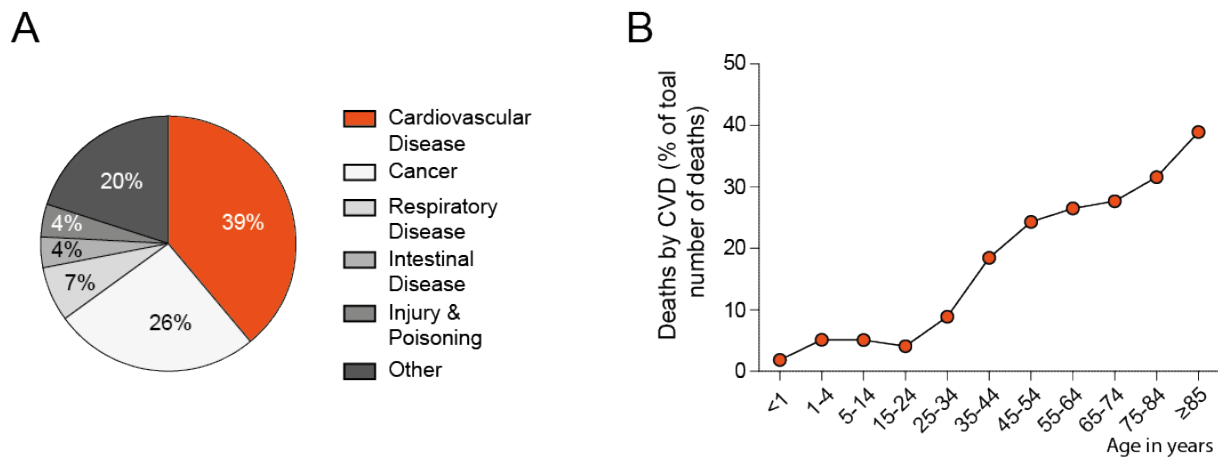


**Figure 7: The risk of death by cardiovascular disease rises with aging. A: 39% of all deaths in Germany in 2014 were due to cardiovascular disease (Source: Statistisches Bundesamt). B: The risk of death by cardiovascular disease rises with aging. Data from 2013 from US Center for Disease Control and Prevention.**

Aging of the vasculature is characterized by thickened intima, endothelial dysfunction, and chronic vascular inflammation<sup>48</sup>. Clinically, these changes result in increased systolic pressure and present a major risk factor for the development of atherosclerosis, stroke, hypertension and arterial fibrillation<sup>48</sup>. Age-related pathologies of vascular dysfunction result in several diseases. Loss of tissue perfusion leads to tissue ischemia<sup>96</sup>. Insufficient vascular growth or vessel regression leads to hypertension, while excessive growth and remodeling leads to age-related macular degeneration<sup>96</sup>. Endothelial barriers become porous in aged individuals and smooth muscle cells migrate into subendothelial spaces and deposit extracellular matrix proteins, which leads to intimal thickening<sup>96</sup>. With advanced age, endothelial cells show a reduced endothelial nitric oxide synthase (eNOS) activity, which results in a reduced abundance of nitric oxide (NO)<sup>97</sup>. NO is a vasodilator and regulates vascular tone, inhibits vascular inflammation, thrombotic events and aberrant cellular proliferation<sup>98</sup>. Absence of NO was furthermore shown to promote endothelial senescence<sup>99</sup>. Atherosclerosis is a chronic inflammatory disease of the endothelium. Atherosclerotic lesion formation usually starts with inflammatory activation of the endothelial monolayer. This leads to increased expression of adhesion molecules and subsequently to infiltration of leukocytes into the subendothelial tissue. The accumulation of monocytes within the vascular wall and the subsequent differentiation into macrophages/dendritic cells plays a critical role in every stage of atherosclerotic lesion formation<sup>31,100</sup>. CD16<sup>+</sup> monocytes were shown to constitutively produce more IL-6, IL-1 $\beta$ , and TNF under basal conditions and stimulation, with older people having a significantly larger proportion of CD16<sup>+</sup> cells than younger people<sup>101,102</sup>. Furthermore, CD16<sup>+</sup> monocytes have increased adherence

and migrate towards endothelial lesions *via* CX3CR1, further contributing to atheroma plaque formation <sup>103</sup>.

#### **1.2.4 IL-6/JAK2/STAT3 Signaling**

The interleukin-6 (IL-6)-Janus Kinase 2 (JAK2)-Signal transducer and activator of transcription 3 (STAT3) pathway mediates signaling from the plasma membrane to the nucleus. IL-6 binds to target cells *via* the low affinity membrane bound IL-6 receptor (IL-6R), which induces homodimerization of glycoprotein 130 (gp130) receptors. The gp130 dimer induces phosphorylation and thus activation of JAK2 which is associated with the intracellular domain of the receptor <sup>104</sup>. Activated JAK2 phosphorylates the gp130 receptor, thereby creating binding sites for cytosolic STAT3 *via* its SH2 domain. Recruited STAT3 is then phosphorylated on tyrosine 705 by JAK2 and this induces homodimerization of two STAT3 molecules, again *via* their SH2 domains. Homodimeric STAT3 dissociates from the receptor and translocates to the nucleus where it acts as a transcription factor for several genes. Phosphorylation of serine 727 was shown to promote STAT3 transcriptional activity, but is not necessary for its function. Endothelial cells do not express IL-6R and are therefore unresponsive to IL-6. A soluble form of IL-6R (sIL-6R) can be generated by shedding from the membrane bound receptor or by alternative splicing <sup>105,106</sup>. sIL-6R can be found in biological fluids where it forms a complex with IL-6 that can bind to gp130 receptors, thus widening the spectrum of IL-6 to non-responsive cells <sup>107</sup>. STAT3 was shown to promote p21 expression *via* transcriptional activation of FOXP3 and by direct binding in the p21 promoter region <sup>108,109</sup>. STAT3 was also shown to upregulate the expression of ICAM-1 in human hepatocellular carcinoma cells and in endothelial cells <sup>110,111</sup>. It furthermore regulated IL-6 expression by direct binding to the IL-6 promoter region in a PKC $\epsilon$ -dependent manner <sup>112,113</sup>.

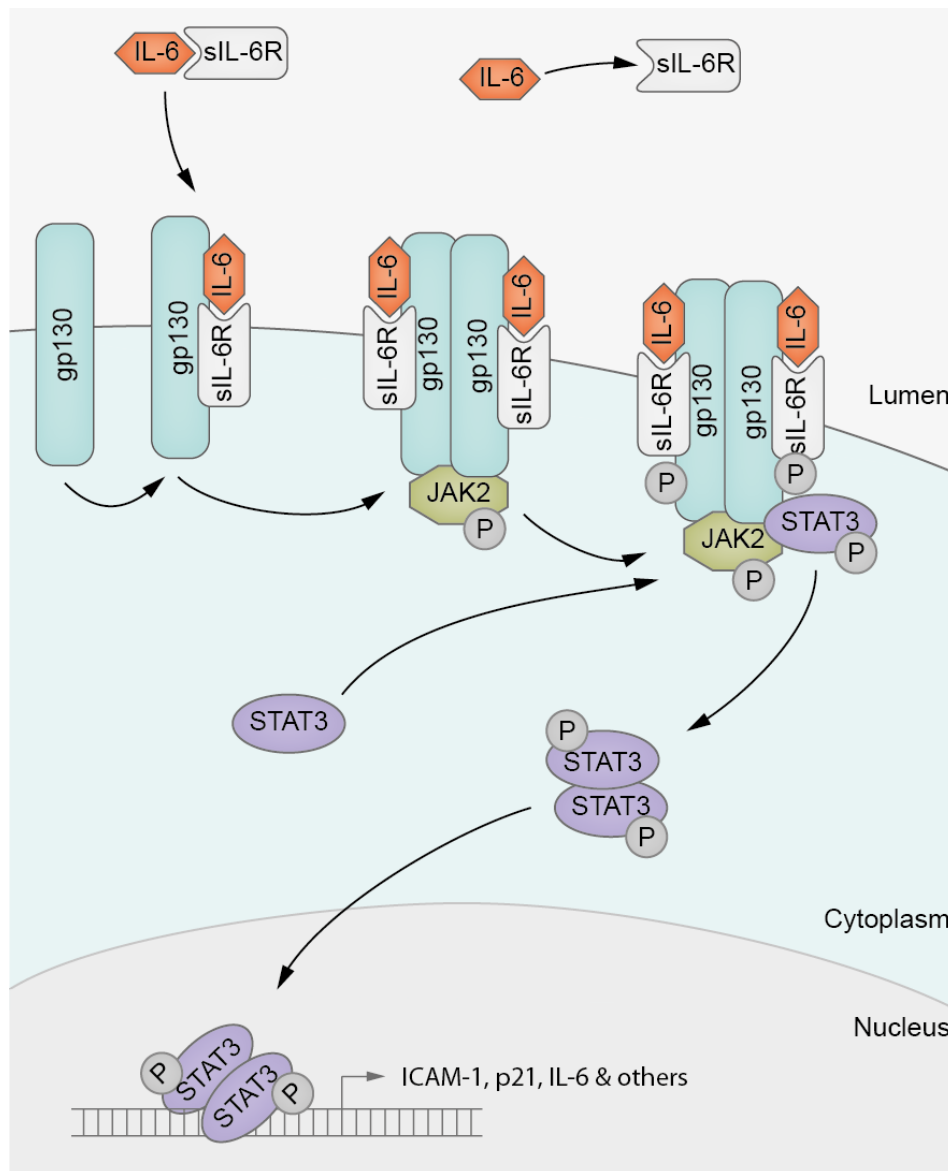


**Figure 8: IL-6/JAK2/STAT3 signaling in endothelial cells.** Interleukin-6 (IL-6) forms a complex with soluble IL-6 receptor (sIL-6R) in blood and binds to EC membrane bound gp130 receptors. Upon ligand binding, gp130 receptors dimerize and phosphorylate the associated phosphokinase JAK2. Phosphorylated JAK2 phosphorylates the gp130 receptor, creating binding sites for STAT3 protein. Upon binding to the gp130 receptor, STAT3 is phosphorylated at TYR705 and this induces dimerization and translocation to the nucleus. In the nucleus STAT3 acts as a transcription factor for several genes, e. g. ICAM-1, p21, and IL-6. Modified from <https://www.cellsignal.com/contents/science-pathway-research-immunology-and-inflammation/jak-stat-signaling-pathway/pathways-il6>

Circulating biomarkers of inflammatory processes, especially C-reactive protein (CRP) and fibrinogen, were shown to be associated with the development of coronary heart disease over many years<sup>114–117</sup>. Although CRP and fibrinogen are regulated by many cytokines, IL-6 plays a central role<sup>118</sup>. Furthermore, increased plasma concentrations of IL-6 predicted both total and cardiovascular mortality over a 5-year period independent of the traditional risk factors for atherosclerosis<sup>119</sup>. A SNP in the IL-6 promoter was previously shown to be associated with longevity<sup>120</sup> and serum IL-6 concentration correlated with age in two independent cohorts<sup>121</sup>. These observations highlight a

central role of IL-6 in cardiovascular disease. Approximately 30% of all circulating IL-6 is produced in subcutaneous adipose tissue, linking obesity with risk for coronary artery disease <sup>122</sup>. IL-6 has a variety of functions, including stimulation of hepatic synthesis of acute-phase reactants, activation of endothelial cells, increased coagulation and promotion of lymphocyte proliferation and differentiation <sup>35</sup>. Inflammatory activation of endothelial cells induces IL-6 secretion together with inflammatory adhesion molecule presentation on the cell surface <sup>123</sup>. As mentioned before, IL-6 plays a central role in propagating the inflammatory response in atherosclerosis development <sup>35</sup>. Consequently, exogenous administered IL-6 significantly enhanced the development of fatty lesions in mice, increasing the size of the fatty streak by 1.9 to 5.1-fold over control animals in C57/Bl6 and ApoE-deficient mice upon high fat diet <sup>124</sup>.

Global STAT3 knockout is embryonically lethal in mice <sup>125</sup>. Induced STAT3 deletion in cardiomyocytes of young mice results in no phenotype under baseline conditions but showed enhanced susceptibility to myocardial ischemia/reperfusion injury and infarction with increased apoptosis, increased infarct size and reduced cardiac function and survival <sup>126</sup>. In aged mice, cardiomyocyte-specific STAT3 knockout resulted in reduced myocardial capillary density and increased interstitial fibrosis <sup>126</sup>. *Vice versa*, cardiomyocyte-specific overexpression of STAT3 resulted in increased myocardial capillary density and increased expression of proangiogenic factors VEGF and VE-cadherin <sup>127</sup>. STAT3 inhibition was shown to promote satellite cell expansion and tissue repair in aged mice <sup>128</sup>. These studies highlight the controversial role of STAT3 in the process of aging. Conditioned medium from STAT3-deficient cardiomyocytes inhibited endothelial cell proliferation and increased fibroblast proliferation, suggesting the presence of paracrine factors attenuating angiogenesis and promoting fibrosis *in vitro* <sup>126</sup>. Proangiogenic STAT3 signaling seems to involve paracrine and autocrine mechanisms in various cells, such as expression and regulation of vascular endothelial growth factor (VEGF) <sup>126,127,129</sup>. VEGF was shown to stimulate tyrosine phosphorylation of STAT3, STAT1 and STAT6 and nuclear translocation of the latter two, but not STAT3 <sup>129</sup>. Taken together, these studies highlight the role of IL-6 in atherosclerosis initiation and progression and also in overall fitness and longevity. STAT3 was shown to play a role during aging and in some studies STAT3 inhibition had positive effects during aging, e. g. during tissue regeneration, in some studies the opposite was the case, for example in regards to angiogenesis.

## 1.3 Noncoding RNAs

### 1.3.1 Noncoding RNAs

Since the complete sequencing of the human genome in 2003, it became clear that only a small portion of the human genome codes for proteins. At the beginning of the human genome project, the highest estimates put the number to 100,000 protein coding genes, but this number shrunk continuously since then. With the first results of the human genome project in 2001, 30,000 protein coding genes were estimated and this number is now cut to 19,000 to 20,000, which corresponds to roughly 2-3% of the whole genome. The ENCYclopedia Of DNA Elements consortium (ENCODE) reported in 2012 that they were able to assign a biochemical function to 80% of the human genome<sup>130</sup>. Even though computational predictions or experimental validations of these numbers are a hard task, it is thought that 70-80% of the human genome is transcribed. This large amount of RNA, besides the small portion of mRNA, was considered as junk RNA for a long time. In recent years it became clear, that these noncoding RNA molecules might be functional. Noncoding RNAs can be further divided into many subclasses. Transfer-RNAs (tRNAs) and ribosomal RNAs (rRNAs) were known for a long time and their role was extensively analyzed. The roles of smaller noncoding RNAs like microRNAs (miRNAs), small nucleolar RNAs (snoRNAs), small nuclear RNAs (snRNAs) and piwi-interacting RNAs (piRNAs) were further studied in recent years. The analysis of longer noncoding transcripts is still in its beginnings and this class of transcripts comprises antisense RNAs, enhancer RNAs, intergenic RNAs, pseudogene RNAs, 3' UTR RNAs and circular RNAs.

### 1.3.2 MicroRNAs

Micro RNAs (miRNAs) are approximately 23 nt long small noncoding RNAs that regulate gene expression post-transcriptionally by binding to the 3' untranslated region of target RNAs<sup>131</sup>. miRNAs were first described in 1993 where lin-4 miRNA regulated the expression of lin-14 in *C. elegans* larval development<sup>132,133</sup>. In 2000, let-7 miRNA was identified to regulate lin-41 in *C. elegans*<sup>134</sup>. Lin-4 and let-7 were then found to be part of a larger class of small noncoding RNAs that were present in *C. elegans*, *Drosophila* and human cells<sup>135-137</sup>. The first human disease associated with miRNAs was chronic lymphatic leukemia<sup>138</sup>. miRNAs are transcribed from nuclear DNA, the majority being transcribed by RNA polymerase II, while some viral miRNAs are transcribed by RNA polymerase III<sup>139,140</sup>. miRNA loci can be found either in intergenic or intronic regions, as well as in exons of coding- and noncoding genes. The resulting primary miRNA (pri-miRNA) contains a ~80 nt miRNA precursor, that forms a stem-loop and the whole pri-miRNA transcript is capped, spliced, and

polyadenylated<sup>141,142</sup>. One single pri-miRNA can contain up to six miRNA precursors. The protein microprocessor complex subunit DiGeorge Syndrome chromosomal region 8 (DGCR8) recognizes the double stranded region of the stem loop structure and positions the catalytic RNase III domain of the endonuclease Drosha to cleave the RNA 11 nt from the base of the stem loop, which results in the precursor miRNA (pre-miRNA)<sup>143,144</sup>. Pre-miRNAs are exported into the cytoplasm in a Ran-GTP dependent manner by exportin-5 and cleaved by RNase III endonuclease Dicer, yielding a 22 nt miRNA:miRNA duplex with a 2-3 nt 3' overhang<sup>145</sup> (Figure 9). Both strands could potentially act as a functional miRNA, but only one is incorporated into the RNA-induced silencing complex (RISC), while the other strand is usually degraded<sup>146</sup>. The RISC contains proteins of the Argonaut family of proteins and the miRNA determines the target RNA of the RISC by its sequence. Binding of the miRNA to the target RNA is determined by the miRNA seed sequence in the 5' region of the miRNA<sup>139</sup>. Depending on the complementarity of the miRNA sequence to its target RNA, the target is either degraded or translation is inhibited. One miRNA usually targets several RNAs, thus one miRNA can regulate a network of genes. miRNAs with similar seed regions may target a similar, but nonidentical set of genes, and to differing degrees<sup>147</sup>.

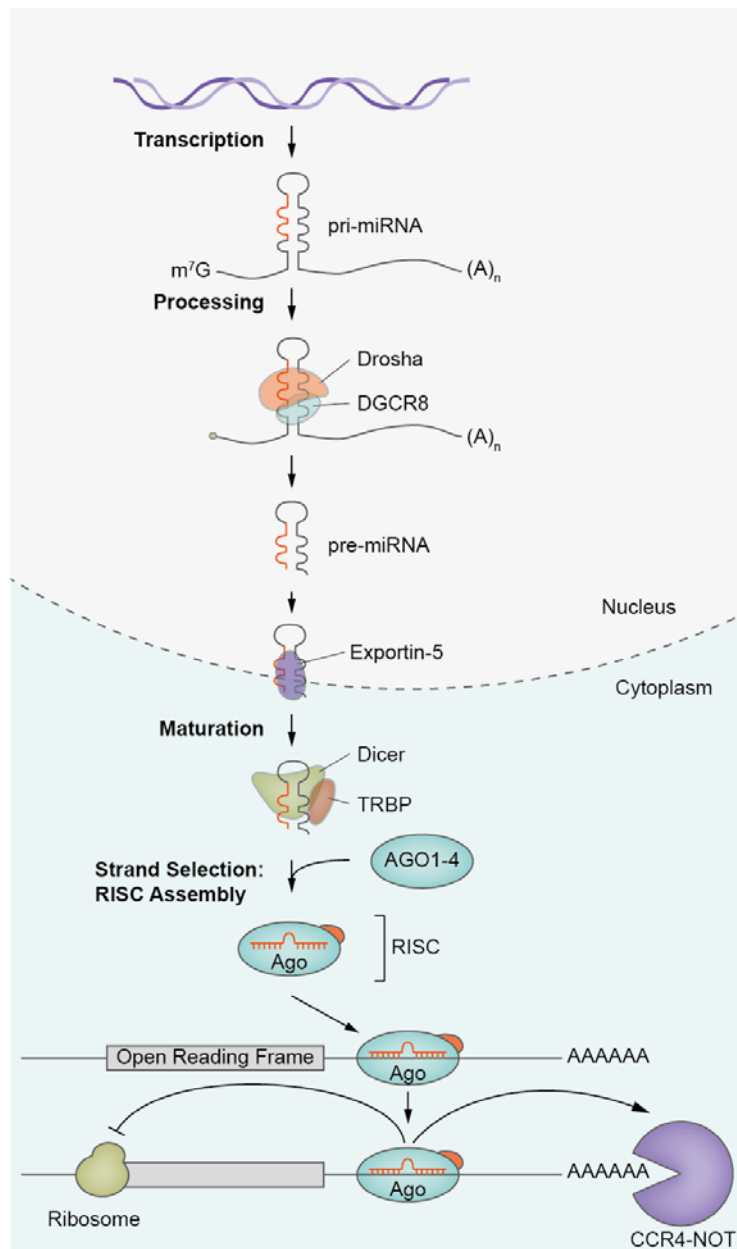


**Figure 9: miRNA Biogenesis:** pri-miRNAs are transcribed from their genomic locus and processed by Drosha and DGCR8 into the pre-miRNA, which is exported into the cytoplasm by Exportin-5. Dicer further processes the pre-miRNA and one strand together with AGO proteins then forms the RNA-induced silencing complex (RISC). RISC is directed to its target by imperfect base pairing of the miRNA to the 3' untranslated region of a target RNA and induces either translation inhibition or degradation. Modified from <sup>148</sup>.

In the cardiovascular system, several miRNAs have been described to play important roles <sup>149,150</sup>. miR-133 was reduced in animal models of cardiac hypertrophy and in patients with hypertrophic cardiomyopathy <sup>151</sup>. Inhibition of miR-133 increased hypertrophy *in vitro* and *in vivo* and miR-133 overexpression preserved cardiac function due to targeting beta-1 adrenergic receptor pathway <sup>152</sup>. Increased and reduced expression of miR-1 led to electrophysiological abnormalities in heart failure patients by targeting insulin growth factor 1 <sup>153,154</sup>. miR-21 enhances neointimal growth and

promotes deposition of extracellular matrix<sup>155-157</sup>. *In vivo* inhibition of miR-21 attenuated fibrotic response and improved cardiac function in mouse models of heart failure<sup>155</sup>. Inhibition of miR-92a reduced endothelial inflammation and promoted angiogenesis and functional recovery in ischemic myocardium<sup>158,159</sup>. miR.34a improved cardiac function after myocardial infarction in mice, attenuated cardiomyocyte apoptosis and telomere shortening<sup>160</sup>.

### **1.3.3 Long Noncoding RNAs**

Long noncoding RNAs (lncRNAs) are RNA molecules with a length of more than 200 nucleotides that do not code for proteins. There are currently 56,018 and 46,475 lncRNAs annotated for humans and mice respectively, which means that there are roughly twice as many lncRNAs than protein coding genes (based on GENCODE version 19, Ensembl 74). lncRNAs can have various functions in cells and depending on their origin in the genome, these transcripts can be divided into several subclasses. Sense lncRNAs overlap with a protein coding gene and the two genes usually share one promoter. Antisense lncRNAs are located on the opposite strand of a protein coding gene and the two genes can overlap. Intronic lncRNAs are transcribed from an intron of a protein coding gene and intergenic lncRNAs are located between two protein coding genes (Figure 10).



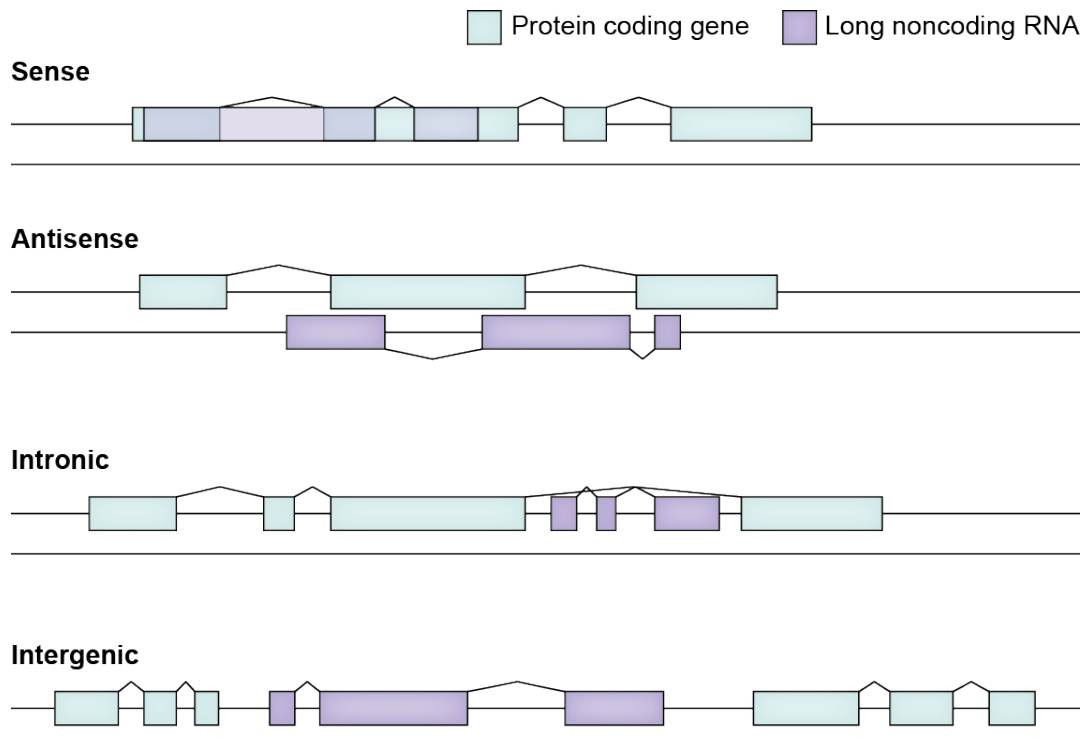


**Figure 10: Long noncoding RNA biotypes.** Long noncoding RNAs (lncRNAs) can be classified depending on their genomic location. Sense lncRNAs are transcribed from the same strand as a protein coding gene, often from intronic and exonic regions. Both genes can potentially share the same promoter. Antisense lncRNAs are located on the opposite strand of a protein coding gene and the overlap can be partial or complete. Intronic lncRNAs are transcribed exclusively from introns of protein coding genes. Intergenic lncRNAs are located between two protein coding genes. Modified from <sup>161</sup>

Numerous functions were shown for lncRNAs, involving direct interaction with proteins, other RNAs or genomic DNA (Figure 11). Direct protein binding of lncRNAs can result in competitive binding of two or more RNAs or of RNA and DNA. Gas5 lncRNA was for example shown to directly bind glucocorticoid receptor (GR) at its DNA binding domain, thus acting as a decoy <sup>162</sup>. Gas5 thereby inhibits binding of GR to genomic DNA and thus inhibits the transcription factor activity of GR. lncRNAs were also shown to bind proteins and bring them into spatial proximity as scaffolds in ribonucleoprotein complexes. HOTAIR lncRNA was shown to bind Polycomb Repressive Complex 2 (PRC2) at a 5' domain and LSD1/CoREST/REST complex at a 3' domain, thus mediating assembly of PRC2 and LSD1 and possibly enabling binding of PRC2 to LSD1 sites and *vice versa* <sup>163</sup>. Epigenetic regulators were also shown to be bound by lncRNAs and HOTTIP, which is transcribed from the 5' region of the *HOXA* locus, bound the adaptor protein WDR5 and targeted WDR5/MLL complexes across *HOXA* via chromosomal looping <sup>164</sup>. While HOTTIP acts *in cis* on the locus of its transcription, HOTAIR was shown to repress transcription *in trans* across 40 kilobases of its locus, again by interaction with PRC2 <sup>165</sup>. lncRNA-mRNA interaction can have multiple effects. MALAT1 was for example shown to regulate alternative splicing by interacting with serine/arginine (SR) splicing factors and influenced the presence of SR and other splicing factors in nuclear speckles <sup>166</sup>. Depletion

of MALAT1 and overexpression of SR proteins changed alternative splicing of a similar set of pre-mRNAs <sup>166</sup>. Even though MALAT1 does not directly interact with mRNAs in this case, it influences mRNA processing. LincRNA-p21 was shown to directly interact with CTNNB1 and JUNB mRNA through several sites of high complementarity and lowering their translation <sup>167</sup>. lincRNA-p21 bound the RNA binding protein HUR, this favored the recruitment of let-7/Ago2 to lincRNA-p21 and this lowered lincRNA-p21 stability <sup>167</sup>. This study highlights a direct lincRNA-mRNA interaction, where levels of the RNA binding protein HUR influenced lincRNA stability and this regulated target protein expression. Target mRNA degradation by lincRNAs was shown function through base-pairing between an Alu-element in the 3' UTR of a mRNA and an Alu-element within lincRNAs, inducing Staufen1-mediated mRNA decay <sup>168</sup>. LincRNAs not only interact with mRNA but also with smaller RNAs. Several lincRNAs were shown to act as competitive endogenous RNAs (ceRNAs) for miRNAs by sponging several of these transcripts and inhibiting them from binding to target mRNAs. ZEB2 lincRNA was shown to act as a ceRNA for PTEN and attenuation of ZEB2 expression activated PI3K/AKT pathway, a process common after loss of PTEN in many cancers <sup>169</sup>.

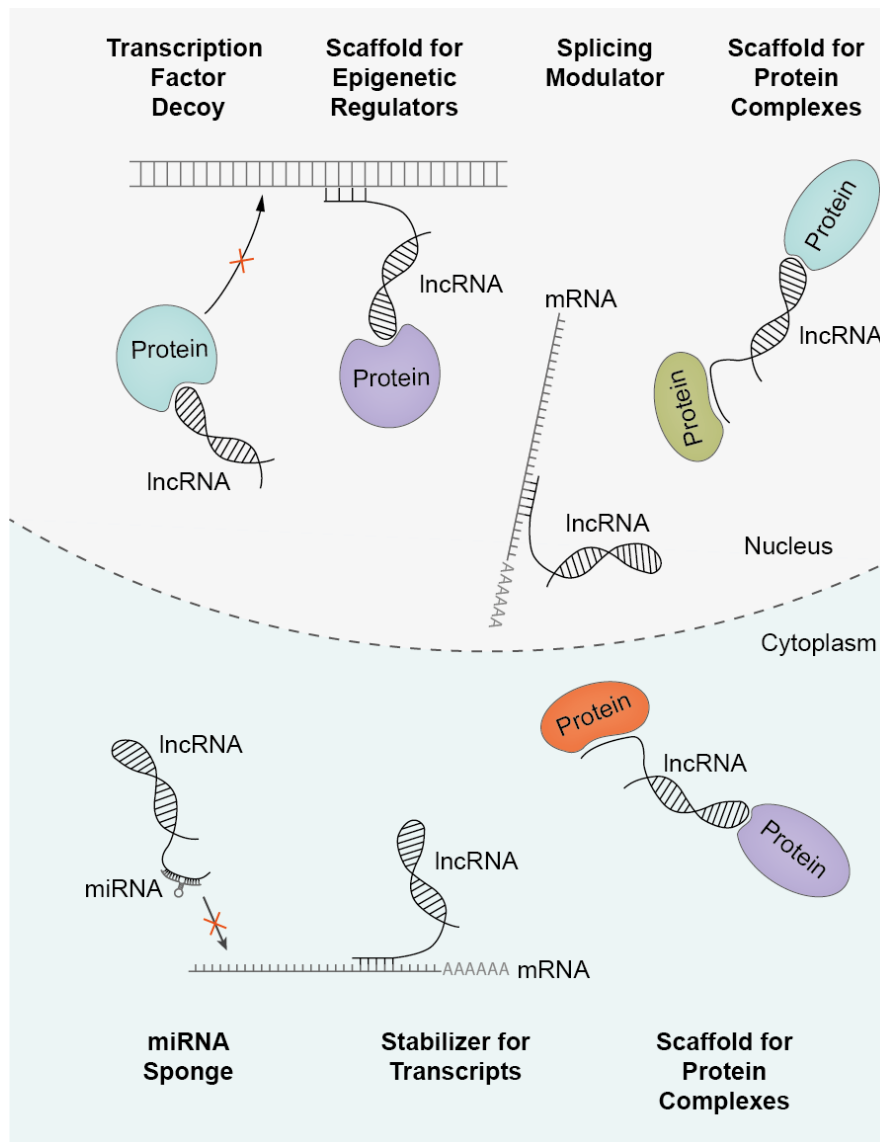


Figure 11: Biotypes of long noncoding RNAs: lncRNAs have different functions. Some depend on transcript localization. Nuclear transcripts can act as decoys for transcription factors, binding those proteins and thus inhibiting them from binding to target DNA. Other nuclear lncRNAs were shown to direct epigenetic regulators to their site of function in the genome. lncRNAs were shown to act as scaffolds for protein complexes by binding proteins and bringing them in spatial proximity, which can happen in both, nucleus and cytoplasm. In the cytoplasm, lncRNAs can act as sponges for miRNAs by direct binding and thus inhibiting miRNAs from binding to target mRNAs. lncRNAs were furthermore shown to directly interact with mRNAs to stabilize or destabilize those transcripts. Modified from <sup>170</sup>.

Several lncRNAs were identified to play a role in the cardiovascular system. Some transcripts were identified as being associated with a disease. Expression of the lncRNA ANRIL was shown to be associated with the risk for coronary and carotid atherosclerosis <sup>171,172</sup>. Others were identified in genetic analysis and subsequently deeper characterized. Analysis of the association of SNPs and myocardial infarction identified a SNP in the locus of the lncRNA MIAT that enhanced transcription of the RNA and changed its binding to an uncharacterized protein <sup>173</sup>. Later, MIAT was shown to enhance cardiac hypertrophy partly by sponging miR-150 <sup>174</sup>. A screen for circulating lncRNAs in

plasma samples from patients with or without left ventricular remodeling after acute myocardial infarction identified the lncRNA LIPCAR, which was downregulated early after AMI, but was higher expressed in later stages<sup>175</sup>. Another study analyzed expression of known lncRNAs in peripheral blood mononuclear cells of patients with AMI and identified HIF-1 AS being higher in patients with AMI compared to healthy controls and ANRIL as being lower<sup>176</sup>. Several transcripts were first identified from *in vitro* screenings and later characterized in detail. MALAT1 expression for example was shown to be increased by hypoxia in endothelial cells *in vitro* and also upon hind limb ischemia *in vivo*<sup>177</sup>. Pharmacological inhibition of MALAT1 expression *in vitro* led to a disturbed formation of vessel-like structures in a spheroid sprouting assay, where its depletion promoted migration of tip-cells but blocked proliferation of stalk cells<sup>178</sup>. Furthermore, both genetic deletion and pharmacological inhibition impaired vascularization in the mouse retina and in the hind limb *in vivo*<sup>178</sup>. MALAT-1 was also higher expressed in patients with AMI compared to healthy controls<sup>176</sup>. The lncRNA SENCER was shown to play a role in smooth muscle cell migration, where its depletion led to a hypermigratory phenotype<sup>179</sup>. Another lncRNA that plays a role in SMCs is lincRNA-p21, which is controlled by p53<sup>180</sup>. lincRNA-p21 repressed SMC proliferation and induces apoptosis and its depletion enhanced neointimal hyperplasia<sup>181</sup>. lincRNA-p21 directly interacted with MDM2 and this enhanced p53 transcriptional activity by releasing p53 from MDM2 repression<sup>181</sup>. Depletion of the lncRNA Meg3 was shown to enhance angiogenic sprouting in a spheroid outgrowth assay *in vitro* and enhanced perfusion upon hind limb ischemia *in vivo*<sup>182</sup>. Depletion of the lncRNA MANTIS resulted in inhibition of angiogenic sprouting and disturbed alignment of ECs to laminar shear stress<sup>183</sup>. MANTIS stabilized the ATPase activity of BRG1 by direct interaction and this was required for nucleosome remodeling and regulated the transcription of key endothelial genes<sup>183</sup>. Screenings of several disease models in mice for regulated lncRNAs suggested a more profound lncRNA regulation in more severe disease states<sup>184</sup>. Relatively few lncRNAs were regulated after early and late transverse aortic constriction (TAC) with mild deterioration of heart function<sup>185</sup>. Similarly, another study found 15 differentially regulated lncRNAs in mouse hearts upon TAC, while the authors identified 135 differentially regulated lncRNAs in heart failure<sup>184</sup>. Taken together, these findings suggest important roles for lncRNAs in cardiovascular disease.

### **1.3.4 The Long Noncoding RNA H19**

H19 was first identified in 1984 in a screen for genes that are upregulated by  $\alpha$ -fetoprotein in the liver and was identified as the 19<sup>th</sup> clone in row H, which gave rise to its name<sup>186</sup>. H19 is highly expressed in the developing embryo, mainly in mesoderm and endoderm-derived tissues. Its

expression is strongly downregulated after birth except for cardiac and skeletal muscle and placenta<sup>187,188</sup> (Figure 12). During tissue regeneration and in several cancers, H19 is upregulated again<sup>189,190</sup>.

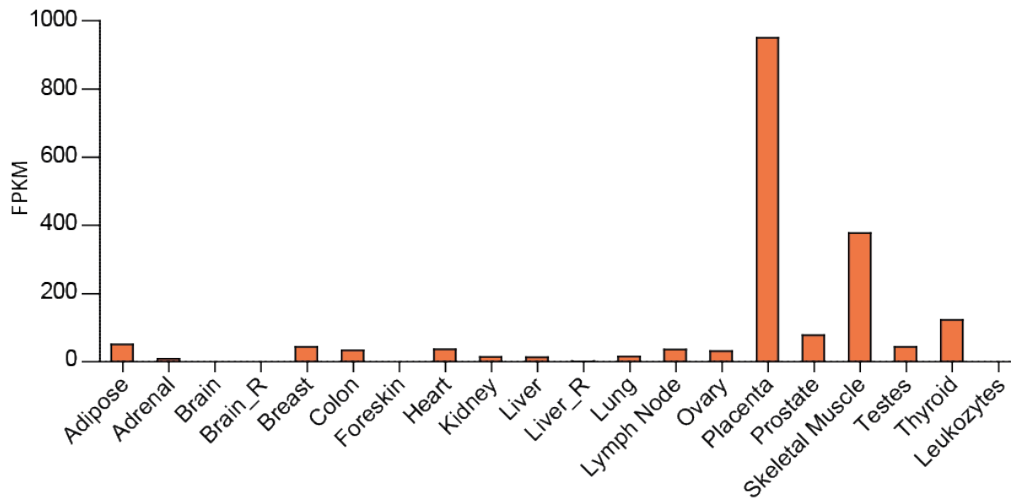


**Figure 12: H19 expression in adult human tissue: H19 is highly abundant in embryos but is shortly downregulated after birth, except for some tissues. In adults, H19 is mainly expressed in placenta and skeletal muscle. Data from noncode.org, transcript ID: NONHSAT017462.2.**

H19 is located on 11p15 in humans and on chromosome 7 in mice<sup>186,191</sup>. The gene contains five exons and is transcribed into a 2.3 kb long capped and polyadenylated RNA. The locus encoding H19 is evolutionary conserved in mammals and the exon distribution in mice and humans is similar despite nearly no sequence conservations is observed. Both mouse and human H19 harbor potential open reading frames, but neither is their distribution conserved, nor was any protein product detected, indicating a function as a noncoding RNA<sup>191</sup>. H19 is located upstream of insulin growth factor 2 (IGF2) and is paternally imprinted<sup>192</sup>. IGF2 and H19 share a distal 3' enhancer sequence downstream of the H19 gene and its deletion results in a downregulation of IGF2 and H19 expression. Located upstream of and within the IGF2 gene are two differentially methylated regions (DMR1&2). The IGF2 and H19 genes are separated by an imprinting control region (ICR) to which transcriptional zinc finger DNA-binding protein repressor (CTCF) binds in an unmethylated state. CTCF binding blocks the interaction between the 3' enhancer element and the promoter of IGF2, while it has no effect on the interaction between the 3' enhancer and the H19 promoter<sup>193</sup>. CTCF was furthermore shown to potentially play a role in initiation of H19 expression and to prevent DNA methylation on the maternal allele and to delay replication during S-phase<sup>194,195</sup>. Under proper somatic imprinting, the ICR and the DMRs are methylated on the paternal allele and not methylated on the maternal allele, allowing CTCF to bind only to the maternal ICR. H19 is then exclusively expressed from the maternal allele, while IGF2 is exclusively expressed from the paternal allele<sup>192</sup>

(Figure 13A). Loss of imprinting is associated with two different syndromes in humans, Beckwith-Wiedemann Syndrome (BWS) and Russel-Silver Syndrome (RSS). In both cases patients show aberrant methylation patterns on 11p15. In the case of BWS patients, the IGF2/H19 locus shows a hypermethylation of the ICR, which is then methylated on both alleles, leading to biallelic expression of IGF2 and to silencing of H19 (Figure 13B). Patients suffering from BWS usually show an overgrowth phenotype of several body parts<sup>196</sup>. Furthermore, these patients are more susceptible for embryonal cancers<sup>196</sup>. The knockout of the H19 gene in mice led to an overgrowth phenotype of approximately 108% compared to WT littermates, while the knockout of H19 and the ICR led to a more severe overgrowth of approximately 127%<sup>197,198</sup>. This overgrowth phenotype mainly results from the biallelic expression of IGF2. Patients suffering from RSS usually show mirrored symptoms compared to BWS patients, mainly resulting in growth defects. In RSS patients, the IGF2/H19 locus is hypomethylated, resulting in biallelic CTCF binding to the ICR and biallelic H19 expression (Figure 13C). The absence of IGF2 during embryogenesis is most likely the reason for the impaired growth phenotype. Overexpression of H19 in mice was lethal after embryonic day 14 in one study and did result in an undergrowth phenotype in another study<sup>199,200</sup>.

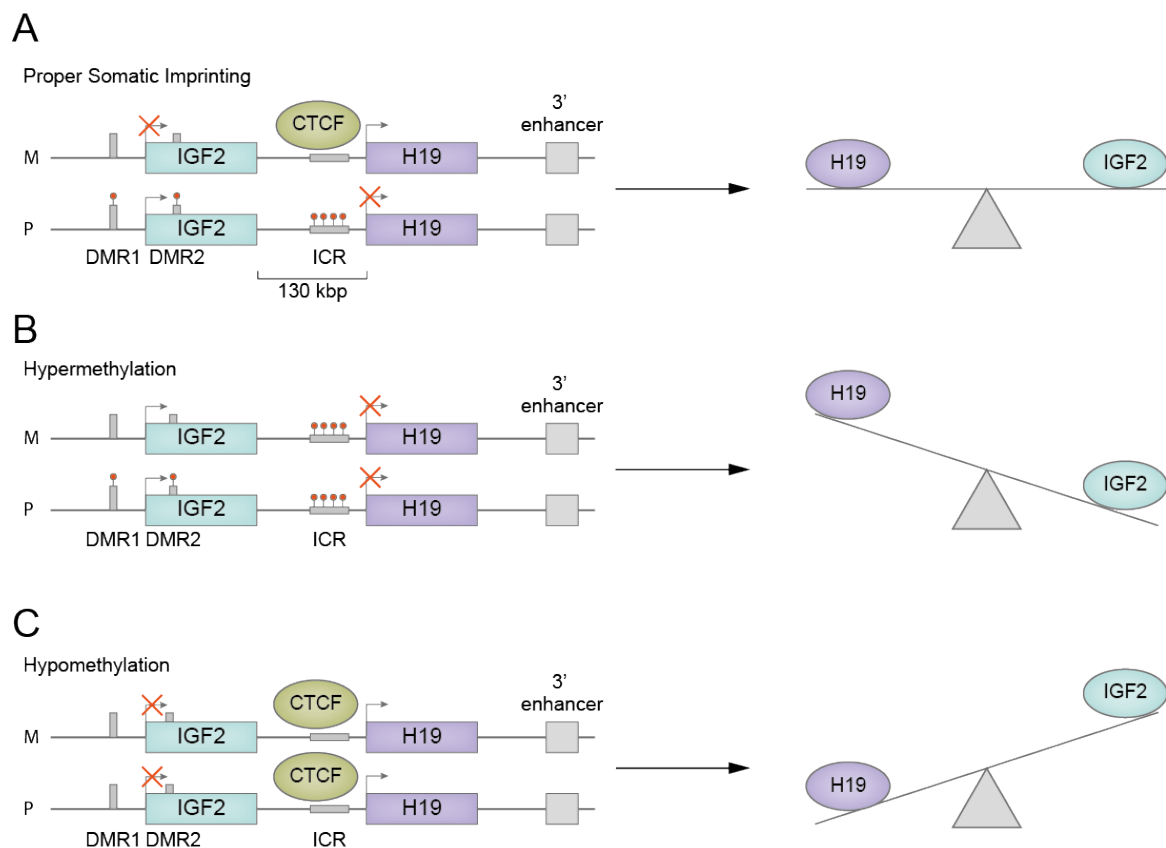


**Figure 13:** H19 and insulin growth factor 2 (IGF2) are located in a highly imprinted region on Chr11p15 in humans and Chr7 in mice. **A:** Under normal somatic imprinting, the differentially methylated regions (DMR) upstream of and within the IGF2 gene and the imprinting control region (ICR) are not methylated on the maternal and methylated on the paternal allele. Transcriptional zinc finger DNA-binding protein repressor (CTCF) binds to the unmethylated ICR on the maternal allele and blocks the interaction between the 3' enhancer and the promoter region of IGF2, leading to

transcription of H19 from the maternal and to transcription of IGF2 from the paternal allele. B: In patients with Beckwith-Wiedemann Syndrome the ICR is methylated on both alleles, leading to the biallelic expression of IGF2 and to an overgrowth phenotype. C: In patients with Russel-Silver Syndrome neither the DMRs, nor the ICR is methylated on any allele, leading to a biallelic expression of H19 and to an undergrowth phenotype. DMR: Differentially methylated region; ICR: Imprinting control region; IGF2: Insulin growth factor 2; CTCF: Transcriptional zinc finger DNA-binding protein repressor. Modified from <sup>193</sup>.

Many different stimuli were shown to regulate H19 expression, mainly related to cancer progression. H19 plays a controversial role in different types of cancer. First *in vitro* studies hinted a tumor suppressor role for H19 <sup>201</sup>. More recently, H19 was described to act as an oncogene through interaction with EZH2 and E-cadherin <sup>202,203</sup>. H19 promoted survival and proliferation of host progenitor cells under hypoxic conditions after injection of prostacyclin-producing human mesenchymal stem cells (PGI<sub>2</sub>-hMSCs) injected into mice subjected to hind limb ischemia. Furthermore, the presence of PGI<sub>2</sub>-hMSCs upregulated H19 in myoblasts under hypoxia in a co-culture *in vitro* <sup>204</sup>. Sun and colleagues show that H19 was significantly higher expressed in estrogen-receptor (ER) positive breast cancer tissue compared to ER-negative tissue. H19 depletion reduced cell survival and blocked estrogen-induced cell growth, while H19 overexpression stimulated proliferation of MCF-7 breast cancer cells <sup>205</sup>. H19 was shown to promote the proliferation of colorectal cancer (CRC) cells by binding to eIF4A3 <sup>206</sup>. H19 was furthermore shown to be the most significant lncRNA associated with CRC patient survival <sup>207</sup>. H19 depletion blocked G1/S-phase transition, reduced cell proliferation and inhibited cell migration <sup>207</sup>. RB1-E2F1 and  $\beta$ -catenin were identified as essential upstream regulators of H19 function and H19 affected the phosphorylation of RB1 by regulating the expression of CDK4 and Cyclin D1 <sup>207</sup>. H19 furthermore interacted with macroH2A, which regulates CDK8 gene transcription <sup>207</sup>. In an esophageal cancer cell line, H19 overexpression promoted proliferation and invasion and endothelial-to-mesenchymal-transition, while H19 depletion had the opposite effect <sup>208</sup>. H19 was upregulated in microvessels from glioma tissues and in glioma-associated endothelial cells cultured in glioma-conditioned medium. Furthermore, H19 inhibited the expression of miR-29a, by direct binding and miR-29a targeted the angiogenesis promoting factor vasohibin, indicating a miRNA-sponge function of H19, although the authors do not claim this <sup>209</sup>. H19 was upregulated in glioblastoma tissue and its expression level was associated with patient survival. Furthermore, it promoted invasion, stemness and tumorigenicity of glioblastoma cells and was associated with increased tumor growth in a murine xenograft model. In the same cells, H19 also promoted angiogenesis in tube formation and matrigel assays <sup>210</sup>. In hepatocellular carcinoma HepG2 cells, H19 was regulated by E2F1 through E2F1 binding sites in the H19 promoter region <sup>211</sup>. YAP1 and H19 expression was found to be associated in bladder cancer tissue and YAP1 enhanced the expression of H19 <sup>212</sup>. H19 was upregulated in bladder cancer tissues and this upregulation promoted bladder cancer cell migration *in vitro* and *in vivo* <sup>212</sup>. H19 interacted

with EZH2 and this resulted in activation of Wnt/ $\beta$ -catenin and subsequent downregulation of E-cadherin <sup>203</sup>. In pancreatic cancer cells H19 expression was increased and knockdown of H19 suppressed cell viability, proliferation and tumor growth, while H19 overexpression had the opposite effects. Knockdown of H19 led to decreased levels of E2F1 and its downstream targets <sup>213</sup>. In mouse embryo fibroblasts, H19 interacted with methyl-CpG-binding domain protein 1 (MBD1) and regulated 5 genes of the previously identified imprinted gene network <sup>214,215</sup>. The H19-MBD1 complex interacted with histone lysine methyl transferases and brought repressive histone marks to the differentially methylated regions of the target gene <sup>214</sup>. In gallbladder cancer, H19 was shown to sponge miR-342-3p and to regulate the abundance of miR-342-3p target FOXM1. Depletion of H19 *in vitro* inhibited invasion and proliferation and H19 silencing *in vivo* led to decreased tumor volumes <sup>216</sup>. H19 is known to be upregulated upon hypoxia in several cell types <sup>217,218</sup>. Matouk and colleagues showed that hypoxia-dependent H19 upregulation diminished p57<sup>kip2</sup> expression on hepatocellular carcinoma and bladder carcinoma cells <sup>219</sup>. High H19 levels promoted tumorigenic potential *in vivo* through regulating Angiogenin and FGF18 expression <sup>217</sup>. In another study, the same authors showed that p53 prevents the induction of H19 upon hypoxia and exogenous p53 was sufficient to repress H19 upregulation upon hypoxia in p53<sup>null</sup> cells. Furthermore, H19 upregulation upon hypoxia was dependent on HIF1- $\alpha$  and in p53<sup>wt</sup> cells, depletion of p53 and overexpression of HIF1- $\alpha$  was necessary to induce H19 significantly upon hypoxia <sup>219</sup>. H19 expression was furthermore shown to be repressed by p53 in HeLa cells <sup>220</sup>. H19 was shown to be regulated by E2F1 through binding sites in its promoter region in breast cancer cells and to directly promote proliferation by repressing p57<sup>kip2</sup> <sup>221</sup>. In corneal epithelial cells, H19 negatively influenced proliferation and regulated cell adhesion molecules <sup>222</sup>.

In regards to the cardiovascular system, H19 was found to be expressed in human atherosclerotic plaques <sup>223</sup>. Interestingly, in the same study, Han and colleagues showed that H19 was expressed evenly in all cells of blood vessels of rabbits at gestational day 20, but was restricted to outer layer vessel wall smooth muscle cells and to interstitial cells with further development <sup>223</sup>. Rat proliferating neointimal cells did not express H19, but in postconfluent, differentiated neointimal cells, H19 was highly abundant, indicating a role in the development and differentiation of blood vessels <sup>224</sup>. H19 was upregulated by hyperhomocysteinemia, an independent risk factor for coronary artery disease (CAD), in aorta and vascular smooth muscle cells, pointing to a potential involvement of H19 in the progression of CAD <sup>225,226</sup>. Polymorphisms in the H19 gene were associated with further risk factors for CAD, namely obesity, birth weight, and blood pressure <sup>227-229</sup> and were directly associated with the risk and severity of CAD in a Chinese population <sup>230</sup>. H19 levels were increased in end-stage and non-end-stage hearts of heart failure patients and in hypertrophic mouse hearts upon transverse aortic constriction surgery <sup>231</sup>. Interestingly, H19 was detectable in left ventricle human heart



samples, but staining for H19 and CD31 indicated a likely vascular localization of H19<sup>231</sup>. Hadji and colleagues found H19 levels to be increased in biopsies of aortic valves of patients suffering from calcific aortic valve disease (CAVD). H19 induced a strong osteogenic phenotype by preventing recruitment of p53 to the NOTCH1 promoter and thus repressing NOTCH1 expression<sup>232</sup>. H19 was also shown to be involved in cardiac fibrosis<sup>233</sup>. H19 levels were elevated in cardiac fibroblast and fibrotic tissue and ectopic H19 overexpression induced cardiac fibroblast proliferation, while H19 silencing had the opposite effect. H19 overexpression furthermore reduced the expression of DUSP5, indicating a role for H19 in cardiac fibrosis through repression of DUSP5/ERK1/2<sup>233</sup>. In HUVECs, depletion of H19 induced p21 expression and reduced proliferation<sup>218</sup>. Furthermore, H19 was shown to possess a pro-angiogenic function through regulation of angiogenin in cancer<sup>217</sup>.

H19 was previously shown to act as a miRNA precursor by giving rise to miR-675<sup>234</sup>. It was proposed that the main physiological role of H19 is to limit placenta growth before birth by regulated processing of miR-675. Interestingly, despite high H19 levels, miR-675 was poorly expressed in mouse embryos<sup>235-237</sup>. miR-675 was only detectable in the placenta from E11.5, despite there being no change in H19 expression, suggesting a tight regulation of the miRNA processing. Keniry and colleagues analyzed miR-675 and H19 copy numbers in different tissues of mouse embryos and found in average 40 and 70 copies per cell in fetal heart and fetal liver respectively for miR-675 and approximately 300 copies of miR-675-5p and 1000 copies of miR-675-3p per placenta cell at the peak of expression. Nevertheless, miR-675 copy numbers never exceeded 1% of H19 copy numbers<sup>235</sup>. Let-7 miRNAs are known to be functional in HeLa cells at similar copy numbers compared to miR-675 in mouse placenta<sup>238,239</sup>. These data support the theory of a tight regulation of miR-675 processing from H19 and Keniry and colleagues identified the RNA binding protein HuR as a regulator of this step<sup>235</sup>. H19 and miR-675 were shown to be upregulated during myoblast differentiation and muscle regeneration. The knockout of H19 in mice altered muscle regeneration and this effect was rescued with exogenous miR-675-3p and -5p<sup>190</sup>. Dey and colleagues show that miR-675 exerts its effects on muscle regeneration by targeting Smad transcription factors and Cdc6<sup>190</sup>. In a gastric cancer cell line, H19 was as well described to mainly act through miR-675 by targeting RUNX1 and thus enhanced proliferation and invasion<sup>240</sup>. H19 was significantly downregulated in a rat model of diabetic cardiomyopathy and its overexpression attenuated oxidative stress, inflammation and apoptosis and improved left ventricular function in rats. Li and colleagues propose that this effect is mediated by miR-675 targeting VDAC1, a protein that is associated with diabetes and plays a role in cardiomyocyte apoptosis<sup>241</sup>. In colorectal cancer, miR-675 was found to target retinoblastoma (RB) and suppression of miR-675 increased RB expression and decreased cell growth and soft agar colony formation of human colorectal cancer cells<sup>242</sup>. Zhou and colleagues showed that repression of miR-675-5p arrested esophageal squamous cell carcinoma cells in G1 phase during cell cycle and reduced

proliferation, migration, colony formation and invasion. Furthermore, tumorigenesis and tumor metastasis was reduced upon miR-675 inhibition *in vivo* due to miR-675-5p targeting RESP2<sup>243</sup>. Overexpression of H19/miR-675 increased the proliferation migration of breast cancer cells *in vitro* and increased tumor growth and metastasis *in vivo* through a regulation of c-Cbl and Cbl-b by miR-675<sup>244</sup>. Liu and colleagues showed that H19 and miR-675 expression is elevated in cardiac hypertrophy and heart failure<sup>245</sup>. Overexpression of H19 reduced cell size, whereas its silencing induced hypertrophy. Inhibition of miR-675 reversed the reduction in cardiomyocyte size upon H19 overexpression, indicating that that miR-675 mediated the inhibitory effect of H19 on cardiomyocyte hypertrophy<sup>245</sup>. miR-675 directly targeted tumor suppressor retinoblastoma (RB) in colorectal cancer cells<sup>242</sup>.

H19 not only gives rise to miRNAs, it was furthermore shown to be able to sponge those short noncoding RNAs. Kallen and colleagues identified 4 binding sites for miRNAs of the let-7 family in the human H19 transcript. Depletion of H19 accelerated muscle differentiation in C2C12 cells and this effect was recapitulated by let-7 overexpression, suggesting an inhibitory function of H19 on let-7 miRNAs. Let-7 overexpression led to a decrease in H19 levels and H19 and let-7 interacted in AGO2 RNPs<sup>246</sup>. Another study identified an interaction between H19 and miRNAs of the miR-17-5p family by miR-CLIP and further confirmed the let-7 binding ability of H19<sup>247</sup>. siRNA-mediated H19 depletion repressed many targets of miR-17-5p and let-7<sup>247</sup>. Gao and colleagues showed that H19 expression decreases in muscle tissue of patients with type-2-diabetes, which leads to an increased bioavailability of let-7 miRNAs. Furthermore, hyperinsulinemia repressed H19 in a KSRP-dependent manner<sup>248</sup>. PI3K/AKT-dependent phosphorylation of KSRP promoted biogenesis of let-7 miRNAs and this led to H19 destabilization<sup>248</sup>. Another study further analyzed the interaction between H19 and KSRP. Giovarelli and colleagues found H19 to directly interact with KSRP in the cytoplasm of C2C12 cells and this promoted the mRNA decay function of KSRP<sup>249</sup>. In colorectal cancer, H19 was shown to antagonize miR-138 and miR-200a and overexpression of H19 promoted EMT by de-repressing miR-138 and miR-200a targets Vimentin, ZEB1 and ZEB2<sup>250</sup>. The ceRNA function for miR-200 was furthermore shown in osteosarcoma cells, where H19 antagonized miRNAs of the miR-200 family and its overexpression promoted metastasis by upregulation of miR-200 targets ZEB1 and ZEB2<sup>251</sup>. In cholangiocarcinoma, H19 expression was induced upon short- and long-term oxidative stress and H19 again functioned as a ceRNA against let-7a and let-7b. IL-6 was identified as a target for let7 miRNAs and overexpression of H19 increased IL-6 protein abundance while H19 depletion decreased IL-6 levels<sup>252</sup>. However, until now, H19 has not been described to be involved in aging of the cardiovascular system.

## 2. Objective

Cardiovascular disease is the leading cause of death worldwide. Life expectancy steadily increases and aging is among the greatest known risk factors for cardiovascular disease, highlighting the growing relevance for new approaches for therapies. Aging of the vasculature is characterized by endothelial dysfunction, impaired angiogenesis, and inflammatory activation, leading to a plethora of different diseases. Noncoding RNAs were shown to be promising targets for new therapeutic approaches, highlighted by the development of several miRNA based therapeutic approaches for different diseases. Extensive studies have shown that long noncoding RNAs possess a great variety of functions through different types of cells and disease states. However, little is known about the role of long noncoding RNAs during aging of the cardiovascular system.

The objective of this work was to elucidate the following:

1. Are long noncoding RNAs regulated during aging of endothelial cells?
2. Does the aging-regulated long noncoding RNA H19 play a functional role in endothelial cells in regards to endothelial function *in vitro* and *in vivo*?
3. Does the aging-regulated long noncoding RNA H19 influence endothelial hallmarks of aging like impaired angiogenesis and increased inflammatory activation?

### 3. Materials and Methods

#### 3.1 Materials

**Table 1: Consumables and manufacturer**

Item	Manufacturer
μ-slide I leuc (0.4)	Ibidi (Martinsried, Germany)
¼" ceramic spheres	MP Biomedicals (Illkirch, France)
48-well cell culture plates Nunclon	Nalge Nunc International (Denmark)
Cell culture dishes (6cm, 10cm)	Greiner Bio-one GmbH (Frickenhausen, Germany)
Cell culture flasks (T25, T75, T175)	Greiner Bio-one GmbH (Frickenhausen, Germany)
Cell scraper	Greiner Bio-one GmbH (Frickenhausen, Germany)
Cell strainer (70 μm)	BD Biosciences (Erembodegen, Belgium)
Combitips (5 ml, 10 ml)	Eppendorf (Hamburg, Germany)
Costar stripette serological pipettes	Corning (Big flats, NY, USA)
Culture Insert 2-well	Ibidi (Martinsried, Germany)
Filter Tips TipOne RPT (10 μl, 20 μl, 100 μl, 200 μl, 1000μl)	Starlab (Ahrensburg, Germany)
Hybond Nitrocellulose membrane	GE Healthcare (Little Chalfont, UK)
Microtubes 2 ml, polypropylene	Sarstedt (Nümbrecht, Germany)
Multiwell cell culture plates (96-well, 24-well, 6-well)	Greiner Bio-one GmbH (Frickenhausen, Germany)
NucleoCasette (Cell Counting)	ChemoMetec A/S (Allerød, Denmark)
Optical 96 well reaction plates	Thermo Fisher Scientific (Waltham, MA, USA)
Optical adhesive covers	Thermo Fisher Scientific (Waltham, MA, USA)
PCR tubes (0.5 and 0.2 ml)	Eppendorf (Hamburg, Germany)
Perfusion set (15 cm, ID 1.6mm)	Ibidi (Martinsried, Germany)
Polypropylene falcon tubes (15 and 50 ml)	Greiner Bio-one GmbH (Frickenhausen, Germany)
Safe lock tubes (1.5 and 2 ml)	Eppendorf (Hamburg, Germany)
Whatman paper	Macherey-Nagel GmbH (Düren, Germany)
96-well qRT-PCR plates	Thermo Fisher Scientific (Waltham, MA, USA)
384-well qRT-PCR plates	Thermo Fisher Scientific (Waltham, MA, USA)

**Table 2: Equipment and manufacturer**

Instrument	Model/type	Manufacturer
Adjustable volume pipettes		Eppendorf (Hamburg, Germany)
Cell counter	Nucleocounter 2000	ChemoMetec A/S (Allerød, Denmark)
Centrifuge (falcon, plates)	5810 R	Eppendorf (Hamburg, Germany)
Centrifuge benchtop	5424 R	Eppendorf (Hamburg, Germany)
CO2 Incubator	Galaxy 170S	Eppendorf (Hamburg, Germany)
Confocal Microscope	LSM 780, Axio Observer	Zeiss (Jena, Germany)
Blood Pressure Analysis System	BP-2000	Visitech Systems
Histology	TPC 15 Duo/Trio	Medite GmbH (Burgdorf, Germany)
Homogenizer	FastPrep24	MP Biomedicals (Solon, OH, USA)
Imaging system	ChemiDoc MP	Bio-Rad (Munich, Germany)
Inhalationsnarkose-Apparat	Trajan 808	Dräger Medical Deutschland GmbH (Lübeck, Germany)
Microplate multimode reader	GloMax®-Multi+with Instinct®	Promega, (Madison, WI, USA)
Microplate reader	Synergy HT	Biotek (Winooski, VT, USA)

Microscope	Axio Observer Z1	Zeiss (Jena, Germany)
Microscope	Axiovert 100	Zeiss (Jena, Germany)
Mini gel electrophoresis setup	Protean Tetra	Bio-Rad (Munich, Germany)
Mini Trans Blot Cell setup		Bio-Rad (Munich, Germany)
Semi Dry Blot Setup	Pierce Power Blot Station	Thermo Fisher Scientific (Waltham, MA, USA)
Multipipette	XStream	Eppendorf (Hamburg, Germany)
Overhead stirrer (homogenizer)	VOS 14	VWR (Leicestershire, UK)
Perfusion pump and fluidic unit	Version 1.1	Ibidi (Martinsried, Germany)
Perfusion unit	Perfusor fm	B.Braun (Melsungen, Germany)
Powersupply	Powerpac HC	BioRad (Munich, Germany)
Real time PCR system	StepOnePlus	Thermo Fisher Scientific (Waltham, MA, USA)
Real time PCR system	Viia-7	Thermo Fisher Scientific (Waltham, MA, USA)
Safety cabinet	Hera safe	Heraeus (Hanau, Germany)
Shaking incubator	3003	GFL GmbH (Burgwedel, Germany)
Shear Stress Setuo	Ibidi Pump System	Ibidi (Martinsried, Germany)
Spectrophotometer	SmartSpec 3000	Bio-Rad (Munich, Germany)
Spectrophotometer	Nanodrop 2000	Thermo Fisher Scientific (Waltham, MA, USA)
Thermocycler	Mastercycler Nexus	Eppendorf (Hamburg, Germany)
Thermomixer compact	Thermomixer C	Eppendorf (Hamburg, Germany)
UV Trans illuminator	T2201	Sigma-Aldrich (St. Louis, MO, USA)
Vortexer	Vortex Genie 2	Scientific Industries (Bohemia, NY, USA)
Water bath		VWR (Leicestershire, UK)

**Table 3: Chemicals and reagents**

Item	Manufacturer
10 mM dNTP Mix	Thermo Fisher Scientific (Waltham, MA, USA)
10x PCR buffer	Thermo Fisher Scientific (Waltham, MA, USA)
2x Fast SYBR green mix	Thermo Fisher Scientific (Waltham, MA, USA)
37% Paraformaldehyde (PFA)	AppliChem (Darmstadt, Germany)
5x Reverse transcriptas buffer	Thermo Fisher Scientific (Waltham, MA, USA)
Acetone	Sigma-Aldrich (St. Louis, MO, USA)
Acetylated Dil LDL	Thermo Fisher Scientific (Waltham, MA, USA)
Acrylamide	AppliChem (Darmstadt, Germany)
Ammonium per sulphate (APS)	Roth (Karlsruhe, Germany)
BCECF	Thermo Fisher Scientific (Waltham, MA, USA)
BD Matrigel Basement Membrane Matrix	BD Bioscience

Biotin isolectin B4	Vector laboratories (Burlingame, CA, USA)
Bovine Serum Albumin (BSA) Fraction V	PAA laboratories (Paching, Austria)
Bradford reagent	Bio-Rad (Hercules, CA, USA)
Bromphenol blue	Merck (Darmstadt, Germany)
Cadaverine AlexaFluor488	Thermo Fisher Scientific (Waltham, MA, USA)
Cadaverine AlexaFluor555	Thermo Fisher Scientific (Waltham, MA, USA)
Calcium dichloride (CaCl <sub>2</sub> )	Merck (Darmstadt, Germany)
CD144 antibody	Pharmingen
CD31 antibody	Dianova
Chloroform	J T Baker (Phillipsburg, NJ, USA)
Collagenase/Dispase mix	Roche (Mannheim, Germany)
Dimethyl sulfoxide (DMSO)	Sigma-Aldrich (St. Louis, MO, USA)
Dispase II	Gibco, Invitrogen (Darmstadt, Germany)
Dithiothreitol (DTT)	AppliChem (Darmstadt, Germany)
DNase and RNase-free water	Gibco, Invitrogen (Darmstadt, Germany)
DNase I	Worthington (Lakewood, NJ, USA)
Donkey serum	DAKO (Jena, Germany)
Dual Luciferase Reporter Assay System	Promega (Madison, WI, USA)
Dynabeads	Thermo Fisher Scientific (Waltham, MA, USA)
Ethanol absolute	Sigma-Aldrich (St. Louis, MO, USA)
Evans blue	Sigma-Aldrich (St. Louis, MO, USA)
Fibronectin	Sigma-Aldrich (St. Louis, MO, USA)
FITC conjugated isolectin B4	Sigma-Aldrich (St. Louis, MO, USA)
Fixation buffer (4% w/v paraformaldehyde)	BD Cytotfix™ (Franklinlake, NJ, USA)
GeneJuice	Merck (Darmstadt, Germany)
Glycerol	AppliChem (Darmstadt, Germany)
Goat serum	DAKO (Jena, Germany)
HCl	Sigma-Aldrich (St. Louis, MO, USA)
Hoechst	AnaSpec (Fremont, CA)
Immobilon western ECL reagent	Merck (Darmstadt, Germany)
Isolectin B4 biotinylated	Vector laboratories (Burlingame, CA, USA)
Isopropanol	Sigma-Aldrich (St. Louis, MO, USA)
Magnesium dichloride (MgCl <sub>2</sub> )	Sigma-Aldrich (St. Louis, MO, USA)
Manganese dichloride (MnCl <sub>2</sub> )	Sigma-Aldrich (St. Louis, MO, USA)
Methanol	Sigma-Aldrich (St. Louis, MO, USA)
Mounting medium	DAKO (Jena, Germany)
Mounting medium	DAKO (Jena, Germany)
Multiscribe Reverse Transcriptase	Thermo Fisher Scientific (Waltham, MA, USA)
MuLV-Reverse-Transcriptase (200 U/μl)	Thermo Fisher Scientific (Waltham, MA, USA)
N,N dimethylformamide	Sigma-Aldrich (St. Louis, MO, USA)
Phenol-Chlorophorm-Isoamylalcohol	AppliChem (Darmstadt, Germany)
Phosphate buffered saline (PBS)	Thermo Fisher Scientific (Waltham, MA, USA)
Potassium chloride (KCl)	AppliChem (Darmstadt, Germany)
Protein block buffer, serum free	DAKO (Jena, Germany)
Protein G Beads	Thermo Fisher Scientific (Waltham, MA, USA)
QIAzol	Qiagen GmbH (Hilden, Germany)
Random hexamer primer	Thermo Scientific (Waltham, MA, USA)
Rat tail collagen type I	Merck (Darmstadt, Germany)
RiboJuice	Merck (Darmstadt, Germany)
RiboLock Rnase Inhibitors	Thermo Fisher Scientific (Waltham, MA, USA)
RIPA buffer	Sigma-Aldrich (St. Louis, MO, USA)
SDS	Roth (Karlsruhe, Germany)
Sodium azide	Sigma-Aldrich (St. Louis, MO, USA)
Sodium bicarbonate	Sigma-Aldrich (St. Louis, MO, USA)
Sodium chloride (NaCl)	J T Baker (Phillipsburg, NJ, USA)

Sodium hydroxide (NaOH)	Roth (Karlsruhe, Germany)
Streptavidin AF-488	Molecular Probes (Eugene, OR, USA)
Streptavidin AF-555	Thermo Fisher Scientific (Waltham, MA, USA)
Sucofin skimmed milk powder	TSI GmbH (Zevern, Germany)
Tamoxifen base	Sigma-Aldrich (St. Louis, MO, USA)
TaqMan Fast Universal PCR Mastermix (2x)	Thermo Fisher Scientific (Waltham, MA, USA)
TEMED	AppliChem (Darmstadt, Germany)
Tris pure	AppliChem (Darmstadt, Germany)
Triton-X-100	Sigma-Aldrich (St. Louis, MO, USA)
tRNA (yeast)	Thermo Fisher Scientific (Waltham, MA, USA)
Tween 20	Sigma-Aldrich (St. Louis, MO, USA)
Zn <sup>2+</sup> fixation solution	Morphisto (Frankfurt, Germany)

**Table 4: Kits**

Name	Manufacturer
BrdU Flow Kit	BD Bioscience (San Jose, CA, USA)
Cignal 45-Pathway Reporter Assay	Qiagen (Hilden, Germany)
Dual luciferase reporter assay	Promega (Madison, WI, USA)
EasyPrep Pro plasmid miniprep kit	Biozym Scientific (Oldendorf, Germany)
IL-6 human ELISA kit	Thermo Fisher Scientific (Waltham, MA, USA)
KOD hot start	Novagen/Merck (Darmstadt, Germany)
Magna RIP <sup>TM</sup> RNA-Binding Protein Immunoprecipitation Kit	Merck (Darmstadt, Germany)
miRNeasy RNA isolation kit	Qiagen (Hilden, Germany)
PCR purification kit	Qiagen (Hilden, Germany)
Plasmid Maxi kit	Qiagen (Hilden, Germany)
QiaQuick Gel extraction kit	Qiagen (Hilden, Germany)

**Table 5: Bacterial strains**

Name	Manufacturer
One Shot TOP10 chemically competent <i>E. coli</i>	Thermo Fisher Scientific (Waltham, MA, USA)
One Shot Stbl3 chemically competent <i>E. coli</i>	Thermo Fisher Scientific (Waltham, MA, USA)

**Table 6: Bacterial media**

Name	Media	Manufacturer
LB Agar capsules	1% Tryptone, 0.5% Yeast extract-B, 1% NaCl, 1.5% Agar-B	MP Biomedicals (Irvine, CA, USA)
LB medium capsules	1% Tryptone, 0.5% Yeast extract, 1% NaCl (pH6.7)	MP Biomedicals (Irvine, CA, USA)
S.O.C medium	2% Tryptone, 0.5% Yeast extract, 10 mM NaCl, 2.5 mM KCl, 10 mM MaCl <sub>2</sub> , 10 mM MgSO <sub>4</sub> , 20 mM glucose	Thermo Fisher Scientific (Waltham, MA, USA)

**Table 7: Plasmids**

Plasmid	Manufacturer/Source
P9.81	Addgene (Cambridge, MA, USA)
pGK	Addgene (Cambridge, MA, USA)
pLenti4/V5	Thermo Fisher Scientific (Waltham, MA, USA)
pMD2	Addgene (Cambridge, MA, USA)

**Table 8: Enzymes**

Enzyme name	Manufacturer
Dispase	Roche (Mannheim, GER)
DNase I	Worthington (Lakewood, NJ, USA)
Multiscribe reverse transcriptase	Thermo Fisher Scientific (Waltham, MA, USA)
MuLV reverse transcriptase	Thermo Fisher Scientific (Waltham, MA, USA)
LR clonase	Thermo Fisher Scientific (Waltham, MA, USA)

**Table 9: Cell culture solutions and supplements**

Item name	Manufacturer
2.5% Trypsin EDTA	Thermo Fisher Scientific (Waltham, MA, USA)
Cryptothanshinone	Sigma-Aldrich (St. Louis, MO, USA)
DMEM/F-12	Thermo Fisher Scientific (Waltham, MA, USA)
DMSO	Sigma-Aldrich (St. Louis, MO, USA)
Dulbecco's Phosphate Buffer Saline (PBS)	Thermo Fisher Scientific (Waltham, MA, USA)
ECGS-H	Promocell (Heidelberg, Germany)
EDTA Solution pH7.4	Thermo Fisher Scientific (Waltham, MA, USA)
EGM single quots	Lonza (Verviers, Belgium)
Endothelial Basal Medium (EBM)	Lonza (Verviers, Belgium)
Fetal Bovine Serum	Thermo Fisher Scientific (Waltham, MA, USA)
Fibronectin from human plasma (0.1 % solution)	Sigma-Aldrich (St. Louis, MO, USA)
Gelatin	Sigma-Aldrich (St. Louis, MO, USA)
Genejuice transfection reagent	Millipore (Millerrica, MA, USA)
Hanks BSS	PAA laboratories (Paching, Austria)
HEPES	Thermo Fisher Scientific (Waltham, MA, USA)
Interleukin-6	Peprtech (Rocky hill, NJ, USA)
Lipofectamine RNAimax	Thermo Fisher Scientific (Waltham, MA, USA)
M199 medium	Sigma-Aldrich (St. Louis, MO, USA)
MCDB131	Thermo Fisher Scientific (Waltham, MA, USA)
MEM non-essential amino acid mix	Sigma-Aldrich (St. Louis, MO, USA)
OptiMEM	Thermo Fisher Scientific (Waltham, MA, USA)
Penicillin-Streptomycin (500x)	Roche (Mannheim, Germany)
Rat tail collagen type I	Merck (Darmstadt, Germany)
Sodium pyruvate	Thermo Fisher Scientific (Waltham, MA, USA)
Soluble Interleukin-6 Receptor $\alpha$	Peprtech (Rocky hill, NJ, USA)
Tumor Necrosis factor alpha (TNF $\alpha$ )	Peprtech (Rocky hill, NJ, USA)
Vascular Endothelial Growth Factor human (VEGF)	R&D Systems GmbH (Wiesbaden, Germany)
Vascular Endothelial Growth Factor mouse (VEGF)	Peprtech (Rocky hill, NJ, USA)

**Table 10: Primary cells and cell lines**

Name	Species	Manufacturer
------	---------	--------------



HEK293FT	<i>Homo sapiens</i>	Clontech (Mountain View, CA, USA)
HeLa	<i>Homo sapiens</i>	
Human umbilical vein endothelial cells (HUVEC)	<i>Homo sapiens</i>	Lonza (Verviers, BEL)
Human coronary artery endothelial cells (hCoAEC)	<i>Homo sapiens</i>	Promocell (Heidelberg, GER)

**Table 11: Mouse strains**

Strain	Provided by
C57BL/6	Charles River Laboratories (Sulzfeld, Germany)
Cdh5CRE-ERT2 <sup>PAC</sup>	Dr. Ralf Adams (Münster, Germany)
H19 <sup>fl/fl</sup>	Dr. Carl Pfeifer (NIH, Bethesda, MD, USA)
Cdh5CRE-ERT2 <sup>PAC</sup> ; H19 <sup>fl/fl</sup>	Own breeding

**Table 12: Primary Antibodies used for immunoblotting and RNA immunoprecipitation**

Antibody	Species	Manufacturer	Use
Ago2	Mouse	Millipore (Darmstadt, Germany)	RNA Immunoprecipitation
P21	Rabbit	Cell Signaling Technology (Danvers, MA, USA)	Western Blot
STAT3	Rabbit	Cell Signaling Technology (Danvers, MA, USA)	Western Blot RNA Immunoprecipitation
pSTAT3(Y705)	Rabbit	Cell Signaling Technology (Danvers, MA, USA)	Western Blot
JAK2	Rabbit	Cell Signaling Technology (Danvers, MA, USA)	Western Blot RNA Immunoprecipitation
αTubulin	Mouse	Thermo Fisher Scientific (Waltham, MA, USA)	Western Blot
αTubulin	Rabbit	Thermo Fisher Scientific (Waltham, MA, USA)	Western Blot
CD144 (mouse)	Rat	Pharmingen	Lung EC Isolation

**Table 13: Secondary antibodies used for immunoblotting**

Antibody	Species	Manufacturer	Use
HRP-linked sheep anti-mouse	Sheep	GE Healthcare (Little Chalfont, UK)	Western Blot
HRP-linked donkey anti-rabbit	Donkey	GE Healthcare (Little Chalfont, UK)	Western Blot

**Table 14: Antibodies used for flow cytometry**

Antibody	Species	Manufacturer	Use
PE-anti-human-CD45	Mouse	Biolegend (San Diego, CA, USA)	Flow Cytometry
APC-anti-human-CD106	Mouse	Biolegend (San Diego, CA, USA)	Flow Cytometry
V450-anti-BrdU	Mouse	BD Bioscience (San Jose, CA, USA)	Flow Cytometry

**Table 15: Primary antibodies for histology.**

Antibody	Species	Manufacturer
Anti-mouse-CD31	Rat	Dianova
$\alpha$ SMA-Cy3 labeled (anti-human)	Mouse	Sigma-Aldrich (St. Louis, MO, USA)
Anti-mouse-CD45	Rat	Abcam

**Table 16: Secondary antibodies used for histology**

Antibody	Species	Manufacturer
AlexaFluor488	Donkey anti-rat	Life Technologies (Carlsbad, CA, USA)
AlexaFluor488	Goat anti-rat	Life Technologies (Carlsbad, CA, USA)
AlexaFluor488	Anti-mouse IgG	Life Technologies (Carlsbad, CA, USA)
AlexaFluor555	Goat anti-rabbit	Life Technologies (Carlsbad, CA, USA)
AlexaFluor647	Goat anti-rat	Life Technologies (Carlsbad, CA, USA)
AlexaFluor 647	Donkey anti-goat	Life Technologies (Carlsbad, CA, USA)

**Table 17: Buffers used for immunoblotting, agarose gels and SDS-PAGE**

Buffer	Component
10x TBE	25 mM EDTA, 890 mM Tris-Base, 890 mM Boric acid, pH 8.0 (adjust with acetic acid)
4x loading buffer	250 mM Tris/HCl pH 8.0, 8% SDS, 40% Glycerin, 0.04% Bromphenolblue, 200 mM DTT
HBSS	400 mg/L KCl, 60 mg/L $\text{KH}_2\text{PO}_4$ , 350 mg/L $\text{NaHCO}_3$ , 8 g/L NaCl, 48 mg/L $\text{Na}_2\text{HPO}_4$
PBS	200 mg/L KCl, 200 mg/L $\text{KH}_2\text{PO}_4$ , 8 g/L NaCl, 2160 mg/L $\text{Na}_2\text{HPO}_4 \cdot 7\text{H}_2\text{O}$
Resolving buffer	1.5 M Tris/HCl pH 8.8, 0.4% SDS
SDS running buffer	25 mM Tris, 96 mM Glycine, 1% SDS
Stacking buffer	0.5 M Tris/HCl, pH 6.8, 0.4% SDS
TBS	250 mM Tris (pH 8), 750 mM NaCl, 12.5 mM KCl
TBST	TBS + 0.2 % Tween (v/v)
Wet blot buffer	48 mM Tris base, 278 mM Glycine, 0.1% SDS

**Table 18: Primers for detection of human RNAs in qRT-PCR**

Target	Sequence forward	Sequence reverse
RPLP0	TCGACAATGGCAGCATCTAC	ATCCGTCTCCACAGACAAGG
GAPDH	ATGGAAATCCCATCACCATCTT	ATGGAAATCCCATCACCATCTT
H19	TCAAGCCTGGGCCTTTGAAT	GGCTGATGAGGTCTGGTTCC
KLF2	CAAGACCTACCAAGAGTTTCG	CATGTGCCGTTTCATGTGC
ICAM-1	ATGCCAGACATCTGTGTCC	TCCTTTTATAGCAACGGGGT
VCAM-1	GGGAAGCCGATCACAGTCAA	CTCCAGCCTGTCAAATGGGT
STAT3	ACCATTGACCTGCCGATGTC	AAGGTGAGGGACTCAAATGTC
IL-6	GCAGAAAAAGGCAAAGAATC	CTACATTTGCCGAAGAGC
p21	AGTCAGTTCCTTGTGGAGCC	CATTAGCGCATCACAGTCGC
p16 <sup>ink4A</sup>	GCACCAGAGGCAGTAACCAT	TTCCCGAGGTTTCTCAGAGC
p53	ACCTATGGAACTACTTCTCTG	ACCATTGTTCAATATCGTCC
HMGA2	GCAGCAGCAAGAACCAACC	CGGCAGACTCTTGTGAGGAT
LYZ	AGTACAAACTACAATGCTG	AAAGCACTGCAGGATAAATG

IGF2	CGTCCCCTGATTGCTCTACC	CGGCAGTTTTGCTCACTTCC
------	----------------------	----------------------

**Table 19: Primers for detection of mouse RNAs in qRT-PCR**

<b>Target</b>	<b>Sequence forward</b>	<b>Sequence reverse</b>
RPLP0	GCGTCCTGGCATTGTCTGT	GAAGGCCTTGACCTTTTCAGTAAG
H19	CAGAGCAAAGGCATCGCAAAG	GCCACGTCCTGTAACCAAAA
p21	GCGGTGTCAGAGTCTAGGG	GTGCCTGTGGCTCTGAATGT

## 3.2 Methods

### 3.2.1 Cell culture

#### Cultivation of primary cells and cell lines

Human umbilical vein endothelial cells (HUVECs) were purchased from Lonza and cultured in endothelial basal medium (EBM; Lonza), supplemented with EGM SingleQuots (Lonza) and 10% fetal calf serum (FCS; Invitrogen (San Diego, CA)). HeLa cells were cultured in DMEM with 10% FCS, D-Glucose, Pyruvate, Penicillin/streptomycin and MEM non-essential amino acid mix (Sigma Aldrich); Hek293T cells were cultured in DMEM with 10% heat inactivated FCS (30 min, 55° C), D-Glucose, Pyruvate and 0.1 mg/mL Penicillin/streptomycin. Cells were cultured at 37° C with 5% CO<sub>2</sub>. Cell numbers were determined with a Nucleocounter NC-2000 (Chemometec A/S). HUVECs were stimulated with 100 ng/mL IL-6 (Peprotech) and sIL-6R $\alpha$  (Peprotech) each in EBM for 10 min (for pSTAT3 Y705 western blots) or 4 h before cell lysates were prepared. 20  $\mu$ M Cryptotanshinone (CPT; Sigma Aldrich) in DMSO was added to cell culture medium 1 h prior to addition of IL-6 and sIL-6R $\alpha$ . Equal volumes of DMSO were used as controls for CPT experiments. For seeding and splitting, cells were washed with 1x PBS and incubated with 1x trypsin-EDTA (Gibco) for 3-7 min at 37° C, 5% CO<sub>2</sub>. The reaction was stopped with full medium. HUVECs were splitted 1:6 for passaging and cell numbers for different cell culture dishes are listed in table 1.

**Table 20: List of cell numbers plated in different cell culture dishes**

Strain	HUVECs	hCoAECs	HeLa
T25	3.5x10 <sup>5</sup>	3.5x10 <sup>5</sup>	2x10 <sup>5</sup>
6 cm	3.5x10 <sup>5</sup>	3.5x10 <sup>5</sup>	2x10 <sup>5</sup>
6-well	1.8x10 <sup>5</sup>	1.8x10 <sup>5</sup>	
12-well	8x10 <sup>4</sup>	8x10 <sup>4</sup>	
24-well	3.6x10 <sup>4</sup>	3.6x10 <sup>4</sup>	
96-well	9x10 <sup>3</sup>	9x10 <sup>3</sup>	

#### Shear stress

10<sup>5</sup> HUVECs were seeded to  $\mu$ -slides 0.4 I Luer (Ibidi) 24 h before the start of the experiment. Slides were connected to Ibidi's pump system and constant unidirectional shear stress of 20 dyn/cm<sup>2</sup> was applied for defined durations. Cells seeded in 6-well dishes served as static controls (7.9\*10<sup>4</sup> cells per well, same density as in  $\mu$ -slide). All cells were incubated at 37° C with 5% CO<sub>2</sub>.

### **Transfection of oligonucleotides to adherent cells**

Cultured cells were transfected at 60-70% confluence with 50 nM LNA GapmeRs (Exiqon) or 66.6 nM siRNAs (Qiagen, Hilden, Germany) using Lipofectamine RNAiMax (Life Technologies) according to the manufacturer's protocol in serum reduced OptiMEM medium (Life Technologies). A siRNA against firefly luciferase (Sigma Aldrich, St. Louis, MO, USA) and a negative control LNA GapmeR (Exiqon) were used in the same concentrations. The medium was changed after 4 hours of transfection to full growth medium. Sequences of the used GapmeRs and siRNAs can be found in Table 18 and Table 19.

### **Lentivirus production and transduction**

Lentiviral particles were generated as previously described<sup>253</sup>. Briefly, Hek293T cells were transfected at 70% confluency with lentivirus plasmids (pGK-Mock, pGK-KLF2, pLenti-Mock or pLenti-H19), packaging plasmids pMD2.G and pCMVΔR8.91 with gene juice transfection reagent (Millipore). 1876 μL OptiMEM were mixed with 47 μL GeneJuice and incubated for 10 min at room temperature. 8 μg overexpression vector together with 2 μg pMD2.G and 6 μg pCMVΔR8.91 in 100 μL OptiMEM were mixed with the OptiMEM-GeneJuice mix and incubated for 20 min at room temperature. The transfection mix was then added to Hek293T cells in 25 mL full growth medium. Cells were transferred to S2 lab and medium was changed after 24 h. 48 h and 72 h after transfection, the medium was collected and virus particles were concentrated by filter centrifugation. Efficiency was tested for each new virus batch.  $3 \times 10^5$  HUVECs were transduced in T25 flasks for 24 h. After virus incubation, cells were washed 3x with PBS and 3x with medium in an alternating order. After 48 h washing was repeated, cells were classified as S1 safety level and passaged for experiments. Overexpression efficiency of target RNA was analyzed with qRT-PCR at least 7 days after transduction.

### **Shear stress**

$10^5$  HUVECs were seeded in μ-slides I<sup>0.4</sup> (Ibidi, Munich, Germany) and exposed to laminar flow 4-24 h after seeding at shear stress of 20 dyn/cm<sup>2</sup> for 24, 48 or 72 h controlled by an Ibidi perfusion system.  $8 \times 10^4$  HUVECs seeded per well of a 24-well dishes were used as static controls.

### **Mouse lung EC isolation**

Mice were sacrificed and the circulation was flushed with HBSS with Ca<sup>2+</sup>/Mg<sup>2+</sup>. Lungs were harvested and stored in HBSS with Ca<sup>2+</sup>/Mg<sup>2+</sup>. Lungs were minced with scalpels, collected in 40 mL HBSS with Ca<sup>2+</sup>/Mg<sup>2+</sup> and filtered through a 40 μm mesh cell sieve. Tissue was transferred to a tube containing 5 mL dispase solution (Dispase II (Roche) 4 U/mL in Ham's F12). Tissue was incubated in

Dispase for 45 min under shaking. Tissue was further homogenized by pipetting the solution up and down using a 1 mL pipette approximately 50 times before incubation for another 30 min at 37° C under shaking. Homogenized tissue was then filtered through a 70 µm mesh cell sieve into 5 mL Ham's F12 +10% FCS and the sieve was rinsed with another 5 mL Ham's F12 +10% FCS. Cells were centrifuged at 290 x g for 5 min at room temperature and resuspended in 6 mL Ham's F12 +10% FCS. After another centrifugation step, the pellet was resuspended in 1 mL Ham's F12 +10% FCS. 5 µL Dynabeads M450 (Dyna 110.07) per lung were washed with HBSS +0.5% BSA three times and incubated with either rat anti-mouse podoplanin (MBL D190-3, 0.45 µL per lung) or rat anti-mouse CD144 (Pharmingen 555289; 0.9 µL per lung) for 1 h under rotation at room temperature. Beads were washed three times with HBSS +0.5% BSA and anti-podoplanin coated beads were resuspended in Ham's F12 and anti-CD144 coated beads were resuspended in HBSS +0.5% BSA. Cells were centrifuged at 290 x g for 5 min and the pellet was resuspended in anti-podoplanin coated Dynabeads and incubated for 30 min under rotation at room temperature. Beads were washed 3 times with 1 mL Ham's F12 +10% FCS and the supernatant was collected and centrifuged at 290 x g for 5 min. The pellet was resuspended in the CD144-coated Dynabeads and incubated for 40 min under rotation at room temperature. The beads were washed two times with HBSS +0.5% BSA and resuspended in D-MEM/F12 +20% FCS + ECGS-H (Promocell, 8 µL/mL for P0 and P1, 4 µL/mL for further passages) and seeded to fibronectin coated 24-well plates. After the first or second passage, the culture was purified again. CD144 coated Dynabeads were prepared as described above and cells were washed twice with HBSS +0.5% BSA. Beads were resuspended in HBSS +0.5% BSA and cells were incubated with beads for 1 h at room temperature. Supernatant was removed and cells were washed twice with HBSS +0.5% BSA. Trypsin was added to cells, the reaction was stopped with PBS and cells were centrifuged for 5 min at 290 x g. Cells were resuspended in PBS, washed three times with PBS in a magnetic rack and resuspended in culture medium and seeded to fibronectin coated culture dishes. For direct RNA isolation, all previous washing steps were performed in HBSS and cells were resuspended in Trizol instead of culture medium.

### **3.2.2 *In vitro* assays**

#### **Proliferation Assay**

Cell proliferation was analyzed using the BrdU Flow Kit (BD Pharmingen). Cells were incubated with 10 mM BrdU for 45 minutes, were harvested by trypsinization and washed once with PBS. Fixation and permeabilization was done by incubating the cells with 100 µL Cytofix/Cytoperm buffer for 30 min at room temperature, followed by incubation with 100 µL Cytoperm Plus buffer for 10 min on ice and 5 min with 100 µL Cytofix/Cytoperm on ice. Cells were then incubated in 100 µL DNase working

solution for 1 h at 37° C followed by antibody staining with either V450-anti-BrdU or FITC-anti-BrdU in 50 µL PermWash buffer. Nuclei were stained with 20 µL 7-AAD solution for 20 min at room temperature. Cells were then transferred to FACS tubes, 300 µL PBS was added and BrdU incorporation and DNA content was analyzed using a FACS Canto II device (BD Bioscience). Cells that were not incubated with BrdU served as negative controls and to adjust laser power. Cells were washed with 1 mL PermWash buffer between all steps.

### **Senescence associated $\beta$ -Galactosidase Staining**

Senescence associated  $\beta$ -Galactosidase activity at pH6.0 was analyzed with the Senescence Associated  $\beta$ -Galactosidase Staining kit (Cell Signaling Technologies #9860). Cells were seeded in 6-well or 12-well plates and transfected 48 h prior to the assay. Fixation was done for 15 min at room temperature in 1x fixative solution (20% formaldehyde, 2% glutaraldehyde in PBS). Staining solution with the chromogenic substrate 5-bromo-4-chloro-3-indolyl- $\beta$ -D-galactopyranoside (X-Gal) was prepared and pH was adjusted to pH6.0 with hydrochloric acid. Staining was done overnight at 37° without CO<sub>2</sub> in a dry incubator. Images were taken with 5x magnification with a Zeiss Axiovert 100 and the number of total cells, as well as the number of stained cells was determined in 5 images per condition and experiment.

### **Adhesion Assay**

HUVECs were transfected and  $3 \times 10^4$  cells were seeded per well in a 96-well plate coated with 2% gelatin one day prior to the start of the assay. Monocytes were isolated from human buffy coats. Approximately 5 mL buffy coat were mixed with 25 mL PBS and this mix was layered over 10 mL Ficoll and centrifuged at  $800 \times g$  for 20 min at 4° C without brake. The monocyte phase was washed two times with PBS, resuspended in PBS and counted.  $8 \times 10^6$  monocytes were stained with 3 µL BCECF for 15 min at 37° C and washed with PBS.  $6 \times 10^4$  monocytes were added to HUVECs per well and cells were incubated for 30 min at 37° C. Wells were washed 7 times with 100 µL PBS and fluorescence was measured before washing and after every washing step.

### **Scratch wound migration assay**

Cells were transfected and seeded 24 h later to 24-well plates with Ibidi 2-well culture insert.  $7 \times 10^4$  cells were seeded per well of the culture insert and  $3 \times 10^5$  cells were seeded per 24-well. 48 h after transfection the 2-well culture insert was removed and gap closure was measured. 10 images were taken per well and gap size was measured at three positions per well immediately after removal of the 2-well culture insert, 3 h, 5 h and 8 h later. Initial gap size was defined as 100% and subsequent

measurements were normalized to initial gap size and displayed as 100% - (percentage of initial gap size).

### **Flow Cytometry**

HUVECs were transfected, detached with 1 mM EDTA solution (pH7.4) for 20 min at 37° C and blocked with 1% BSA for 5 min at room temperature. Cells were incubated with respective antibodies for 30 min at 4° C, washed with PBS, fixed with 4% paraformaldehyde and subjected to flow cytometry analysis.

## **3.2.3 Molecular Biology**

### **RNA purification**

Cells grown in cell culture plastic ware were washed 1x with PBS and lysed with Qiazol Reagent (Qiagen, Hilden, Germany) for 5 min at room temperature. Organs were homogenized in Trizol reagent with ceramic beads (MP Biomedicals) 2x 20 s at 20 m/s and centrifuged for 5 min at 1000 x g. RNA was then isolated from Trizol suspension using either Qiagen miRNeasy kit with DNase digest or Zymo DirectZol RNA purification kit (with DNase digest). RNA was eluted in 30 µL ddH<sub>2</sub>O and RNA concentration was measured with Nanodrop Spectrophotometer (Thermo Fisher).

### **RNA purification with phenol/chloroform/isoamylalcohol**

Cells were lysed with different methods. Equal volumes of phenol/chloroform/isoamylalcohol were added to the cell lysate and mixed by vortexing. Samples were centrifuged for 10 min at maximum speed and the aqueous phase of the solution was transferred to a new reaction tube. 2.5 volumes of 100% ethanol were added and the samples were incubated at -20° C over night. Samples were then centrifuged for 15 min at maximum speed at 4° C and 1 mL 70% ethanol was added to the pellet. Samples were again centrifuged for 15 min at maximum speed at 4° C and pellets were resuspended in 30 µL ddH<sub>2</sub>O. RNA concentration was measured with Nanodrop Spectrophotometer (Thermo Fisher).

### **Reverse Transcription of long RNAs**

Up to 1 µg RNA was reverse transcribed with 50 U Multiscribe or M-MLV (both ThermoFisher) reverse transcriptase in the presence of 1x PCR Buffer (ThermoFisher), 5 mM MgCl<sub>2</sub> (ThermoFisher), 1 mM of each dNTP (ThermoFisher) and 400 ng random hexamer primers (ThermoFisher). RNase



activity was inhibited with 10 U RNase inhibitor (ThermoFisher) per reaction. The reaction was done under following conditions

**Table 21: Thermocycler-program for reverse transcription of long RNAs**

Step	Temperature [°C]	Time
1	20	10 min
2	43	75 min
3	95	5 min
4	10	∞

### Reverse Transcription of miRNAs

Taqman assays specific for each miRNA were used according to the manufacturer's protocol (Life Technologies).

**Table 22: Reagents for reverse transcription of miRNAs**

Reagent	Amount
RT Primer	3 µL
dNTPs 100 mM	0.15 µL
Multiscribe Reverse Transcriptase	50 Units
RNase Inhibitor	0.19 µL
PCR Buffer	1.5 µL
RNA (2 ng/µL)	5 µL
H <sub>2</sub> O	<i>ad</i> 15 µL

**Table 23: Thermocycler-program for reverse transcription of miRNAs. Steps 2 and 3 were repeated 40 times.**

Step	Temperature [°C]	Time
1	16	30 min
2	42	30 min
3	85	5 min
4	10	∞

### Detection of long RNA expression

Analysis of expression of long RNAs was done by qRT-PCR with Fast SYBR Green Master Mix (Applied Biosystems) in Applied Biosystems StepOne Plus or Viia7 devices. Ribosomal protein, large, P0 (RPLP0) or glyceraldehyde-3-phosphate dehydrogenase (GAPDH) were used for normalization. Gene expression analysis was done using the  $2^{-\Delta CT}$  method.

**Table 24: Reagents for qRT-PCR Analysis of long RNA expression.**

Reagent	Amount in 96-well plate	Amount in 384-well plate
2x SYBR Green Fast Master Mix	10 µL	5 µL
Primer fw	500 nM	500 nM
Primer rv	500 nM	500 nM

cDNA	12.5 ng	6.25 ng
H <sub>2</sub> O	<i>ad</i> 20 µL	<i>ad</i> 10 µL

**Table 25: Thermocycler program for expression level detection of long RNAs. Steps 2 and 3 were repeated 40 times. Melt curves were analyzed in steps 4 and 5 and temperature was increased 0.3° C per cycle in step 5.**

Step	Temperature [°C]	Time
1	95	20 s
2	95	3 s
3	60	30 s
4	95	15 s
5	60-95	15 s

### Detection of miRNA expression

The levels of miRNAs were detected using miRNA specific TaqMan Assay (ThermoFisher)

**Table 26: Reagents for qRT-PCR with TaqMan reagents**

Reagent	Amount
Primer (20x)	1 µL
TaqMan Fast Master Mix	10 µL
Product from reverse transcription reaction	3 µL
H <sub>2</sub> O	<i>ad</i> 20 µL

**Table 27: Thermocycler program for qRT-PCR for TaqMan Assays. Steps 2 & 3 were repeated 40 times.**

Step	Temperature [°C]	Time
1	95	20 s
2	95	1 s
3	60	20 s

### Protein Extraction

Cells were lysed with 150 µL RIPA lysis buffer (Sigma Aldrich) supplemented with proteinase and phosphatase inhibitors for 15 min on ice. Lysates were cleared by centrifugation for 10 min at 10.000 *x g* and 4° C. Protein content was analyzed with Pierce BCA Protein Assay kit (Thermo Scientific) or Bradford assay.

### Western Blot analysis

Equal amounts of protein were loaded on SDS gels, run at 100 V constant and blotted on nitrocellulose membranes with 0.45 or 0.22 µm pores. Blotting was done using semi-dry method with 100 V for 3-7 min, depending on protein size. Tubulin  $\alpha$  was used as loading controls.

## **Microarrays**

Microarray analysis of HUVEC total RNA was performed on the human GeneChip Gene 2.0 ST platform (Affymetrix, Santa Clara, CA), as previously described<sup>160</sup>. The Database for Annotation, Visualization and Integrated Discovery (DAVID) bioinformatics resources were utilized for pathway analysis of gene ontology terms<sup>254,255</sup>.

## **RNA Immunoprecipitation**

HUVECs were crosslinked with 50 mJ/cm<sup>2</sup> UV light and lysed with total lysis buffer (50 mmol/l Tris-HCl pH8, 150 mmol/l NaCl, 0.5% NP-40 and protease inhibitors). The lysates were cleared by centrifugation at 10,000 x *g* and incubated with protein G magnetic beads (Life Technologies) coated with antibodies listed in Table 15 for 4 h @ 4° C and then washed with lysis buffer with 0.05% NP40. RNA was recovered after protein digestion with Proteinase K and nucleic acids isolated by phenol/chloroform/isoamyl extraction and analyzed by qRT-PCR.

## **ELISA**

The expression of human IL-6 was determined with human IL-6 ELISA kit (Invitrogen) according to the manufacturer's instructions. HUVECs were lysed with RIPA buffer and the protein content was analyzed with Pierce BCA Protein Assay kit (Thermo Scientific). 10 µg total protein was used per sample for the ELISA and signals were analyzed with a Promega GloMax Multi+ device.

## **Transcription factor activity Assay**

To analyze transcription factor activity upon knockdown or overexpression of a gene, the Cignal 45-Pathway reporter array (Qiagen) was used. 2x10<sup>6</sup> HeLa cells were seeded to 15 cm dishes and transfected after 24 h with si Ctrl or siH19. Same amount of H19 overexpressing and mock transduced HeLa cells were seeded to 15 cm dishes. 48 h after seeding cells were reverse transfected with the respective plasmids. 50 µL OptiMEM was added to each well of the 96-well Cignal Reporter Plate and incubated at room temperature for 5 min. 6 mL OptiMEM were mixed with 240 µL Lipofectamin 2000 and incubated for 5 min at room temperature. 50 µL of the OptiMEM/Lipofectamin mix were added to each well of the Cignal Reporter Plate and incubated for 20 min at room temperature. Cells were trypsinized and the reaction was stopped with OptiMEM +10% FCS. 2.07x10<sup>6</sup> cells were resuspended in 6 mL OptiMEM and 50 µL of the cell suspension was added per well, which resulted in a cell number of 1.725x10<sup>4</sup> per well. 100 µL full growth medium without Penicillin/streptomycin was added after 4 h. The medium was changed to full growth medium 24 h after reverse transfection. Dual Luciferase Reporter Assay (Promega) was used for

luminescence detection. 48 h after reverse transfection cells were washed with PBS and 20  $\mu\text{L}$  1x passive lysis buffer was added per well and incubated for 15 min at room temperature followed by 20 min at  $-80^\circ\text{C}$ . The plate was thawed and luminescence was detected using Promega GloMax Multi+ device. 100  $\mu\text{L}$  LAR II were added per well, firefly luciferase signal was detected, 100  $\mu\text{L}$  Stop & Glo Reagent were added and Renilla luciferase signal was detected. Firefly RLU were divided by Renilla RLU for normalization.

### **3.2.4 Animal Experiments**

#### **Ethics**

All mice experiments were carried out in accordance with the principles of laboratory animal care as well as according to the German national laws. The studies have been approved by the local ethic committee (Regierungspräsidium Darmstadt, Hessen, Animal Application number: FU1050).

#### ***Ex vivo* aortic ring assay**

Aortic rings were prepared as previously described<sup>256</sup>. Mice were sacrificed, the circulatory system was flushed with HBSS + $\text{Mg}^{2+}/\text{Ca}^{2+}$ , aortae were harvested and cut in approximately 1 mm long rings in HBSS+ $\text{Mg}^{2+}/\text{Ca}^{2+}$ . For overexpression, the same lentiviral stocks and concentrations as for cultured cells were used. Transduction was done for 24 h in OptiMEM (Life Technologies). Depletion of H19 was done with a mouse-specific LNA GapmeR against H19 or GapmeR control A (Exiqon, Vedbaek, Denmark) for 24 h in OptiMEM with Lipofectamine RNAiMax (Life Technologies). Aortic rings were embedded in collagen gel, consisting of 1x medium 199 (Sigma Aldrich) with 4.4 mM  $\text{NaHCO}_3$  and 1 mg/mL Collagen type I. pH of the collagen mix was adjusted with NaOH until the pH indicator of the medium 199 turned red. 50  $\mu\text{L}$  collagen matrix were added to wells of a flat-bottom 96-well plate and one aortic ring was added per well with the luminal axis parallel to the bottom of the well. Polymerization was done for 10-15 min at room temperature followed by 1 h at  $37^\circ\text{C}$  5%  $\text{CO}_2$ . 150  $\mu\text{L}$  DMEM/F12 +2.5% FCS and Penicillin/Streptomycin was added supplemented with 30 ng/mL VEGF. Medium was changed every second day and aortic rings were fixated for 30 min with 4% paraformaldehyde after 7 days. Mosaic pictures were taken with a Zeiss Axiovert microscope with 5x magnification. The cumulative sprout length was determined with Zeiss Axiovision software.

#### **Tamoxifen administration**

Mice were injected intraperitoneally with 2 mg tamoxifen in 100  $\mu\text{L}$  peanut oil seven times during three weeks prior to surgery or experiment.

### **Hind limb ischemia surgery**

The proximal part of the *Arteria femoralis superficialis* was removed surgically under anesthesia with buprenorphine (0.1 mg/kg body weight every 8-12 h for 24 h). Buprenorphin and carprofen were used for subsequent analgesia for 3 days post-surgery and Ampicillin (1 mg/10g body weight) was used for infection prophylaxis. Leg and toe perfusion was analyzed 7, 14 and 21 days post-surgery by laser-doppler velocimetry measurement and the animals were sacrificed 21 days post-surgery. Animal health was monitored daily with animal health score sheets. 10 µm sections of the frozen soleus muscle were used for morphological analysis. For analysis of capillary density, frozen sections were stained with lectin to visualize endothelial cells and laminin for visualization of cell membranes. For analysis of smooth muscle actin covered blood vessels, frozen sections were stained with mouse anti-SMA antibody and wheat germ agglutinin was used to visualize myocyte membranes. CD45<sup>+</sup> cells were visualized using rat anti-CD45 antibody and myocyte membranes were stained using wheat germ agglutinin. Antibodies and reagents are listed in Table 15. Images were taken with a Zeiss Axiovert Microscope and images were analyzed using ImageJ.

### **Blood Pressure analysis**

Blood Pressure and pulse rate were analyzed with a Visitech Systems BP2000 device in the lab of Prof. Ralf Brandes. The measurement was started 14 days after start of tamoxifen administration. 15 consecutive measurements were done per day for 10 days. The last 10 measurements from days 5-10 were used for analysis.

### **3.2.5 Statistics**

Data are expressed as Means ± SEM. GraphPad Prism 5 was used for statistical analysis. Data were tested for Gaussian distribution with Kolmogorov-Smirnov test (with Dallal-Wilkinson-Lilliefors p value) and paired or unpaired student's t-test or Mann-Whitney test was performed when comparing two groups. Analysis of variance (ANOVA) followed by Bonferroni's correction or Kruskal-Wallis test with Dunns correction was performed for multiple comparisons. Outliers within a group were detected with a Grubbs' outlier test and significant outliers (p<0.05) were excluded from the analysis. Statistical significance was depicted as follows: \*p<0.05, \*\*p<0.01, \*\*\*p<0.001, n.s. = not significant.

## 4. Results

### 4.1 H19 is repressed by aging and induced by KLF2

In order to identify lncRNAs that are regulated with age, a microarray of tissues and cells of 2 and 20 months old mice was analyzed<sup>160,257</sup>. H19 was the most profoundly age-dependent downregulated lncRNA in mouse endothelium. The H19 transcript was downregulated with ageing in endothelial cells isolated from lungs and not regulated in whole hearts. In whole aortas, there was a nonsignificant trend towards a downregulation of H19 with age, while it was not expressed in bone marrow mononuclear cells (Figure 14A). In a second cohort of mice of the same age, whose tissues were analyzed by qRT-PCR, H19 was again not regulated in whole hearts. To determine which cells of the aorta are responsible for the decrease of H19 levels, aortas were dissected into aortic media/adventitia and aortic intima. In aortic intima, H19 was significantly repressed with aging, while in aortic media/adventitia, H19 was not regulated (Figure 14B).

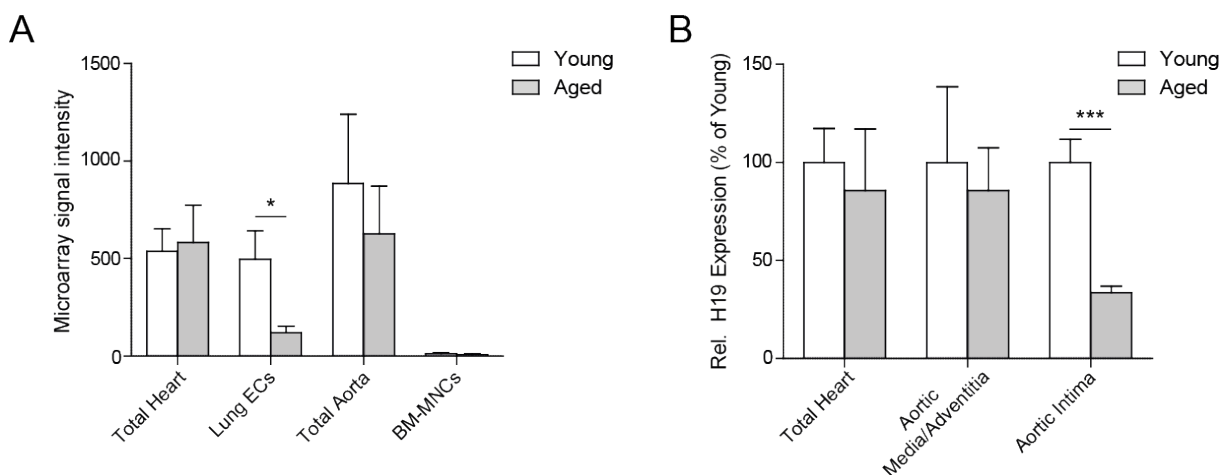


**Figure 14: H19 was downregulated with aging in endothelial cells from different vascular beds *in vivo*.** A: RNA from indicated tissues from 2 and 20 months old mice was isolated and H19 expression was analyzed in a microarray analysis. B: RNA from indicated tissues was isolated from 2 and 20 months old mice (not identical cohort to A). H19 expression was analyzed with qRT-PCR. Statistical significance was depicted as follows: \* $p < 0.05$ , \*\*\* $p < 0.001$ ,  $n \geq 3$ .

H19 is highly expressed in embryos, but in general poorly expressed in most tissues after birth, except for placenta, skeletal muscle, and heart<sup>190</sup>. To gain insight into the aging-dependent regulation of H19, the promoter region of human H19 was analyzed for transcription factor binding sites that are conserved between humans and mice using rVista software<sup>258</sup>. Several evolutionary conserved transcription factor binding sites were identified within 1000 base pairs upstream of the H19 transcription start site (Figure 15A). The binding sites for the Krüppel-like-factor (KLF) transcription factor family were of special interest, as KLF2 is known to play an atheroprotective role

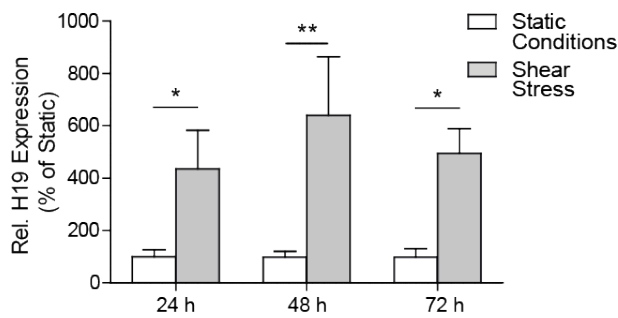
in endothelial cells <sup>12</sup>. To test whether KLF2 regulates H19 expression, the transcription factor was overexpressed in HUVECs using a lentivirus system. Overexpression of KLF2 led to an approximately 8-fold induction of H19 expression compared to mock transduced control HUVECs (Figure 15B).



**Figure 15: The promoter region of H19 harbors numerous conserved binding sites for transcription factors. A: Transcription factor binding sites were identified using rVista software. KLF2 is known to play an atheroprotective role in ECs and KLF binding sites were therefore of special interest. B: KLF2 was overexpressed in WT HUVECs using a lentivirus system and the expression of H19 was analyzed with qRT-PCR at least 7 days after transduction. Statistical significance was depicted as follows: \* $p < 0.05$ ,  $n \geq 3$ .**

Krüppel-like-factor 2 is one of the key transcription factors that are upregulated by laminar shear stress in HUVECs <sup>12</sup>. HUVECs were exposed to laminar shear stress at 20 dyn/cm<sup>2</sup> for 24, 48, and 72 hours and the expression of H19 was analyzed by qRT-PCR. H19 was already upregulated after 24 hours of laminar shear stress and its expression remained constant over 72 hours (Figure 16A). Flow-induced KLF2 upregulates a subset of genes, which protect endothelial cells <sup>12</sup>. To test whether the upregulation of H19 upon shear stress is dependent on KLF2, HUVECs were transduced with short hairpin RNAs (shRNAs) against KLF2 and firefly luciferase as control, and exposed to laminar shear stress for 72 hours. The transduction did not influence the expression of H19 under static conditions and did not influence the upregulation of H19 upon shear stress exposure, but after inhibition of KLF2, the induction of H19 upon shear stress was completely abolished (Figure 16B). Because of the significant upregulation of H19 by KLF2 and the known shear stress mimicking effect of KLF2 *in vitro*, most loss of function experiments hereafter were performed in KLF2 overexpressing HUVECs.

A



B

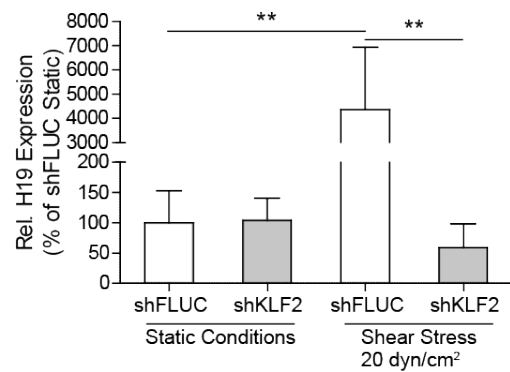


**Figure 16: H19 is upregulated by laminar shear stress and this upregulation is dependent on KLF2.** A: WT HUVECs were exposed to laminar shear stress (20 dyn/cm<sup>2</sup>) for 24 h, 48 h, and 72 h or cultured under static conditions, RNA was isolated and the expression of H19 was analyzed with qRT-PCR. B: HUVECs were transduced with shRNA against KLF2 (shKLF2) or firefly luciferase as control (shFLUC) and exposed to laminar shear stress at 20 dyn/cm<sup>2</sup> or cultured under static conditions for 72 h. RNA was isolated and the expression of H19 was analyzed with qRT-PCR. Statistical significance was depicted as follows: \*p<0.05, \*\*p<0.01, n≥3.

In summary, H19 is repressed with aging *in vivo* and, in the tested tissues, H19 is exclusively repressed in endothelial cells from two different vascular beds. Shear stress induced the expression of H19 in a KLF2 dependent manner.

#### 4.2 H19 can be pharmacologically inhibited with siRNAs and LNA GapmeRs and overexpressed with lentivirus

To study the role of H19 in endothelial cells, pharmacological inhibition strategies were used to deplete H19 *in vitro*. H19 can be silenced by siRNAs and LNA GapmeRs to approximately 37% and 46% compared to controls respectively (Figure 17A&B) and it can be overexpressed using a lentivirus system (Figure 17C).



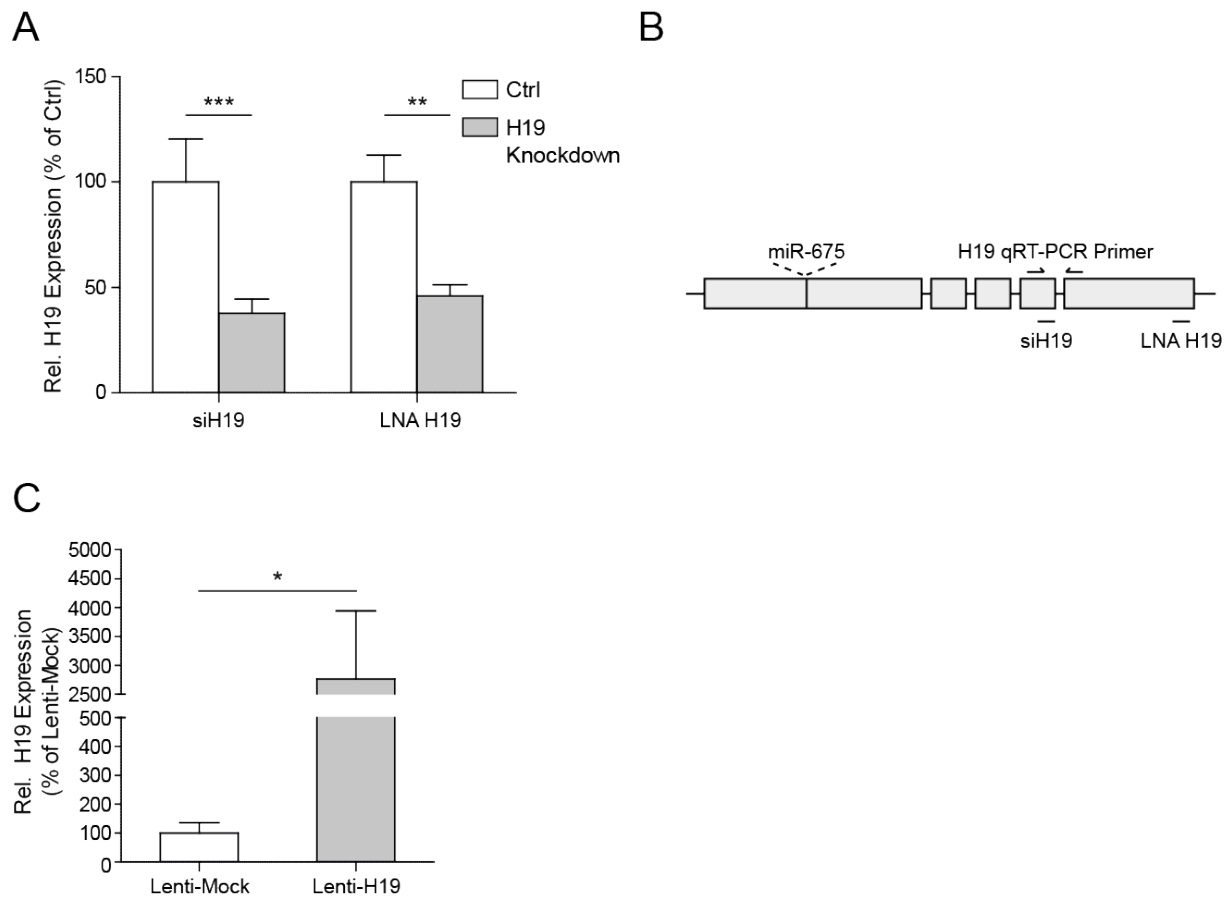


**Figure 17: H19 can be pharmacologically depleted and overexpressed *in vitro*.** A: KLF2 overexpressing HUVECs were transfected with siRNA directed against H19 or firefly luciferase as control (66.6 nM) or with LNA GapmeRs directed against H19 or control sequence (50 nM). RNA was isolated 48 h after transfection and H19 expression was analyzed with qRT-PCR. B: Graphical representation of H19 gene with binding sites for siRNA and LNA GapmeRs as well as localization of the primers for qRT-PCR and localization of miR-675. C: Lentivirus particles were generated with human H19 sequence (ENST00000412788.5). WT HUVECs were transfected with H19 carrying lentivirus or mock virus. RNA was isolated at least 7 days after transduction and H19 expression was analyzed with qRT-PCR. Statistical significance was depicted as follows: \* $p < 0.05$ , \*\* $p < 0.01$ , \*\*\* $p < 0.001$ ,  $n \geq 3$ .

### 4.3 H19 does not function *via* known mechanisms in endothelial cells

LncRNAs were shown to mediate histone modifications before<sup>259</sup>. To determine whether H19 regulates endothelial function *via* histone interactions, the subcellular localization of H19 was first assessed, alongside with the nuclear lncRNA MALAT-1 and ribosomal protein large subunit P0 (P0) mRNA, by separating HUVEC nuclei and cytoplasm and subsequent qRT-PCR. H19 was predominantly located in the cytoplasm of HUVECs, comparable to the mRNA of P0 and in contrast to the known nuclear lncRNA MALAT-1<sup>260</sup> (Figure 18A). Physical interaction with histones was tested in RNA immunoprecipitation (RIP) experiments against histone H3, H3K27me3, and H3K9me3. H19 did not bind to any of these histones (Figure 18B).

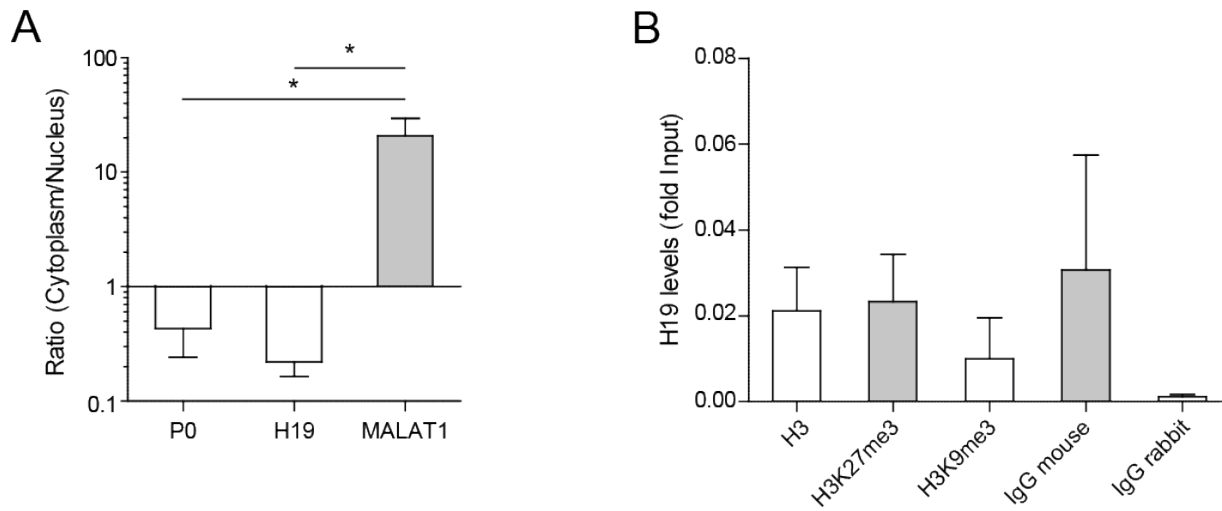
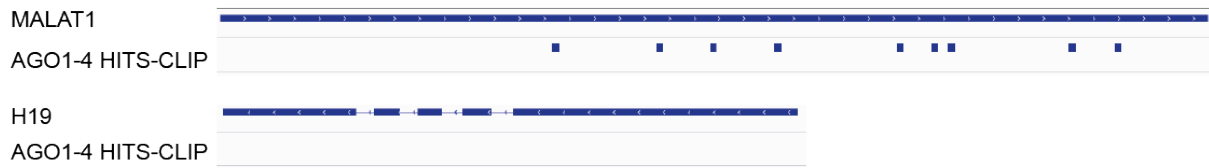


**Figure 18: H19 is predominantly located in the cytoplasm of HUVECs and does not physically interact with histones. A:** Nuclear and cytoplasmic RNA was isolated from KLF2 overexpressing HUVECs and gene expression was analyzed with qPCR. **B:** RNA immunoprecipitation against histone H3 and its trimethylated forms was performed from lysates of WT HUVECs and H19 expression was analyzed with qPCR. The abundance of H19 is depicted as fold input. Statistical significance was depicted as follows: \* $p < 0.05$ ,  $n \geq 3$ .

H19 was previously described to bind miRNAs and act as a sponge<sup>246,247</sup>. Publicly available AGO HITS CLIP data from HUVECs were analyzed for possible miRNA binding sites in the H19 transcript. MALAT1 was used as a control for comparison<sup>150</sup>. MALAT1 showed several binding sites for AGO proteins. In contrast, the H19 transcript did not bind to AGO proteins (Figure 19A). Kallen *et al.* showed that the H19 transcript harbors 4 binding sites for miRNAs of the let-7 family<sup>246</sup>. To test whether H19 binds let-7 miRNAs in ECs, target genes of let-7a were identified using microRNA.org target gene predicting tool<sup>261</sup>. 15 of these genes were analyzed in the microarray data from HUVECs upon H19 depletion. None of the let-7a target genes was significantly regulated upon siRNA mediated H19 depletion, although HMGA2 showed a trend towards reduced mRNA expression and SMARCD1 mRNA showed a trend towards higher expression upon H19 depletion (Figure 19B).

A



B

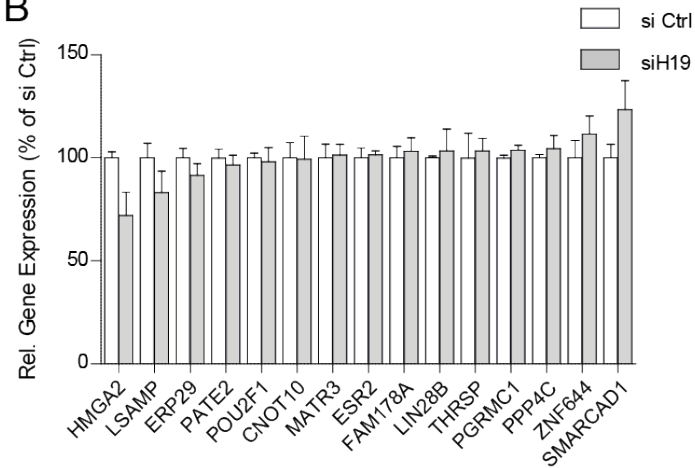


**Figure 19: H19 does not interact with AGO proteins and predicted target genes of let-7a were not regulated.** A: AGO HITS CLIP data from HUVECs were analyzed for binding of AGO proteins to MALAT1 and H19. MALAT1 showed a total of 9 binding sites for AGO proteins, while the H19 transcript did not bind AGO proteins. Screenshot from Integrative Genomics Viewer (IGV, Broad Institute). B: KLF2 overexpressing HUVECs were transfected with siRNA directed against H19 and subjected to microarray analysis 48 h after transfection and 15 predicted let-7a target genes were analyzed.  $n \geq 3$ .

H19 is known to act as a precursor for miR-675<sup>234</sup>. To analyze if this miRNA plays a role in HUVECs, its expression upon KLF2 overexpression, H19 overexpression, and H19 depletion in KLF2 overexpressing HUVECs was analyzed. miR-675-5p showed a nonsignificant trend towards reduced expression upon KLF2 overexpression (Figure 20A). Both, miR-675-3p and -5p were upregulated upon lentiviral H19 overexpression in HUVECs (Figure 20B). Upon siRNA-mediated H19 depletion, miR-675-5p showed a nonsignificant trend towards increased expression (Figure 20C). miRNA-675 target genes were predicted with microrna.org target prediction tool and analyzed in HUVECs upon H19 depletion<sup>261</sup>. FANCA showed a nonsignificant lower expression, while LNPEP, SYDE1, TUBB4, LRIG2, and RNF103 showed a similar nonsignificant increase in expression compared to si Ctrl (Figure 20D).

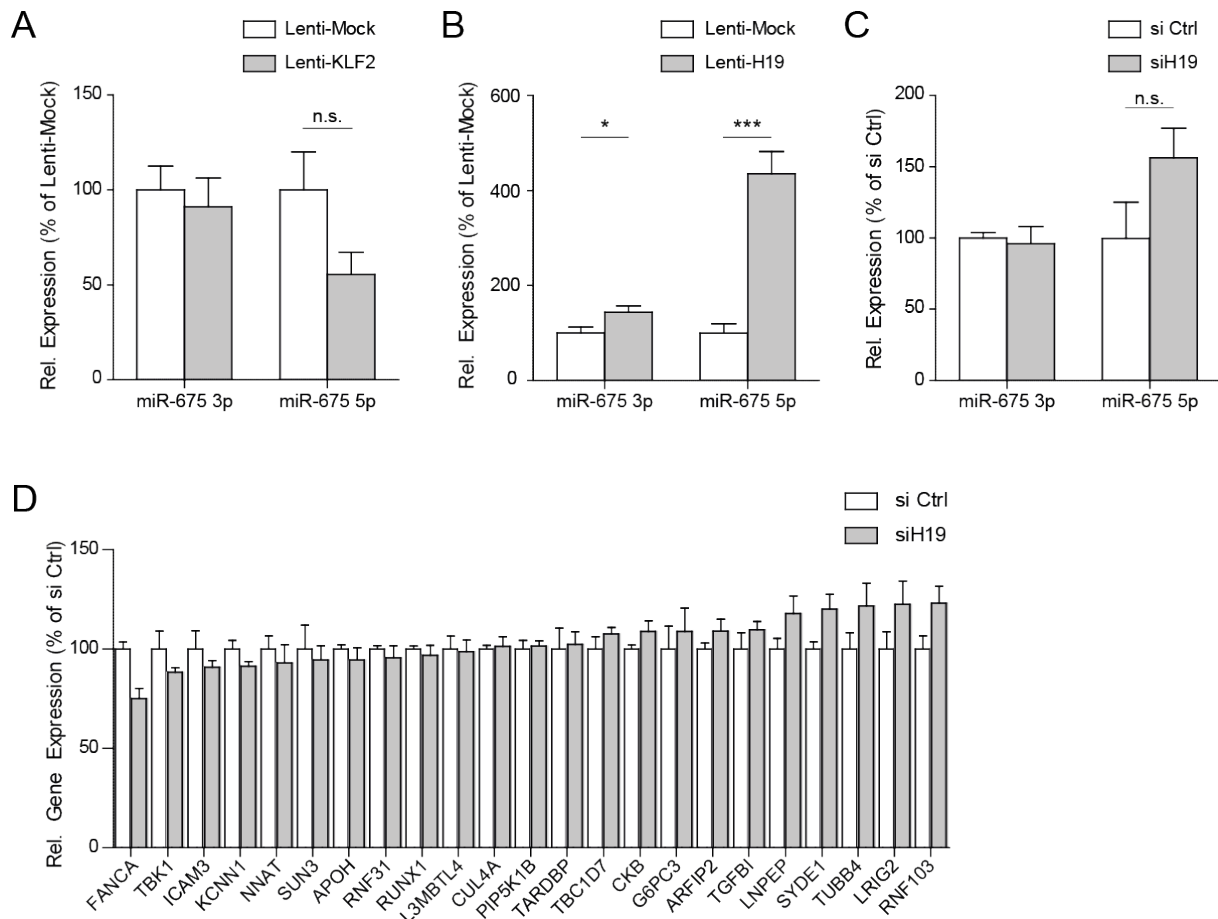


**Figure 20: miR-675 5p was upregulated upon H19 overexpression, while KLF2 overexpression and siRNA-mediated H19 depletion did not change miR-675 levels.** A: WT HUVECs were transduced with lentivirus carrying human KLF2 gene or empty vector and miR-675 expression was analyzed at least 7 days after transduction with qRT-PCR. B: WT HUVECs were transduced with lentivirus carrying H19 gene or empty vector and miR-675 expression was analyzed at least 7 days after transduction with qRT-PCR. C: WT HUVECs were transfected with siRNA directed against H19 or firefly luciferase and miR-675 expression was analyzed with qRT-PCR. D: KLF2 overexpressing HUVECs were transfected with siRNA directed against H19 and subjected to microarray analysis 48 h after transfection. Predicted miR-675 target genes were analyzed. Statistical significance was depicted as follows: \* $p < 0.05$ , \*\*\* $p < 0.001$ , n.s. = not significant,  $n \geq 3$ .

Several lncRNAs were shown to possess a function on their neighboring genes in *cis* and the effect of H19 depletion or overexpression on IGF2 was analyzed in HUVECs. IGF2 was significantly higher expressed in the absence of H19 and showed a trend towards reduced expression upon H19 overexpression (Figure 21A&B). IGF2 was previously described to induce expression of VEGF and to promote tumor angiogenesis<sup>259</sup>. To test whether IGF2 induced upregulation of VEGF upon H19 depletion plays a role in endothelial cells, expression of VEGF mRNA was analyzed upon H19 depletion. VEGF levels were not changed upon H19 depletion in HUVECs (Figure 21C).

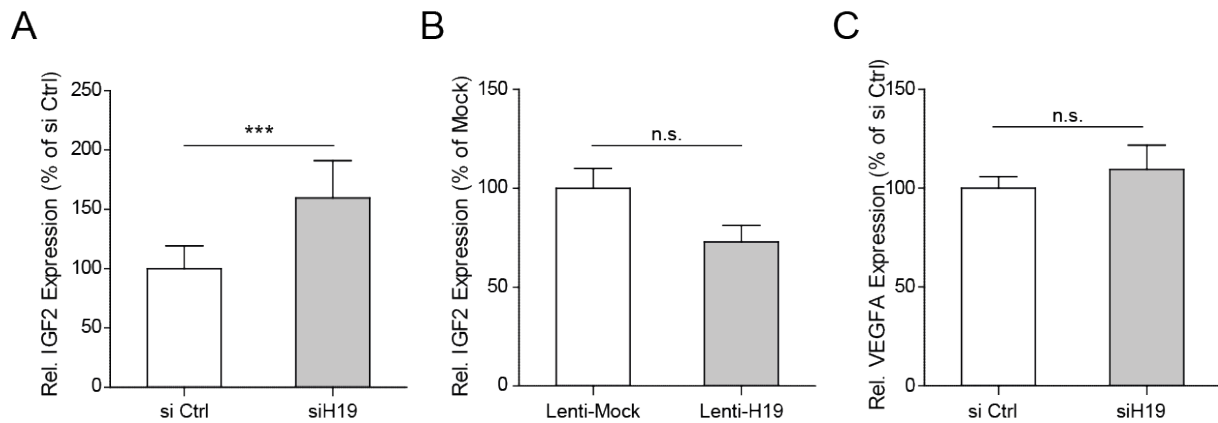


**Figure 21:** Insulin growth factor 2 (IGF2) mRNA was upregulated upon H19 depletion and downregulated upon H19 overexpression, while the IGF2 target VEGFA was not regulated. **A:** KLF2 overexpressing HUVECs were transfected with siRNA directed against H19 or control and IGF2 expression was analyzed by qRT-PCR 48 h after transfection. **B:** WT HUVECs were transduced with lentivirus carrying H19 gene or empty vector and IGF2 expression was analyzed at least 7 days after transfection by qRT-PCR. **C:** KLF2 overexpressing HUVECs were transfected with siRNA directed against H19 and subjected to microarray analysis 48 h after transfection. VEGFA expression was analyzed. Statistical significance was depicted as follows: \*\*\* $p < 0.001$ , n.s. = not significant,  $n \geq 3$ .

Taken together, despite its predominant cytoplasmic localization, H19 can be pharmacologically depleted with siRNAs and LNA GapmeRs. H19 was not bound to histones in HUVECs and its depletion did not change expression levels of target genes of let-7a miRNA, which was shown to be bound by H19. Interestingly, KLF2-mediated H19 upregulation, lentivirus-mediated H19 overexpression, and siRNA-mediated H19 depletion did change levels of the endogenously encoded miRNA miR-675, but this regulation was not consistent. Furthermore, H19 depletion did change levels of its neighboring gene IGF2, but levels of IGF2-regulated gene VEGF were not changed.

#### 4.4 Depletion of H19 delays proliferation and promotes senescence in endothelial cells

To gain more unbiased insights about the function of H19 in ECs, a microarray analysis was performed. H19 was depleted with siRNAs in HUVECs and total RNA was subjected to analysis. 241 genes were up- and 103 genes were downregulated more than 1.5-fold respectively in H19-depleted HUVECs compared to control transfected cells (Figure 22A). The most regulated single genes were analyzed by qRT-PCR in an independent experiment in HUVECs upon siRNA mediated H19 depletion. These genes included the inflammation associated gene lysozyme (LYZ), Hyaluronan Synthase 2 (HAS2), which was shown to be involved in extracellular matrix remodeling and the proliferation marker MKI67 (Figure 22B). Pathway analysis was performed using DAVID bioinformatics resources software and the most regulated pathways upon H19 depletion in HUVECs were identified<sup>254,255</sup> (Figure 22C). Figure 22D shows enrichment plots of the top enriched pathway from Figure 22C and

the additional 2 pathways “G2/M Checkpoint” and “E2F targets”. The core enriched genes of the most enriched pathway Cell Cycle (GO:0007049) are highlighted in black in Figure 22A.

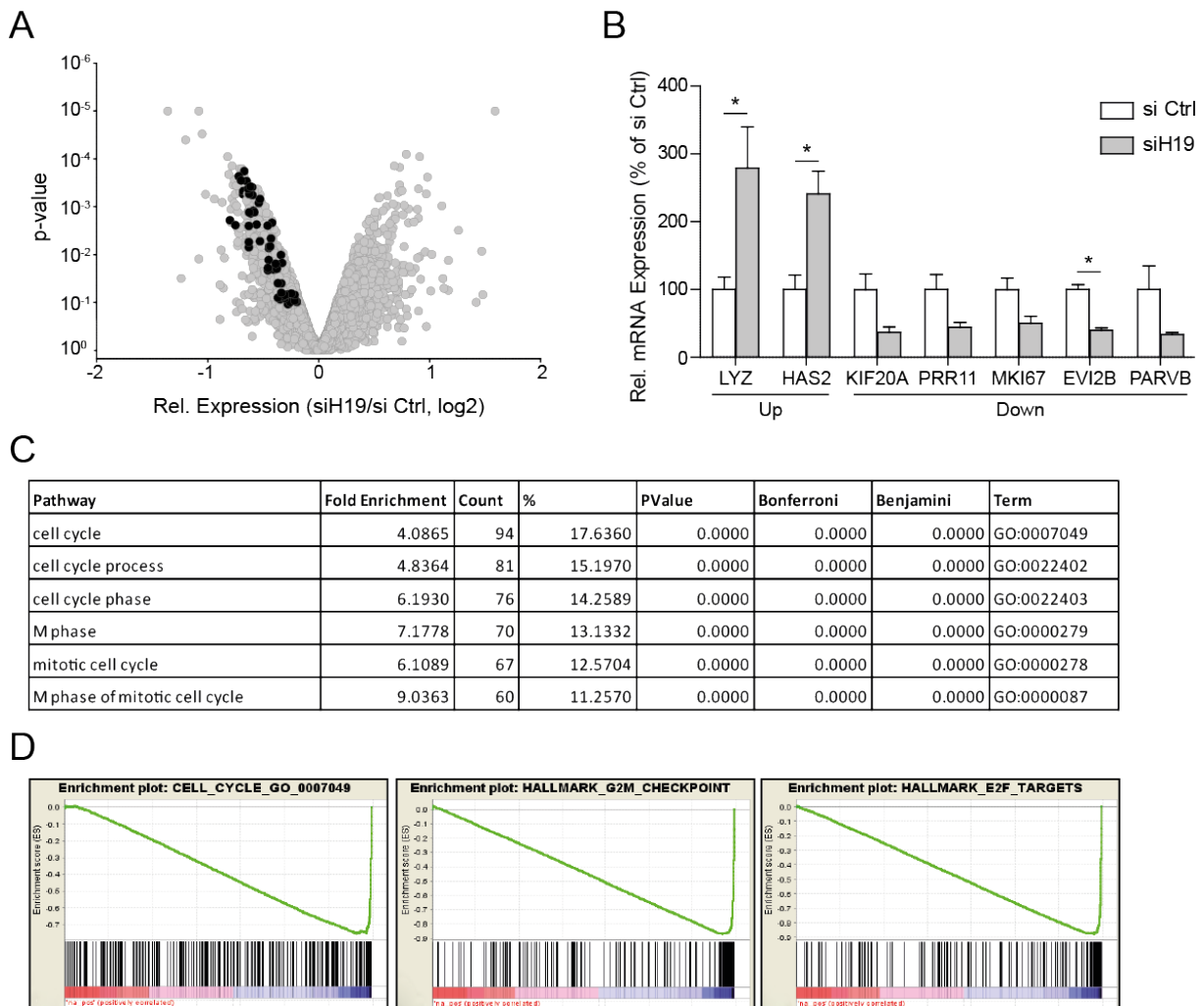


**Figure 22: Microarray analysis in KLF2 overexpressing HUVECs upon H19 depletion followed by gene set enrichment analysis led to the identification of several regulated pathways. A: Volcano Plot showing all genes and p-values in HUVECS 48 h after H19 depletion. Core enriched genes of the pathway Cell Cycle (GO:0007049) are highlighted in black. B: The most regulated genes were confirmed by qRT-PCR in an independent experiment after siRNA-mediated H19 depletion in HUVECs. “Up” and “Down” denotes the regulation of the respective genes in the microarray. C: List of the top 6 regulated pathways in HUVECs upon H19 depletion. The pathways were sorted by the percentage of the core enriched genes. D: Enrichment Plots of Pathways Cell Cycle (GO0007049), G2/M Checkpoint (Hallmark\_G2/M\_Checkpoint) and E2F Targets (Hallmark\_E2F\_Targets). Statistical significance was depicted as follows: \*p<0.05, n≥3.**

To functionally verify the regulation of cell cycle upon H19 depletion in HUVECs, a BrdU proliferation assay was performed, where incorporation of the thymidine analogue bromodesoxyuridine into the genome is analyzed. H19 was depleted with siRNAs in HUVECs or hCoAECs for 48 h or overexpressed for at least 7 days before the start of the assay. Upon depletion of H19, cells accumulate in G0/G1 phase (+17.8% for HUVECs, +7.9% for hCoAECs) and less cells were present in G2/M phase (-22% for

HUVECs) or entered S-phase (-60% for HUVECs, -49% for hCoAECs) (Figure 23A&B). When H19 was overexpressed, no change in cell numbers was detected in the cell cycle phases (Figure 23C).

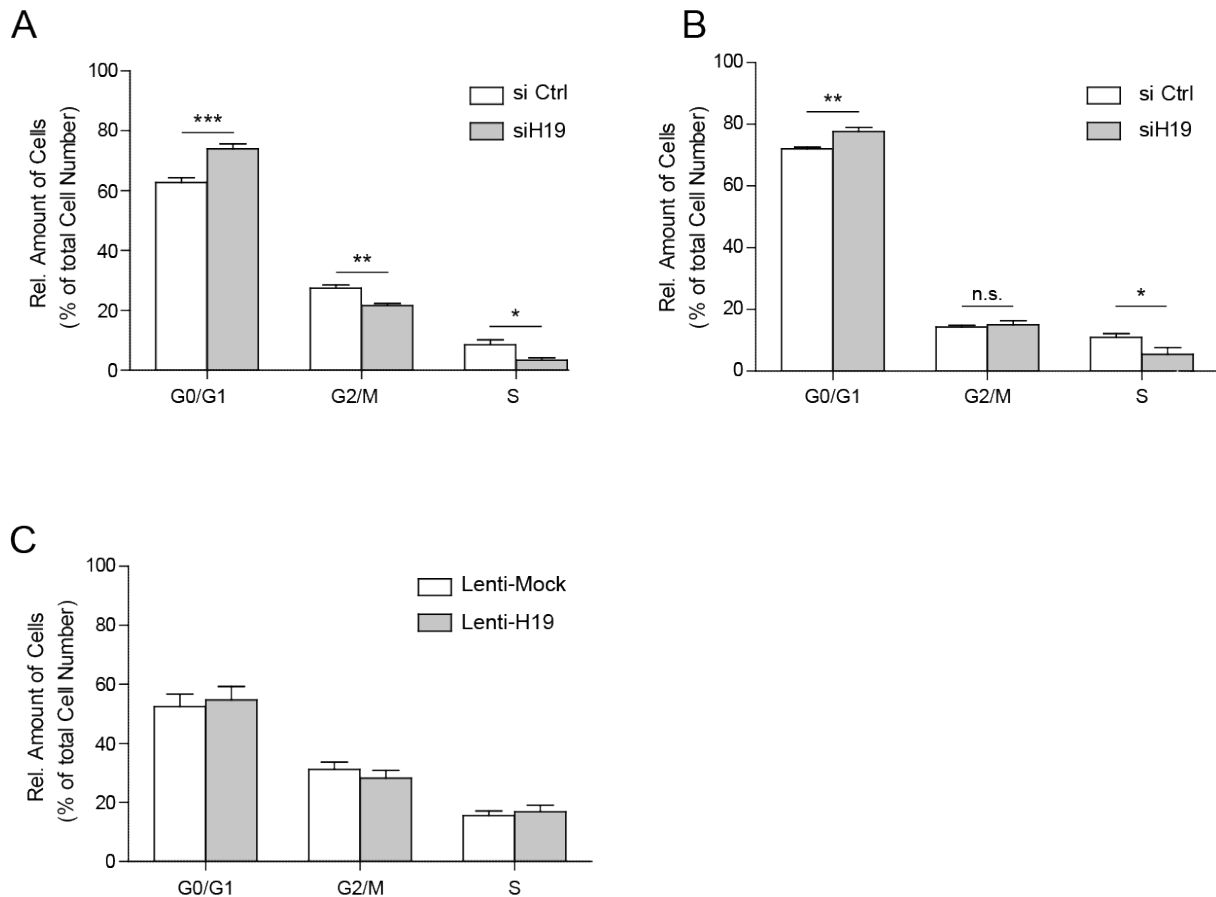


**Figure 23: Depletion of H19 delays proliferation, while overexpression of H19 has no effect in a BrdU assay in HUVECs. A:** KLF2 overexpressing HUVECs were transfected with siRNA directed against H19 or firefly luciferase. 48 h after transfection, BrdU was added to the culture medium and HUVECs proliferated 4 h in the presence of BrdU. Cells were fixed, permeabilized, stained with anti-BrdU antibody and subjected to flow cytometry. **B:** hCoAECs were transfected with siRNA directed against H19 or firefly luciferase. 36 h after transfection, BrdU was added to the culture medium and hCoAECs proliferated 12 h in the presence of BrdU. Cells were fixed, permeabilized, stained with anti-BrdU antibody and subjected to flow cytometry. **C:** WT HUVECs were transduced with lentivirus carrying H19 or mock sequence and incubated with BrdU for 4 h at least 7 days after transduction. Cells were fixed, permeabilized, stained with anti-BrdU antibody and subjected to flow cytometry. Statistical significance was depicted as follows: \* $p < 0.05$ , \*\* $p < 0.01$ , \*\*\* $p < 0.001$ ,  $n \geq 3$ .

H19 was previously described to regulate proliferation *via* regulation of and interaction with numerous proteins. H19 was shown to regulate the expression of CDK4 and Cyclin D1, thereby affecting the phosphorylation of RB1 and it was furthermore shown to interact with macroH2A thereby regulating CDK8<sup>207</sup>. However, none of the genes were regulated upon H19 depletion, and only CDK8 showed a slight nonsignificant upregulation (Figure 24A). Knockdown of H19 was shown to reduce E2F-1 abundance and expression of several E2F-1 target genes<sup>213</sup>. Indeed, depletion of H19 led to a nonsignificant trend towards reduced expression of E2F-1 and its downstream targets, and to a more robust repression of Cyclin A2 expression (Figure 24B). p57 was identified to be repressed upon hypoxia-induced H19 upregulation in different cancers<sup>217</sup>, but pharmacological inhibition had

no effect on p57 levels in HUVECs (Figure 24C). H19 overexpression repressed DUSP5 and its targets ERK1 (MAPK3) and ERK2 (MAPK1), indicating a role of H19 in cardiac fibrosis<sup>233</sup>. Upon H19 depletion, DUSP5 showed a nonsignificant trend towards increased expression in HUVECs, but its targets MAPK1 and MAPK3 were not regulated on mRNA level (Figure 24D). H19 was shown to prevent p53 recruitment to the NOTCH1 promoter, thus reducing NOTCH1 expression<sup>232</sup>. NOTCH1 mRNA expression was not changed upon H19 depletion in HUVECs (Figure 24E). Furthermore, H19 was previously reported to possess a pro-angiogenic function in hepatocellular and bladder carcinoma through regulation of angiogenin<sup>217</sup>. Angiogenin expression was not changed upon H19 depletion in HUVECs (Figure 24F).



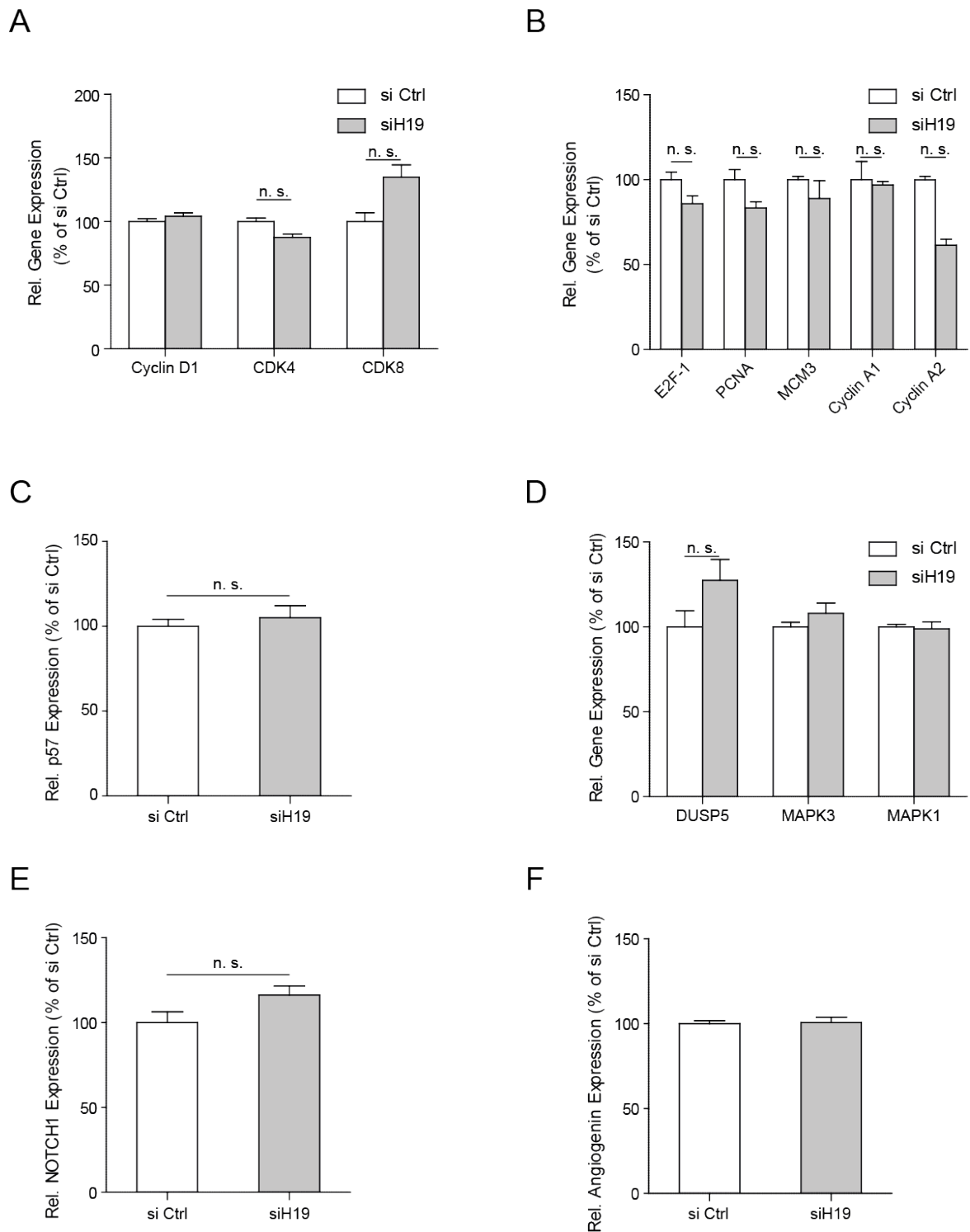


**Figure 24:** H19 was already described to interact with numerous proliferation regulating proteins and most of these interaction partners did not show a significant regulation. **A:** KLF2 overexpressing HUVECs were transfected with siRNA directed against H19 and subjected to microarray analysis 48 h after transfection. Expression of cyclin D1, CDK4, and CDK8 was analyzed. **B:** KLF2 overexpressing HUVECs were transfected with siRNA directed against H19 and subjected to microarray analysis 48 h after transfection. Expression of E2F-1 and its target genes PCNA, MCM3, cyclin A1 and cyclin A2 was analyzed. **C:** KLF2 overexpressing HUVECs were transfected with siRNA directed against H19 and subjected to microarray analysis 48 h after transfection. Expression of p57 was analyzed. **D:** KLF2 overexpressing HUVECs were transfected with siRNA directed against H19 and subjected to microarray analysis 48 h after transfection. Expression of DUSP5 and its downstream effectors ERK1 (MAPK3) and ERK2 (MAPK1) was analyzed. **E:** KLF2 overexpressing HUVECs were transfected with siRNA directed against H19 and subjected to microarray analysis 48 h after transfection. NOTCH1 expression was analyzed. **F:** KLF2 overexpressing HUVECs were transfected with siRNA directed against H19 and subjected to microarray analysis 48 h after transfection. Expression of Angiogenin was analyzed.  $n \geq 3$ .

To further characterize the effect of H19 depletion on endothelial cell function, senescence was analyzed, since the accumulation of cells in G0/G1 phase is an indicator for cellular senescence. Senescent cells have a  $\beta$ -galactosidase activity at pH6.0, which can be used to visualize senescent cells in a population. Upon siRNA-mediated depletion of H19, a higher percentage of HUVECs (Figure 25A), as well as of hCoAECs (Figure 25B) showed a senescence-associated  $\beta$ -galactosidase activity.

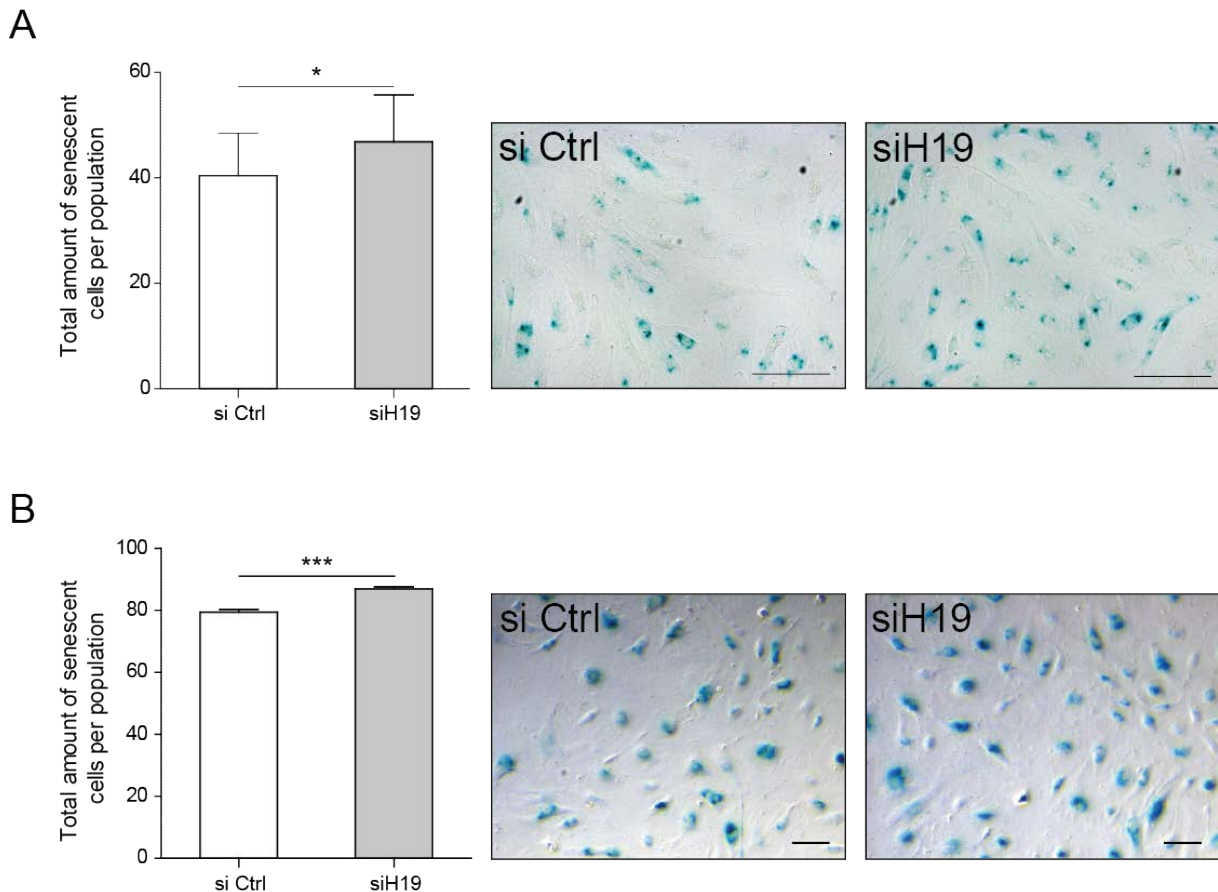


**Figure 25: Depletion of H19 in endothelial cells *in vitro* promotes senescence. A:** KLF2 overexpressing HUVECs were transfected with siRNA directed against H19 or firefly luciferase and senescence associated  $\beta$ -galactosidase activity was analyzed 48 h after transfection. **B:** hCoAECs were transfected with siRNA directed against H19 or firefly luciferase and senescence associated  $\beta$ -galactosidase activity was analyzed 48 h after transfection. The scale bar denotes 100  $\mu$ m. Statistical significance was depicted as follows: \* $p < 0.05$ , \*\*\* $p < 0.001$ ,  $n \geq 3$ .

Senescence is established by two major pathways, the p53/p21 pathway and the p16<sup>ink4A</sup>/pRB pathway. To test whether depletion of H19 influences one of these pathways, the expression of p16<sup>ink4A</sup>, p21, and p53 was analyzed in HUVECs upon siRNA-mediated depletion of H19. The expression of p21 was induced on the mRNA level (Figure 26A), as well as on the protein level (Figure 26B) upon H19 depletion with siRNAs 48 h after transfection. Upon lentiviral H19 overexpression in HUVECs, a trend towards the repression of p21 expression was visible (Figure 26C). p53 was neither regulated upon siRNA-mediated H19 depletion, nor upon lentiviral H19 overexpression (Figure 26A&B). p16<sup>ink4A</sup> expression was induced upon siRNA-mediated depletion of H19 in HUVECs (Figure

26A) and there was a trend towards a repression of p16<sup>ink4A</sup> expression upon lentiviral H19 overexpression (Figure 26C).

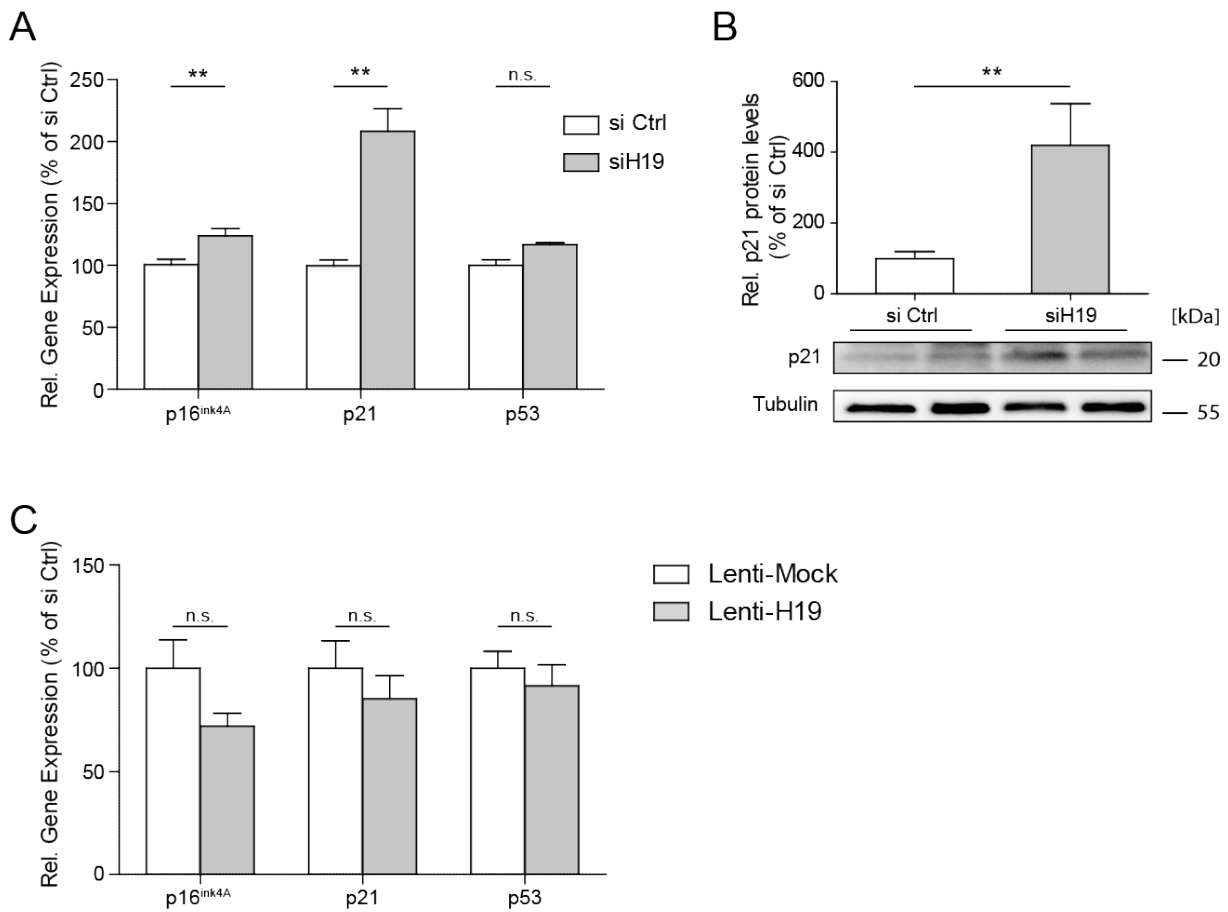


**Figure 26: The expression of p16<sup>ink4A</sup> and p21 was induced upon H19 depletion, while the expression was not changed upon H19 overexpression. P53 was not regulated. A:** KLF2 overexpressing HUVECs were transfected with siRNA directed against H19 or firefly luciferase. 48 h after transfection, expression of p16<sup>ink4A</sup>, p21 and p53 mRNA was analyzed with qRT-PCR. **B:** KLF2 overexpressing HUVECs were transfected with siRNA directed against H19 or firefly luciferase. 48 h after transfection, expression of p21 protein was analyzed by immunoblotting. **C:** WT HUVECs were transduced with lentivirus carrying H19 gene or empty vector. The expression of p16<sup>ink4A</sup>, p21 and p53 mRNA was analyzed at least 7 days after transduction with qRT-PCR. Statistical significance was depicted as follows: \*p<0.05, \*\*p<0.01, n≥3.

In summary, microarray analysis identified an association of H19 depletion with reduced proliferation in HUVECs, which was then confirmed in *in vitro* experiments. H19 was shown to regulate proliferation in different cell types before, but none of the known mechanisms could be confirmed in HUVECs. Loss of H19 also led to more senescence in HUVECs and hCoAECs and cell cycle regulators p16<sup>ink4A</sup> and p21 were identified to be upregulated upon H19 depletion.

## 4.5 H19 does not influence migration *in vitro*

To further verify the effects of H19 on EC function, a scratch wound assay was performed. H19 was depleted in HUVECs and migration was analyzed 48 h after transfection (Figure 27A). siRNA-mediated depletion of H19 did not change migration of HUVECs in a time course experiment (Figure 27B&C).

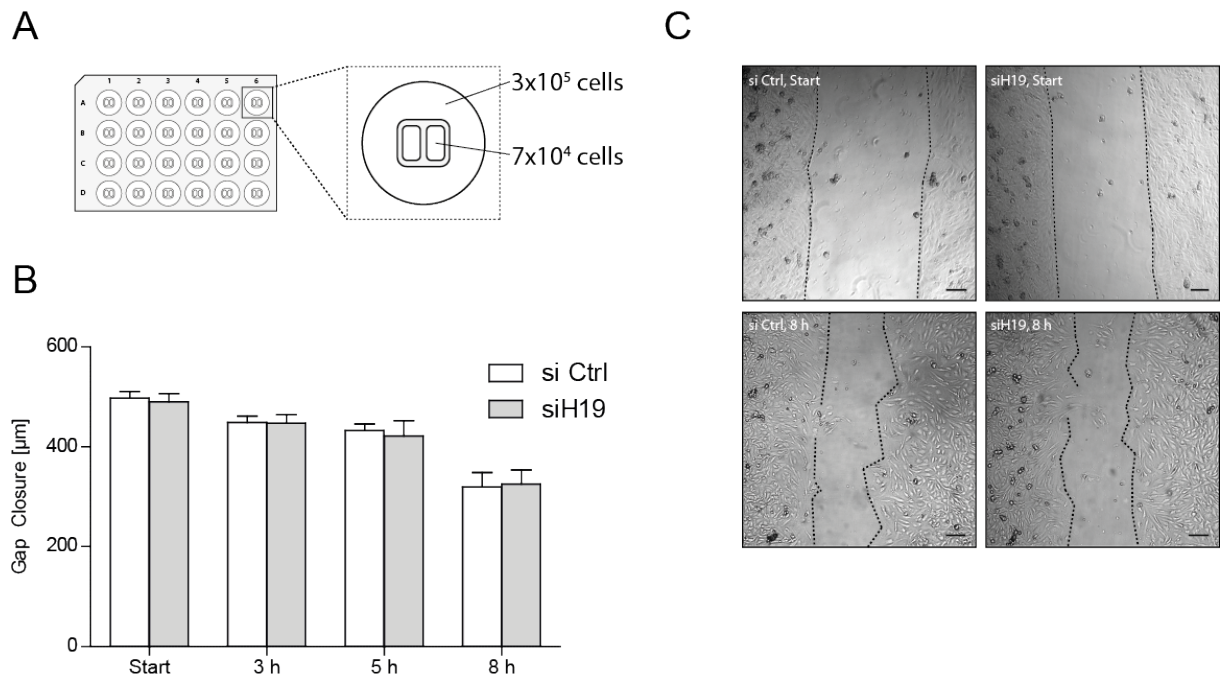


**Figure 27:** siRNA-mediated depletion of H19 did not alter migration of HUVECs. **A:** KLF2 overexpressing HUVECs were transfected with si Ctrl or siH19 and were seeded to 24-well plates with a 2-well silicone insert. **B:** The inserts were removed 24 h after seeding and 48 h after transfection and the gap closure was measured immediately after removal of the insert (Start) and after 3, 5 and 8 h at fixed  $\mu\text{m}$  positions. **C:** Example images immediately after removal of the insert (Start) and after 8 h. The scale bar denotes 100  $\mu\text{m}$ ,  $n \geq 3$ .

In conclusion, the depletion of H19 led to the inhibition of several proliferation-related pathways in HUVECs. miR-675 was not consistently regulated upon H19 depletion and overexpression or KLF2 overexpression and presumably does not play a role in ECs. Furthermore, H19 likely does not act as microRNA sponge in ECs, as it was not associated with AGO proteins. Additionally, target genes of let-7 miRNAs were not regulated upon H19 depletion. Functionally, H19 depletion did not influence migration of HUVECs, but proliferation was delayed upon siRNA-mediated depletion of H19 and a higher percentage of HUVECs entered senescence compared to control transfected cells. The cell cycle regulators p16<sup>ink4A</sup> and p21 were upregulated upon depletion of H19, but not upon overexpression, while p53 was not regulated.

#### **4.6 H19 depletion impairs endothelial cell function *ex vivo* and *in vivo***

Endothelial cells from aged individuals show less angiogenesis *in vitro*<sup>262</sup>. To address the effects of H19 *in vivo* in regard to a functional contribution of H19 to the aged EC phenotype, an *ex vivo* aortic ring assay was performed. Aortic rings were prepared from 2 and 20 months old mice and the sprouting capacity was analyzed. In addition, H19 was depleted in aortic rings of young animals, where H19 baseline expression is high, with mouse-specific LNA GapmeRs. Using a lentivirus system, human H19 was overexpressed in aortic rings of aged animals, where H19 is normally poorly expressed. H19 expression was analyzed in whole aortic rings using qRT-PCR. H19 was repressed with aging and mouse-specific LNA GapmeRs against H19 reduced its abundance in aortic rings of young animals to levels comparable to old animals (Figure 28A). Overexpression of human H19 in aortic rings of aged animals was successful (Figure 28B). As expected, the cumulative sprout length of aortic rings from aged mice was reduced compared to young mice by approximately one third. In line with the reduction of H19 abundance upon LNA GapmeR treatment in aortic rings from young mice is a reduction of cumulative sprout length by approximately one third, which is comparable to the reduction observed between young and aged animals. Overexpression of human H19 in aortic rings from aged mice rescued the impaired sprouting phenotype of aged animals partially and restored cumulative sprout length to levels comparable to sprout lengths of young animals (Figure 28C&D).

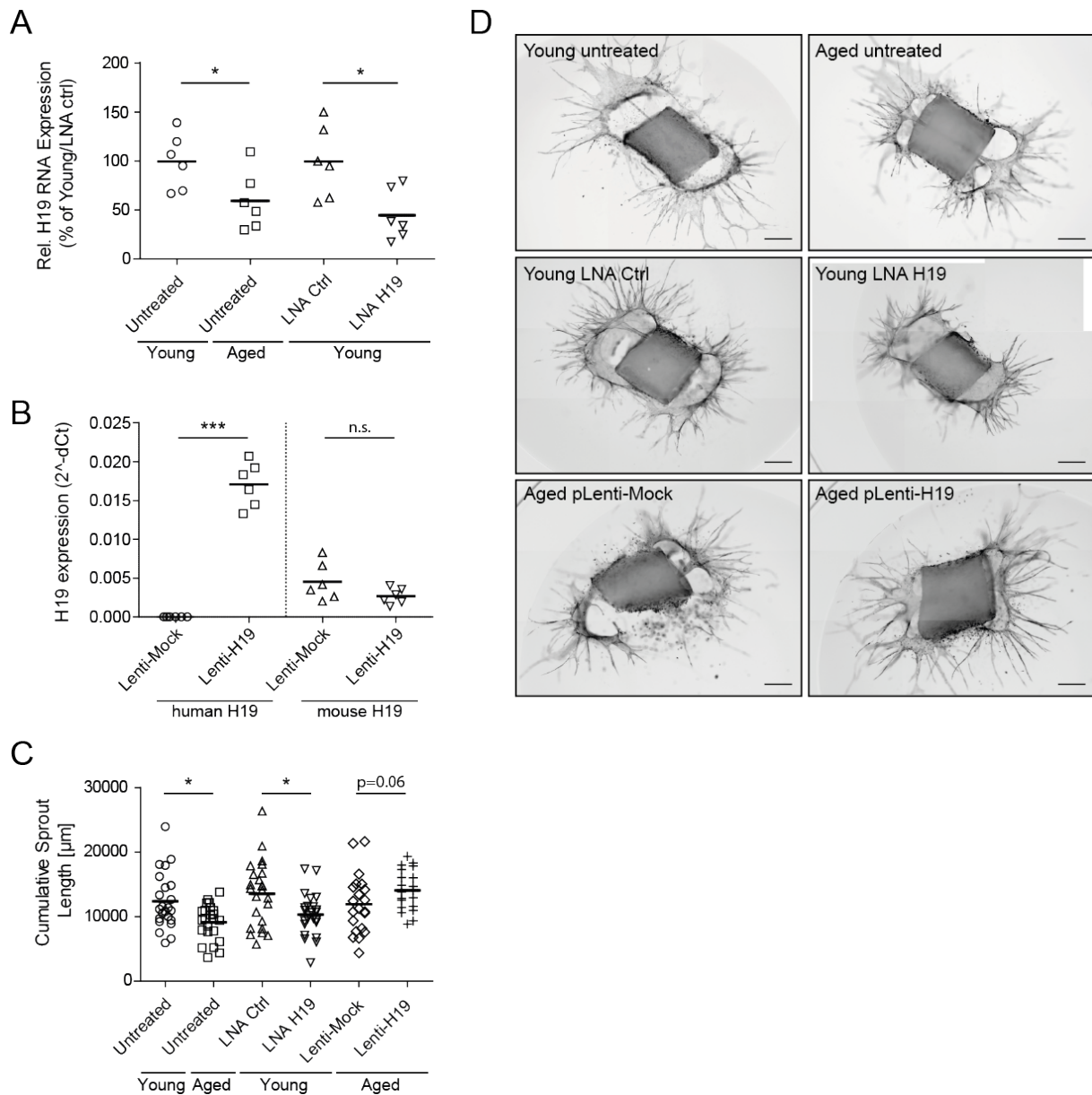


**Figure 28: Depletion of H19 led to impaired angiogenic sprouting in an *ex vivo* aortic ring assay and overexpression of human H19 rescued the impaired sprouting of aged aortic rings. A:** RNA from aortic rings was isolated and the expression of mouse H19 in aortic rings was analyzed with qRT-PCR. n=6 per group **B:** Aortic rings from aged mice were transduced with lentivirus carrying H19 gene or empty vector and the expression of human and mouse H19 was analyzed after 5 days with qRT-PCR. n=6 per group **C/D:** The cumulative sprout length of aortic rings was analyzed. ECs were stained with fluorophore coupled isolectin and fluorescent images are displayed inverted. The scale bar denotes 500  $\mu m$ . Statistical significance was depicted as follows: \* $p < 0.05$ , \*\* $p < 0.01$ , \*\*\* $p < 0.001$ .

To further validate the findings from the aortic ring assay, H19<sup>fl/fl</sup> mice were bred with a Cdh5(PAC)-CreERT line to obtain inducible endothelial-specific H19 KO mice (referred to as H19<sup>IEC-KO</sup>). Cre-negative littermates were used as control (referred to as Ctrl). Lung endothelial cells from these mice were isolated, cultivated and H19 as well as p21 expression was analyzed. H19 levels showed a heterogenic response to tamoxifen injection with an overall reduction of H19 abundance of 60% in H19<sup>IEC-KO</sup> mice compared to Ctrl mice, although this effect was not statistically significant (Figure 29A). p21 showed a nonsignificant trend towards upregulation in lung ECs of H19<sup>IEC-KO</sup> mice compared to

Ctrl mice (Figure 29B). Total hearts were isolated from the same animals and H19 expression was analyzed. H19 was not detectable in three out of five animals and poorly expressed in the remaining two. Compared to Ctrl animals, H19 levels were significantly reduced (Figure 29C).

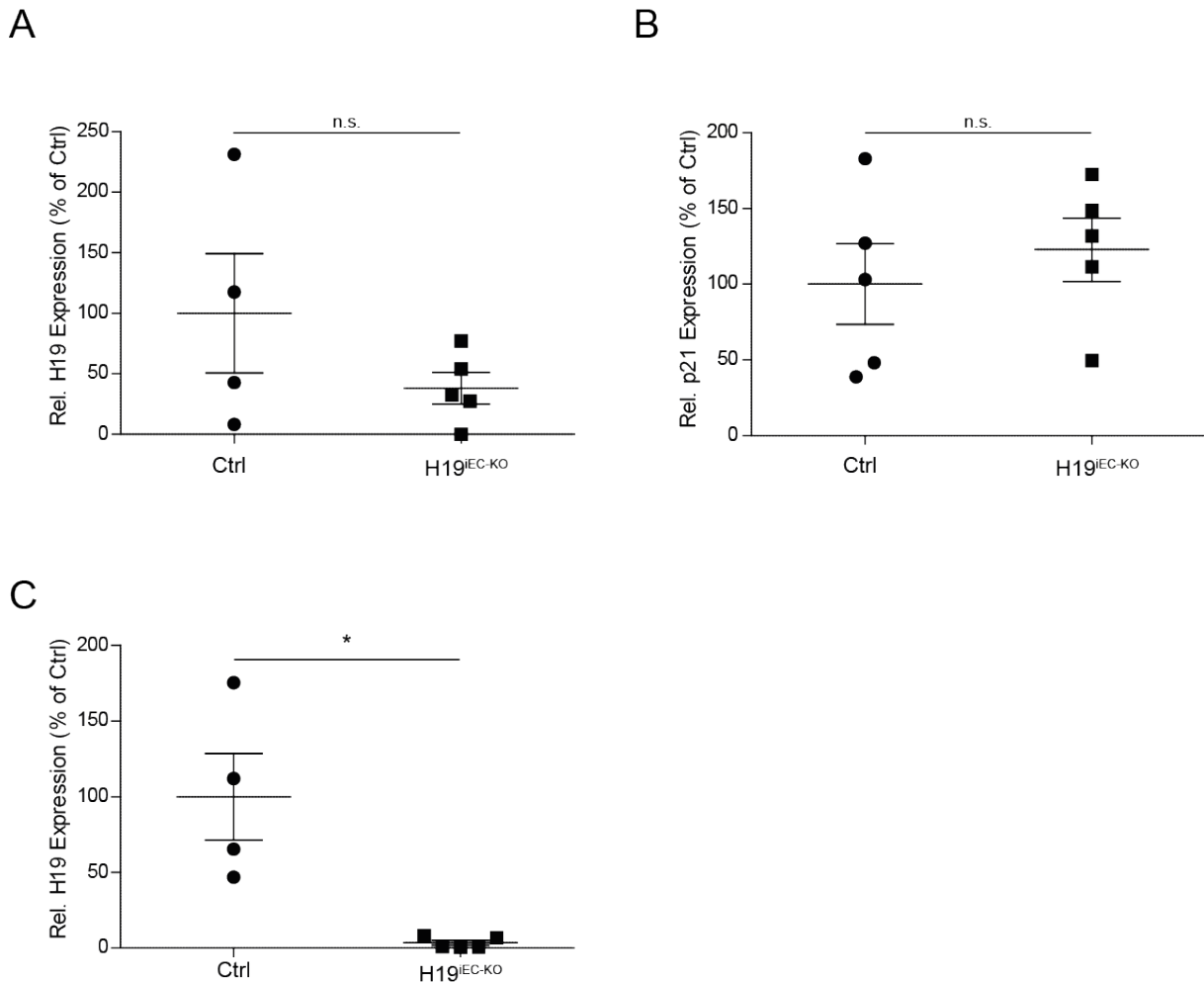


**Figure 29:** H19 was less expressed in lung ECs of H19<sup>iEC-KO</sup> animals compared to Ctrl littermates, while p21 was slightly upregulated. In whole hearts of H19<sup>iEC-KO</sup> animals, H19 expression was abolished compared to Ctrl littermates. **A:** Lung ECs from H19<sup>iEC-KO</sup> animals and Ctrl littermates were isolated, RNA was isolated and H19 expression was analyzed with qPCR. **B:** Lung ECs from H19<sup>iEC-KO</sup> animals and Ctrl littermates were isolated, RNA was isolated and p21 mRNA expression was analyzed with qPCR. **C:** RNA from whole hearts of H19<sup>iEC-KO</sup> animals and Ctrl littermates was isolated and H19 expression was analyzed with qPCR. Statistical significance was depicted as follows: \*p<0.05, n≥3.

Cdh5(PAC)-CreERT2-H19-flox mice (H19<sup>iEC-KO</sup>) and Cre-negative H19<sup>flox/flox</sup> and H19<sup>flox/+</sup> littermates (Ctrl) were subjected to femoral artery ligation and subsequent analysis. Toe perfusion was analyzed 14 and 21 days post-surgery and H19<sup>iEC-KO</sup> mice showed a trend towards increased perfusion consistent over the two time points (Figure 30A). To analyze the effect of H19 depletion on EC function, animals were sacrificed 21 days after surgery and capillary density in the soleus muscle of the ischemic leg was analyzed. H19<sup>iEC-KO</sup> animals showed less capillaries in the ischemic leg compared to Ctrl littermates (Figure 30B). Larger blood vessels contain smooth muscle cells in their *tunica*

*media* and this makes them distinguishable from smaller blood vessels. To further characterize the contradictory effects on perfusion *versus* capillary density, the abundance of smooth muscle cell actin (SMA) covered blood vessels in the soleus muscle of the ischemic legs was analyzed. H19<sup>iEC-KO</sup> mice had more collaterals in the ischemic tissue compared to Ctrl littermates (Figure 30C). Monocyte influx was previously shown to facilitate arteriogenesis and a staining for CD45<sup>+</sup> cells revealed an increased leukocyte infiltration into the soleus muscle of H19<sup>iEC-KO</sup> mice compared to Ctrl littermates (Figure 30D). SMA<sup>+</sup> blood vessels were further analyzed depending on their size. H19<sup>iEC-KO</sup> animals showed an increase in vessels with a diameter of 20-50  $\mu\text{m}$  (Figure 30E). Vessels with a diameter of 50-100  $\mu\text{m}$  were only detectable in two Ctrl animals, while vessels of that size were present in all H19<sup>iEC-KO</sup> animals (Figure 30F). Vessels of more than 100  $\mu\text{m}$  in diameter were detectable in two Ctrl animals and in 3 H19<sup>iEC-KO</sup> animals (Figure 30G).



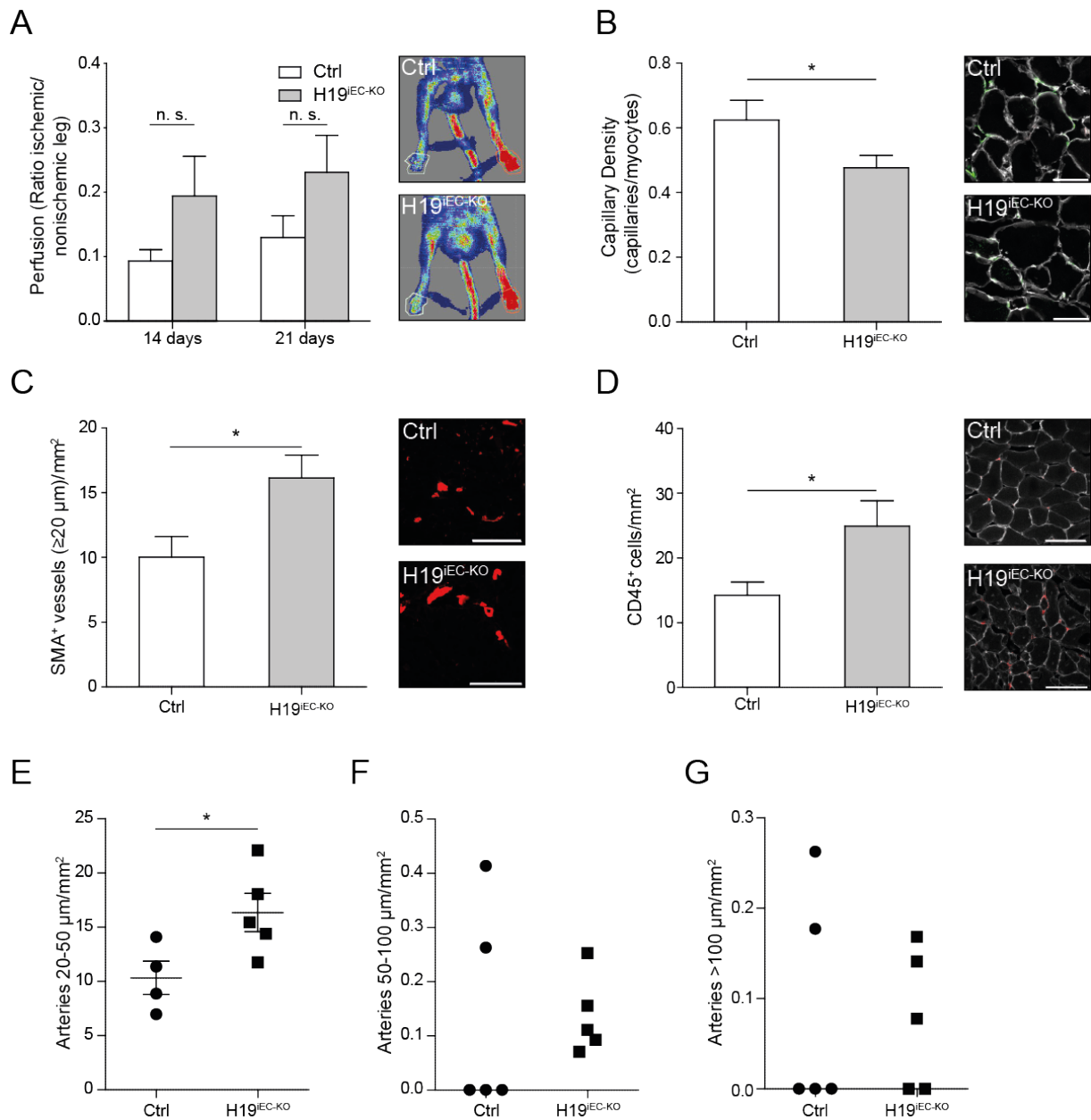


**Figure 30: Femoral artery ligation in endothelial-specific H19 knockout animals led to a decrease in angiogenesis, but an increase in arteriogenesis and leukocyte infiltration.** A: Toe perfusion was measured by laser Doppler imaging 14 and 21 days after femoral artery ligation. n=5 per group. B: Capillary density was analyzed 21 days post-surgery in the soleus muscle of the ischemic legs by staining for lectin (green) and laminin (white). n=5 per group. The scale bar denotes 50  $\mu\text{m}$ . C: The number of smooth muscle covered cell blood vessels in the soleus muscle of the ischemic legs was analyzed 21 days post-surgery by staining for smooth muscle actin (SMA, red). n=5 per group. The scale bar denotes 200  $\mu\text{m}$ . D: The number of leukocytes in the soleus muscle of the ischemic leg was analyzed by staining for CD45 (red) and WGA (white) 21 days post-surgery. n=5 per group. The scale bar denotes 100  $\mu\text{m}$ . E-G: The number of smooth muscle cell covered blood vessels was analyzed depending on their diameter 21 days post-surgery by staining for smooth muscle actin (SMA). n=5 per group. Statistical significance was depicted as follows: \* $p < 0.05$ . Surgery and laser doppler velocimetry were performed by Ariane Fischer (Institut of Cardiovascular Regeneration).

Increased blood pressure is a characteristic of clinical aging<sup>48</sup>. Blood pressure and pulse were analyzed in H19<sup>iEC-KO</sup> mice and Ctrl littermates 14 days after start of tamoxifen administration for 10 days. EC-specific H19 deletion led to an increase in systolic blood pressure and to a trend towards

increased diastolic blood pressure (Figure 31A&B). Pulse rate was analyzed under the same conditions and EC-specific H19 deletion did not alter pulse rate *in vivo* (Figure 31C).

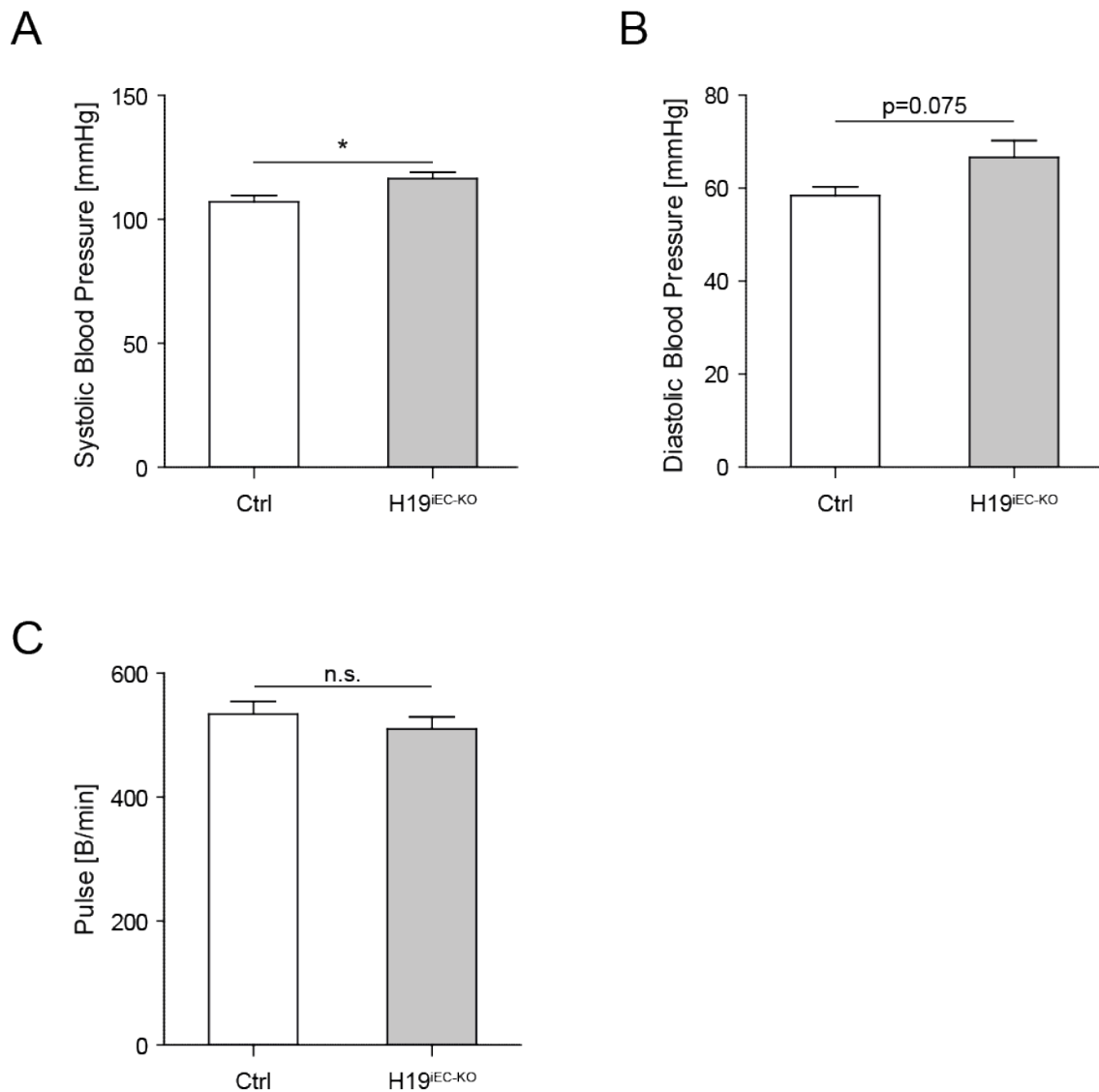


**Figure 31: EC-specific deletion of H19 led to increased blood pressure and did not affect pulse rate *in vivo*.** A: Systolic blood pressure was analyzed in H19<sup>IEC-KO</sup> mice and Ctrl littermates 14 days after start of tamoxifen administration for 10 days. Days 5-8 are depicted. n=5 per group. B: Diastolic blood pressure was analyzed in H19<sup>IEC-KO</sup> mice and Ctrl littermates 14 days after start of tamoxifen administration for 10 days. Days 5-8 are depicted. n=5 per group. C: Pulse rate was analyzed in H19<sup>IEC-KO</sup> mice and Ctrl littermates 14 days after start of tamoxifen administration for 10 days. Days 5-8 are depicted. n=5 per group. Statistical significance was depicted as follows: \*p<0.05.

In summary, these results show that the loss of H19 expression impairs EC function in regards to angiogenesis and that exogenous H19 is sufficient to partially rescue this effect. Endothelial-specific knockout of H19 *in vivo* impairs angiogenesis and increases systolic blood pressure, but facilitates arteriogenesis and inflammatory activation of the tissue at the same time.

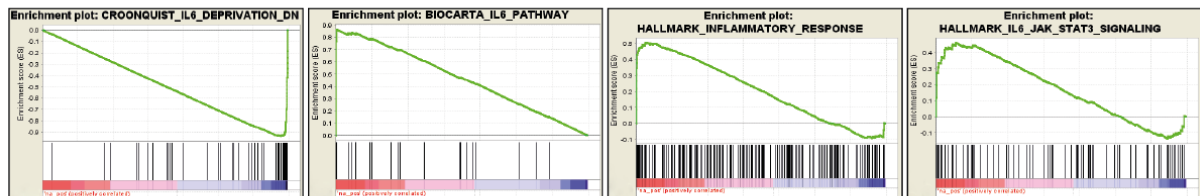
## 4.7 H19 induces inflammatory signaling *in vitro*

To analyze the mechanism by which H19 exerts its function on ECs, the microarray analysis from HUVECs upon H19 depletion was further analyzed for regulated pathways. Gene set enrichment analysis indicated an involvement of H19 in inflammatory processes and more specifically in IL-6/STAT3 signaling (Figure 32A, B&C). IL-6 and IL-6R $\alpha$  expression was upregulated upon H19 depletion on mRNA and protein level (Figure 32C, D&E).

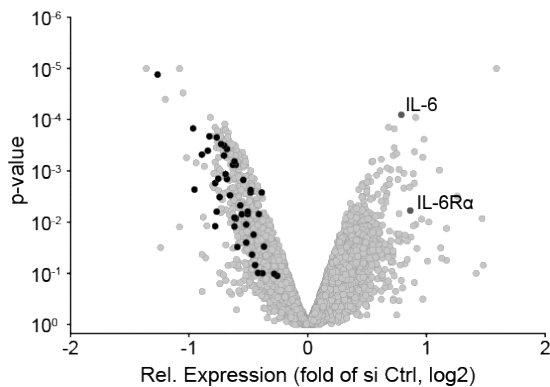
A

Name	Enrichment Score	Normalized Enrichment Score	Nominal p-value	FDR q-value	FWER p-value
Croonquist_IL6_Deprivation_DN	-0.93602115	-2.9599833	0	0	0
Biocarta_IL6_Pathway	0.8637345	2.542158	0	0.21295314	0.18
Hallmark_Inflammatory_Response	0.50658095	2.0259628	0.03324808	0.29194787	0.406
Hallmark_IL6_JAK_STAT3_Signaling	0.46306673	1.6785727	0.059793815	0.368042	0.686

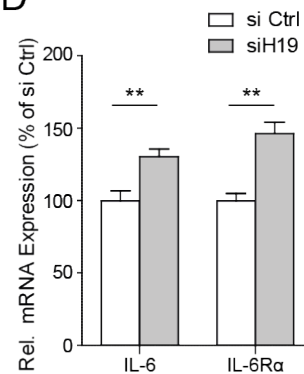
B



C



D



E

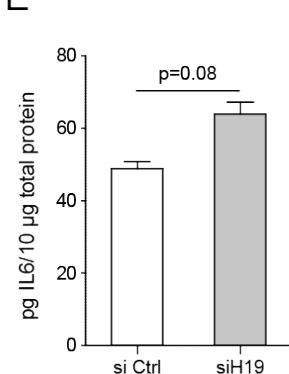


**Figure 32: siRNA-mediated H19 depletion in HUVECs and subsequent microarray analysis identified several inflammation-associated pathways to be differentially regulated.** A: KLF2 overexpressing HUVECs were transfected with siRNA directed against H19 or firefly luciferase. RNA was isolated 48 h after transfection and was subjected to microarray analysis (see Figure.22) A scan for inflammation related pathways was done using gene set enrichment analysis database (Broad Institute). B: Enrichment plots of the pathways mentioned in A. C: Volcano plot showing all genes and p-values in HUVECs 48 h after H19 depletion. Core enriched genes of the pathway Croonquist\_IL6\_Deprivation are highlighted in black and IL-6 and IL-6R $\alpha$  are highlighted in dark grey. D: KLF2 overexpressing HUVECs were transfected with siRNA against H19 or firefly luciferase and RNA was isolated 48 h after transfection. IL-6 and IL-6R $\alpha$  mRNA expression was analyzed with qRT-PCR. E: KLF2 overexpressing HUVECs were transfected with siRNA against H19 or firefly luciferase and RNA whole cell lysates were prepared 48 h after transfection. ELISA against IL-6 detected intracellular IL-6 protein levels. Statistical significance was depicted as follows: \* $p < 0.05$ , \*\* $p < 0.01$ ,  $n \geq 3$ .

To analyze if an upregulation of adhesion molecules upon H19 depletion contributes to the observed leukocyte infiltration *in vivo*, the expression of intercellular adhesion molecule 1 (ICAM-1) and

vascular adhesion molecule 1 (VCAM-1) was analyzed in HUVECs upon siRNA-mediated H19 depletion. Both genes were upregulated upon H19 depletion on mRNA level (Figure 33A). Furthermore, cell surface presentation of ICAM-1 and VCAM-1 was increased as well upon siRNA-mediated depletion of H19 (Figure 33B). Monocytes were isolated from human blood samples and adhesion to HUVECs upon H19 depletion was tested. No differences between si Ctrl and siH19 transfected cells, stimulated with IL-6 for 24 h, were detected in initial adhesion, but as stringency was increased with washing, monocyte adhesion to HUVECs was increased (Figure 33C). To further test if H19 itself is regulated by inflammatory activation, HUVECs were stimulated with tumor necrosis factor  $\alpha$  (TNF- $\alpha$ ) and H19 expression was analyzed. H19 was downregulated in a time-dependent manner in WT and KLF2 overexpressing HUVECs (Figure 33D).

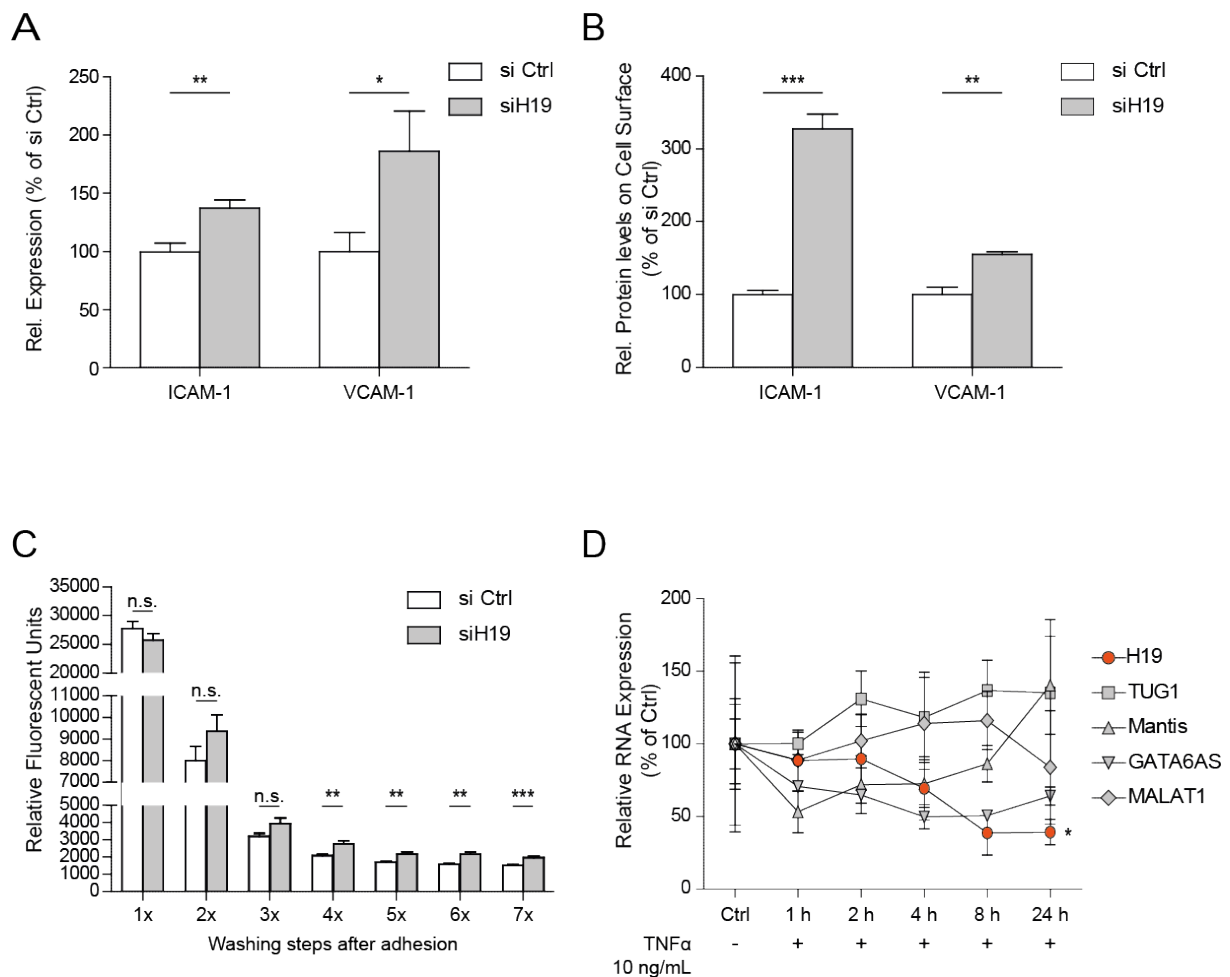


**Figure 33: Depletion of H19 facilitates upregulation of adhesion molecules and increases monocyte adhesion. Inflammatory activation of HUVECs represses H19 expression.** A: KLF2 overexpressing HUVECs were transfected with siRNA directed against H19 or firefly luciferase and RNA was isolated 48 h after transfection. ICAM-1 and VCAM-1 mRNA expression was analyzed with qRT-PCR. B: WT HUVECs were stimulated with IL-6 and siL6R $\alpha$  for 16 h, detached and stained with antibodies against ICAM-1 and VCAM-1 on the cell surface. Cells were analyzed by flow cytometry. C: Monocytes were isolated from human blood samples and added to confluent HUVEC monolayer 48 h after transfection of HUVECs with siRNA directed against H19 or firefly luciferase. Monocytes were stained with BCECF and adhered to HUVECs for 30 min. Fluorescence was measured after every washing step. si Ctrl and siH19 transfected WT HUVECs were stimulated with 100 ng/mL IL-6 and siL-6R $\alpha$  for 24 h prior to the assay. Untransfected WT HUVECs were stimulated with

20 ng/mL TNF- $\alpha$  for 24 h prior to the assay and served as positive control. Monocytes without HUVECs served as negative control. Statistical significance was depicted as follows: \* $p < 0.05$ , \*\* $p < 0.01$ , \*\*\* $p < 0.001$ , n.s. = not significant,  $n \geq 3$ . D: WT and KLF2 overexpressing HUVECs were stimulated with 10 ng/mL TNF- $\alpha$  and H19 expression was analyzed by qRT-PCR at different time points. \* $p$ -for-trend  $< 0.05$ ,  $n \geq 3$ .

In conclusion, depletion of H19 induces inflammatory signaling in HUVECs, especially of the IL-6/JAK2/STAT3 axis. Accordingly, adhesion molecules ICAM-1 and VCAM-1 were upregulated upon H19 depletion and this resulted in increased monocyte adhesion. Furthermore, inflammatory stimulation of HUVECs repressed H19 expression.

#### 4.8 H19 exerts its function mainly through inhibition of STAT3 activation

To gain more insights into how H19 regulates endothelial cell functions, a high throughput luciferase reporter assay for transcription factor activity was performed. HeLa cells were either transfected with siRNAs against H19 or control, or transduced with lentivirus carrying the H19 gene or empty vector. The different cells were then transfected with two plasmids, one carrying a firefly luciferase downstream of a transcription factor binding site and the other carried a renilla luciferase under the control of a CMV promoter as transfection control. After 24 h, transcription factor activity was calculated by luminescence measurement (Figure 34A). Signal transducer and activator of transcription 3 (STAT3) was the only transcription factor that showed consistent effects, as it was more active upon H19 depletion and less active upon H19 overexpression (Figure 34B).

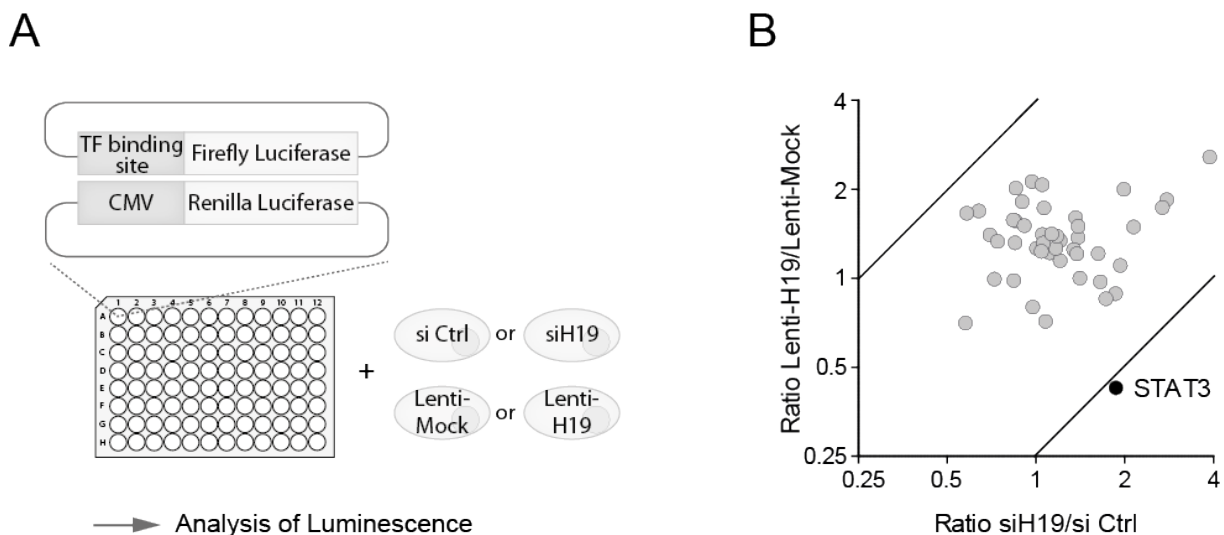


**Figure 34:** A luciferase reporter assay for transcription factor activity revealed STAT3 as being differentially active upon H19 depletion and overexpression. **A:** Schematic representation of the assay. HeLa cells were transfected with siRNAs directed against H19 or firefly luciferase or transduced with a lentivirus carrying either the H19 gene or empty vector. Cells were then transfected with plasmids carrying firefly luciferase gene downstream of transcription factor binding site and renilla luciferase gene under control of a CMV promoter. Luminescence was analyzed 48 after transfection/ $\geq 7$  days after transduction and 24 h after plasmid transfection. **B:** Analysis plot of firefly/renilla luminescence for all tested transcription factors.

To analyze whether the reason for the differential activity of STAT3 is a change in its expression, the mRNA and protein expression of STAT3 was analyzed in HUVECs upon siRNA-mediated depletion of H19. After H19 depletion STAT3 expression was slightly increased on the mRNA and protein level (+38% and +52% respectively) (Figure 35A&B). STAT3 is phosphorylated at TYR705 mainly by Janus Kinase 2 (JAK2) and this phosphorylation induces dimerization and translocation to the nucleus, where STAT3 acts as a transcription factor for several genes. The amount of phosphorylated compared to non-phosphorylated protein was analyzed and STAT3 phosphorylation at TYR705 was significantly increased upon siRNA-mediated H19 depletion (+194%), while phosphorylation at SER727 was not changed (Figure 35B). Furthermore, the levels of JAK2 phosphokinase were not changed upon siRNA-mediated H19 depletion (Figure 35C). These data suggest that H19 regulates the activity of the transcription factor STAT3 by specifically modulation of phosphorylation at tyrosine 705.

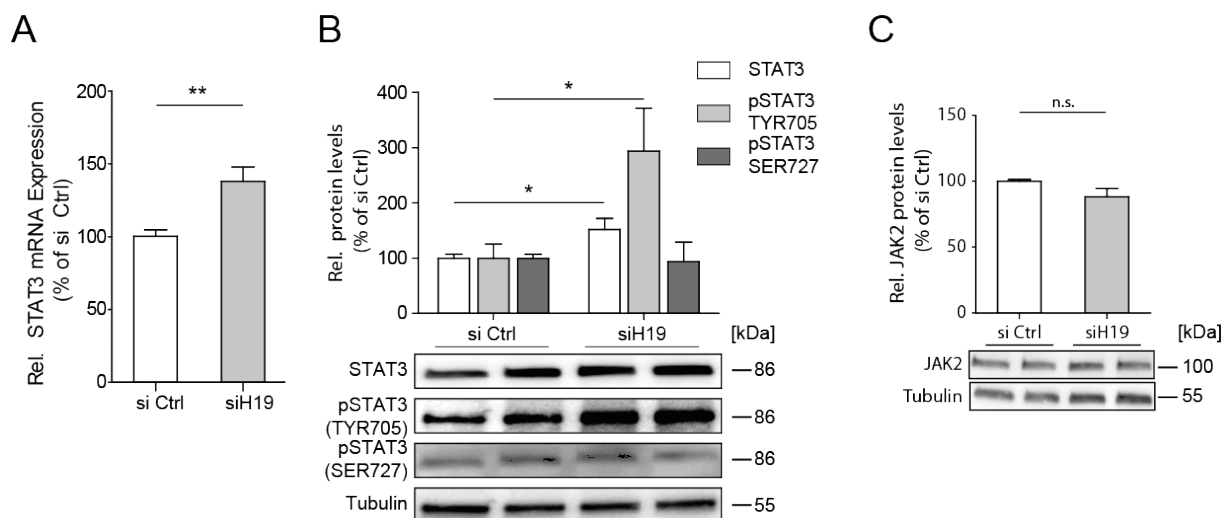


**Figure 35: STAT3 expression and activation were increased upon H19 depletion in HUVECs. A:** KLF2 overexpressing HUVECs were transfected with siRNA directed against H19 or firefly luciferase and RNA was isolated 48 h after transfection. STAT3 mRNA expression was analyzed with qRT-PCR. **B:** KLF2 overexpressing HUVECs were transfected with siRNA directed against H19 or firefly luciferase and whole cell lysates were prepared 48 h after transfection. STAT3 protein expression as well as phosphorylated STAT3 abundance was analyzed with immunoblot. **C:** KLF2 overexpressing HUVECs were transfected with siRNA directed against H19 or firefly luciferase and whole cell lysates were prepared 48 h after transfection. JAK2 protein expression was analyzed with western blot. Statistical significance was depicted as follows: \* $p < 0.05$ , \*\* $p < 0.01$ , n.s. = not significant,  $n \geq 3$ .

STAT3 was shown to act as a transcriptional activator for p21 and ICAM-1<sup>108,109</sup>. Cryptotanshinone (CPT) is a known inhibitor of STAT3 phosphorylation at TYR705 and it thereby inhibits STAT3 activation<sup>263</sup>. 20  $\mu\text{M}$  CPT efficiently blocked the phosphorylation of STAT3 (Figure 36A). In order to confirm that the effect of H19 on EC function is mediated by STAT3 activation, Interleukin-6 together with soluble IL-6 receptor were added to WT HUVECs to stimulate STAT3 signaling and CPT was used to block STAT3 activation upon H19 depletion. HUVECs were incubated with 20  $\mu\text{M}$  CPT for 5 hours,

and IL-6 and siL-6R $\alpha$  were added 1 hour after CPT. The inhibition of STAT3 activation abolished the effects of H19 on mRNA expression of p21, ICAM-1, VCAM-1 and HAS2, indicating that the effect of H19 depletion on these genes is dependent on STAT3 activation (Figure 36B, C, D&E).

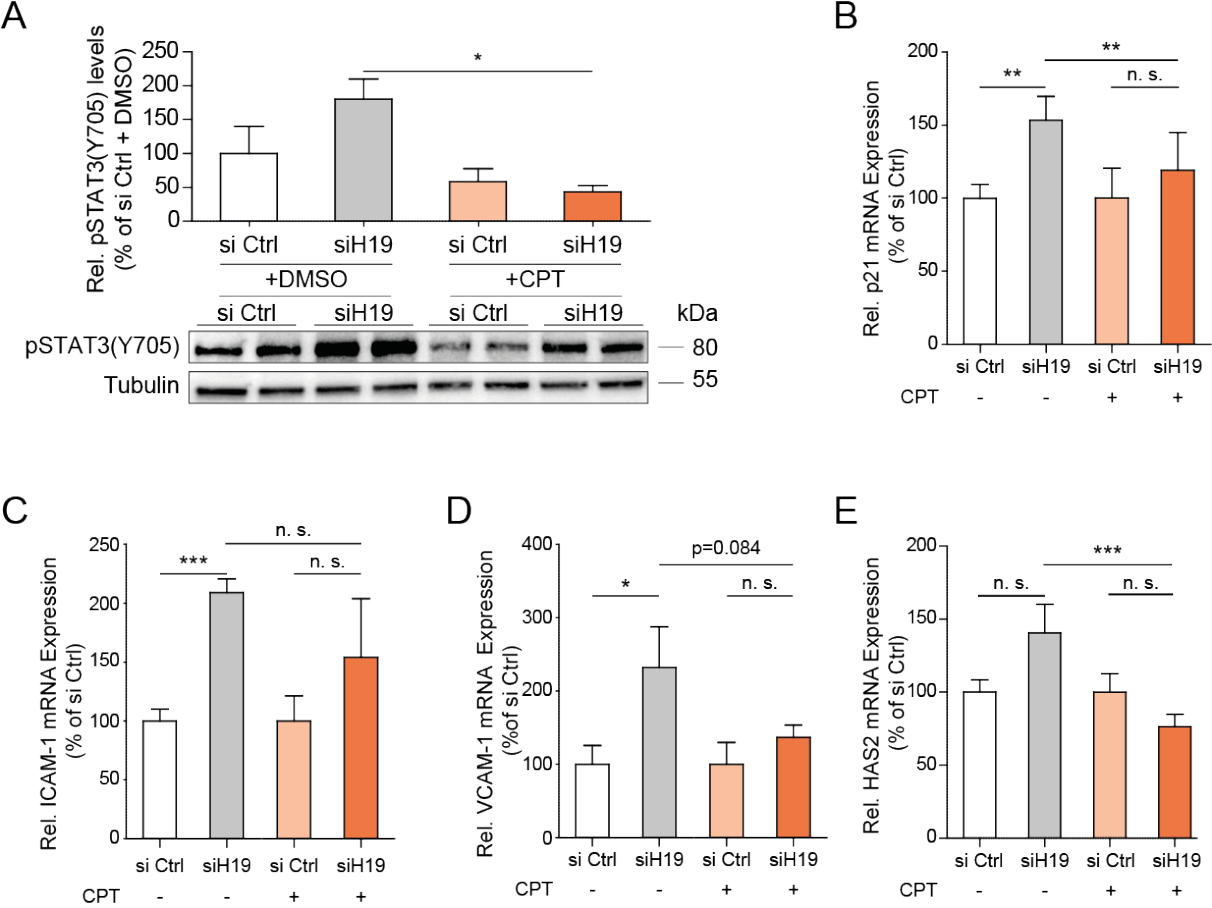


**Figure 36: Inhibition of STAT3 activation with Cryptotanshinone abolished the effect of H19 on gene expression. A:** CPT was added to HUVEC medium 1 h prior to stimulation with IL-6 and siL-6R $\alpha$  (10 ng/mL each) and pSTAT3 (TYR705) levels were analyzed by western blot. **B/C/D:** CPT was added to HUVEC medium to 20  $\mu$ M end concentration 1 h prior to stimulation with IL-6 and siL-6R $\alpha$  (10 ng/mL each) and the expression of p21 (B), ICAM-1 (C), VCAM-1 (D) and HAS2 (E) was analyzed by qPCR. Statistical significance was depicted as follows: \* $p < 0.05$ , \*\* $p < 0.01$ , \*\*\* $p < 0.001$ ,  $n \geq 3$ .

To functionally analyze the dependence of H19 on STAT3 activation, a BrdU proliferation assay was performed. H19 was depleted with siRNAs in WT HUVECs, STAT3 signaling was induced with 10 ng/mL IL-6 and siL-6R $\alpha$  and STAT3 activation was inhibited with 20  $\mu$ M CPT. The effects of depletion of H19 on proliferation were abolished upon inhibition of STAT3 activation (Figure 37).

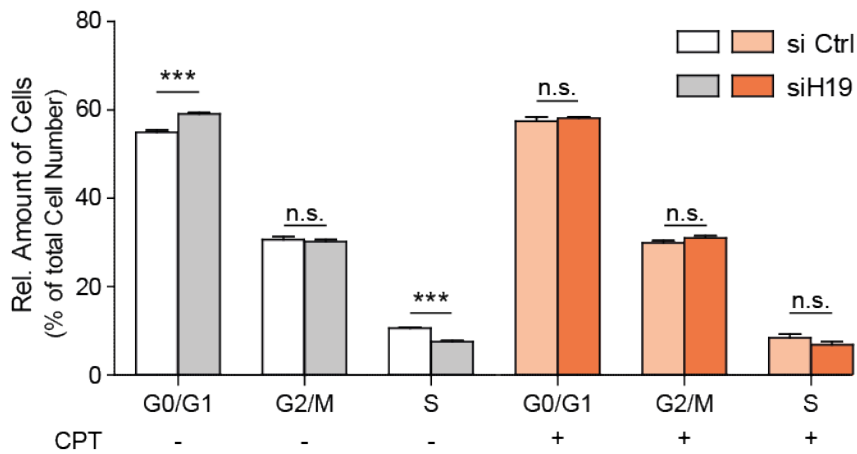


**Figure 37:** HUVECs were incubated with 20  $\mu$ M CPT for 1 h prior to the addition of 10 ng/mL IL-6 and siL-6R $\alpha$  I. After 4 h BrdU was added and cells proliferated in the presence of BrdU for 4 h before the start of the assay. Statistical significance was depicted as follows: \* $p < 0.05$ , \*\* $p < 0.01$ , \*\*\* $p < 0.001$ ,  $n \geq 3$ .

In summary, H19 regulates the expression and phosphorylation of STAT3 at TYR705 and thus its activation, while STAT3 phosphorylation at SER727 is not regulated. Inhibition of STAT3 activation was sufficient to abolish the effects of H19 depletion on mRNA expression of p21, ICAM-1, VCAM-1 and HAS2. Furthermore, inhibition of STAT3 activation abolished the effect of H19 on proliferation.



## 5. Discussion

### 5.1 Expression of H19 is tightly regulated

Ageing diminished H19 expression in mouse endothelium from two different vascular beds. No regulation occurred in total heart and the smooth muscle cell rich aortic media and adventitia (Figure 14). According to data analysis from noncode.org and previous studies, H19 is highly expressed during development, but silenced shortly after birth in most tissues, except for placenta, skeletal muscle, and heart<sup>187,188</sup>. The promotor region of H19 harbors several evolutionary conserved binding sites for the transcription factor Krüppel-like factor 2 (KLF2), which is known to be upregulated under physiological shear stress in endothelial cells (Figure 16)<sup>12</sup>. Indeed, lentiviral overexpression of KLF2 in HUVECs significantly induced H19 expression, suggesting that H19 might as well be highly abundant in the endothelium *in vivo* under physiological conditions (Figure 15). Accordingly, laminar shear stress also induced H19 expression in a KLF2-dependent manner (Figure 16). How H19 expression is regulated during aging remains unclear. We showed that shear stress induced H19 expression in a KLF2-dependent manner and that inflammatory activation diminished H19 expression. KLF2 was shown to be repressed with ongoing age<sup>264</sup> and this might lead to reduced H19 expression during aging. Vascular aging is usually accompanied by increased inflammatory activation<sup>48</sup> and we showed that stimulation of HUVECs with TNF- $\alpha$  reduced H19 expression. We therefore hypothesize that at least two mechanisms regulate H19 during the process of aging, one being the reduced expression of KLF2 and the other the increase in inflammatory activation. Nevertheless, additional work needs to be done to experimentally prove the regulation of H19 by these processes.

### 5.2 Loss of H19 promotes senescence and counteracts proliferation

We used a loss of function approach to study the role of H19 in endothelial cells. H19 can be pharmacologically inhibited with siRNAs and, despite being localized mainly in the cytoplasm, also by LNA GapmeRs, although not as efficiently as with siRNAs (Figure 17A). Overexpression can be achieved by lentiviral transduction (Figure 17B). Previous studies indicated that H19 might regulate gene expression epigenetically, but RNA immunoprecipitation experiments did not show a direct interaction of H19 with histone H3 in HUVECs (Figure 18B). Furthermore, the predominantly cytoplasmic localization of H19 in HUVECs makes a histone modifying role unlikely (Figure 18A). An unbiased exon array analysis in HUVECs upon H19 depletion identified several regulated single genes

and pathways (Figure 22A). Expression levels of the seven most regulated single genes were confirmed in an independent experiment (Figure 22B). The highest regulated single gene was lysozyme (LYZ), which plays an important role in the immune response and acts as an antimicrobial agent by catalyzing hydrolysis of 1,4-beta linkages between N-acetylmuramic acid and N-acetyl-D-glucosamine residues in peptidoglycan of bacterial cell walls. Lysozyme was shown to possess sequestering properties for advanced glycation end products (AGEs) in diabetic nephropathy and it significantly reduced AGE induced IL-6 mRNA *in vitro*<sup>265</sup>. Lysozyme had positive effects in diabetic nephropathy and reduced nephrotoxic effects of AGE through preventing production and release of inflammatory mediators<sup>266</sup>. Interestingly, the loss of H19 expression led to an upregulation of lysozyme. If lysozyme also has an anti-inflammatory function in other cells types, its upregulation upon loss of H19 would be beneficial for aging cells. But if lysozyme does prevent production and release of inflammatory mediators in other organs and cell types is unclear. Furthermore, if lysozyme is upregulated in an H19-dependent manner *in vivo* is unclear and would require further studies. Lysozyme was suggested to play a role during cartilage calcification, most likely *via* interaction with hyaluronan<sup>267</sup>. Interestingly, hyaluronan synthase 2 (HAS2) was the second most upregulated gene upon H19 depletion in HUVECs. HAS2 produces hyaluronan (HA), a component of the extracellular matrix. HA is enriched in advanced atherosclerotic plaques and is secreted by smooth muscle cells during atherogenesis<sup>268,269</sup>. Furthermore, HA was shown to be involved in vascular remodeling<sup>270,271</sup>. Endothelial cells were also shown to produce HA upon pro-inflammatory stimuli which increased adhesive capacity and recruitment of immune cells<sup>272,273</sup>. Mice that overexpressed HAS2 in smooth muscle cells showed increased vascular stiffness and, in an ApoE background, increased atherosclerotic plaque formation in the aorta<sup>274</sup>. Inhibition of HA production reduced neointima formation, and overexpression of HAS2 in vascular SMCs promoted neointima formation after cuff-mediated vascular injury in mice<sup>275</sup>. Furthermore, blood vessels of aged individuals were shown to contain more HA, and senescent SMCs were shown to enhance HA production *in vitro*<sup>276-281</sup>. HAS2 was shown to be induced by STAT3 activation, which might explain the upregulation upon H19 depletion<sup>282</sup>. These results are striking and show that H19 could potentially influence vascular remodeling. The regulation of HAS2 by H19 might provide an explanation for the age- and pathology-mediated regulation of HA synthesis.

When looking at the repressed genes upon H19 depletion, marker of proliferation KI-67 (MKI67) was among the most repressed genes and gene ontology analysis revealed regulation of many cell cycle related pathways (Figure 22B&C). MKI67 is commonly used as a marker for proliferating cells and H19 depletion repressed the expression of this gene. Accordingly, H19 depletion was negatively associated with many proliferation-related pathways (Figure 22D). Ma *et al.* reported that H19 promoted proliferation through E2F-1 in pancreatic ductal adenocarcinoma and H19 depletion

indeed negatively regulated E2F pathways in HUVECs<sup>213</sup> (Figure 22D). Analysis of EC proliferation revealed that H19 depletion indeed reduced proliferation in HUVECs and hCoAECs, while H19 overexpression had no effect (Figure 23). These results are in line with several studies that found pro-proliferative effects of H19, mainly in the background of cancer. Sun and colleagues reported a pro-proliferative effect of H19 in estrogen-induced proliferation of a breast cancer cell line, although they did not provide a mechanism or regulated genes through which H19 might mediate its function in these cells<sup>205</sup>. Han and colleagues report that H19 depletion led to an arrest of colorectal cancer cells in G0/G1 cell cycle phase and they observed decreased cyclin D1, Cyclin E1 and CDK4 expression and increased p21 expression<sup>206</sup>. H19 directly bound eIF4A3 and H19 overexpression decreased transcription factor binding to the abovementioned genes, resulting in their regulation<sup>206</sup>. In HUVECs, eIF4A3 was not regulated upon H19 depletion, which is not surprising, given the fact that H19 only binds and does not alter eIF4A3 levels. eIF4A3 targets Cyclin D1, Cyclin E1 and CDK4 were not regulated as well in HUVECs upon H19 depletion, suggesting that this effect might not play a role in endothelial cells. Another study showed that H19 regulates phosphorylation of RB1 through regulation of Cyclin D1 and CDK4 in colorectal cancer cells and that H19 interacts with macroH2A to regulate CDK8<sup>207</sup>. CDK8 showed a trend towards upregulation upon H19 depletion, which is in contrast to the results Ohtsuka and colleagues postulated, where H19 silencing reduced CDK8 expression<sup>207</sup> (Figure 24A). Taken together, a Cyclin D1 and CDK4-dependent regulation of RB1 and a regulation of CDK8 expression by H19 seems unlikely in endothelial cells. Ma and colleagues report that depletion of H19 in pancreatic cancer cells led to G0/G1 arrest accompanied by decreased E2F-1 levels and its target genes PCNA, MCM3, Cyclin A1 and Cyclin A2<sup>213</sup>. E2F-1 expression was not changed upon H19 depletion and of the abovementioned E2F1 target genes, only Cyclin A2 showed a regulation, although not significantly (Figure 24B). However, pathway analysis after H19 depletion in HUVECs revealed a strong association of H19 with E2F-1 target genes (Figure 22D). It is unknown if this association is the cause or consequence of the G0/G1 accumulation of cells upon H19 depletion (Figure 23A&B). E2F-1 is known to be involved in G1/S-transition during cell cycle progression and as it is not regulated upon H19 depletion, it is likely that the association of H19 with E2F-1 targets is just a consequence of the G0/G1 arrest. A study by Ayesh and colleagues showed that H19 repressed p57<sup>kip2</sup> and therefore promoted cell growth under stress stimuli<sup>189</sup>. p57<sup>kip2</sup> expression was not changed upon H19 depletion in HUVECs (Figure 24C). Tao and colleagues showed that H19 repressed DUSP5, ERK1 and ERK2 in cardiac fibroblasts and alters DUSP5/ERK1/2 axis in cardiac fibroblast proliferation and fibrosis<sup>233</sup>. DUSP5 was upregulated upon H19 depletion in HUVECs and might influence proliferation of ECs, but as neither ERK1 (MAPK3), nor ERK2 (MAPK1) were regulated upon H19 depletion in HUVECs, this is unlikely (Figure 24D). Our results demonstrate that H19 depletion leads to an accumulation of endothelial cells in G0/G1 cell cycle phase and this is also the case in

cellular senescence. As senescence plays an important role during aging, the role of H19 in senescence was analyzed by staining for senescence-associated  $\beta$ -galactosidase. In HUVECs and hCoAECs, depletion of H19 led to more senescence (Figure 25). Senescence is usually established by two pathways, the p53/p21 pathway and the p16<sup>ink4A</sup>/pRB pathway, and H19 might influence proliferation and senescence through alteration of these pathways. In line with this hypothesis, H19 depletion led to increased levels of p16<sup>ink4A</sup> and p21, but interestingly not to an increase in p53 expression (Figure 26). Two groups already reported that H19 repressed p21 expression in colorectal cancer cells as well as in HUVECs, but both studies did not analyze senescence<sup>206,218</sup>. A regulation of p16<sup>ink4A</sup> by H19 was not reported so far, but interestingly, p53 was shown as an upstream regulator of H19<sup>202,220</sup>. H19 prevented p53 binding to the NOTCH1 promoter and thus repressed NOTCH1 expression<sup>232</sup>. Indeed, NOTCH1 expression showed a trend towards upregulation upon H19 depletion in HUVECs, but this effect was not significant (Figure 24E). However, H19 might regulate proliferation and senescence independently of p53 and also likely independently of the upstream p53 regulators ATM and ARF. p53 is induced and stabilized by ATM and ARF upon DNA damage and pathway analysis of HUVECs after H19 depletion did not identify DNA-damage related pathways. It is likely that H19 directly influences p21 levels and thus regulates cell cycle progression and senescence. p21 inhibits the activity of all members of the cyclin/CDK family and p21-mediated cell cycle arrest prevents S-phase entry<sup>67</sup>. This is reflected by results of the pathway analysis upon H19 depletion in HUVECs, where H19 depletion negatively affected cell cycle progression (Figure 22). Additionally, p16<sup>ink4A</sup> was induced upon H19 depletion and H19 might also directly influence p16<sup>ink4A</sup> levels. However, Stein and colleagues showed that prolonged p21-mediated cell cycle arrest leads to p16<sup>ink4A</sup> upregulation<sup>69</sup>. It remains unclear whether H19 directly influences p16<sup>ink4A</sup> levels or if this upregulation is a secondary effect. p16<sup>ink4A</sup> inhibits CDK4 and CDK6 activity and thus inhibits pRB phosphorylation<sup>70,71</sup>. RB1 was identified as an upstream regulator of H19 together with E2F-1 and in the same study the authors showed that H19 also regulated RB1 phosphorylation by regulating CDK4 and Cyclin D1<sup>207</sup>. As mentioned above, this is not the case in HUVECs, but whether RB1 regulates H19 expression remains unclear. Interestingly, overexpression of H19 failed to significantly regulate p16<sup>ink4A</sup>, p21 and p53, although all genes show a trend towards decreased expression (Figure 26C). H19 was shown to be involved in migration and invasiveness of tumor cells before and as migration is an important process during angiogenesis, a scratch wound assay was performed with HUVECs upon H19 depletion. Interestingly and in contrast to results from other studies and other cell types, H19 did not have an effect on EC migration *in vitro* (Figure 27).

In summary, depletion of H19 led to less proliferation and more senescence in endothelial cells from two different vascular beds. Inhibition of cell cycle progression was not established by known H19 functions, but we identified the cell cycle regulators p16<sup>ink4A</sup> and p21 being upregulated upon

depletion of H19. Furthermore, lysozyme and hyaluronan synthase 2 were upregulated upon pharmacological inhibition of H19, indicating that H19 might be involved in extracellular matrix remodeling.

### **5.3 H19 is required for proper endothelial cell function *ex vivo* and *in vivo***

To further confirm the effects of H19 observed *in vitro*, an *ex vivo* strategy was used to analyze the effect of H19 on angiogenic sprouting. In an *ex vivo* aortic ring assay, aortic ECs from aged mice showed an impaired angiogenic capacity compared to young animals. This is not surprising, as it was already shown that human endothelial cells isolated from aged donors show impaired angiogenesis compared to neonatal ECs<sup>262</sup>. H19 was also less expressed in the aorta of aged mice compared to young animals, which is in line with our expectations and was already observed before (Figure 14 & Figure 28A). Pharmacological inhibition of H19 in aortic rings of young animals was sufficient to reduce the cumulative sprout length to levels observed in aged animals (Figure 28B). Several factors play a role in reducing the angiogenic capacity of aged ECs, likely senescence and stem cell exhaustion. Ahluwalia and colleagues showed that reduced VEGF expression in aged ECs due to impaired nuclear transport of pSTAT3 and pCREB are likely the reason for the impaired sprouting of aged ECs. However, neither VEGFA, nor VEGFB or VEGFC are regulated upon H19 depletion in HUVECs. Furthermore, depletion of H19 led to an increase in STAT3 activity. H19 was less abundant in aortic rings from aged mice and we therefore expect an increase in nuclear transport of pSTAT3 in aged endothelial cells, although we did not analyze that. However, STAT3 was shown before to mediate a paracrine effect from cardiomyocytes to endothelial cells and cardiomyocyte-specific overexpression of STAT3 resulted in an increase in myocardial capillary density<sup>127</sup>. Transfection of aortic rings with LNA GapmeRs against H19 not only targets endothelial cells, but all other aortic cells as well. Smooth muscle cells are highly abundant in the aorta and if H19 functions *via* the same mechanisms in smooth muscle cells as it does in endothelial cells, STAT3 activity should be increased upon transfection with LNA GapmeRs against H19. As mentioned above, STAT3 overexpression in cardiomyocytes increased myocardial capillary density *via* secretion of VEGF<sup>127</sup>. If the same was true for smooth muscle cells, higher STAT3 activity upon H19 depletion should induce VEGF secretion and lead to more angiogenic sprouting. As the cumulative sprout length of aortic rings upon H19 depletion is reduced, we can exclude already known STAT3-dependent pathways as mediators of the impaired angiogenic capacity in the aortic rings.

More strikingly, overexpression of human H19 in aged mouse aortic rings was sufficient to rescue the impaired sprouting upon aging (Figure 28A&B). These findings are perfectly in line with the previous

results from our *in vitro* experiments that H19 depletion results in premature senescence. The depletion of H19 in aortic rings from young animals potentially results in premature senescence as well and thus reduces proliferative capacity. Most likely H19 overexpression in aortic rings from aged mice promotes proliferation and counteracts senescence, although this was not observed *in vitro*. Interestingly, human H19 was sufficient to promote sprouting in the aged aortic rings, despite poor sequence conservation between species. Likely, the secondary or tertiary structure is conserved along with potential interaction partner binding motifs. It is unknown if H19 binds the same proteins in humans and mice, but these results suggest that this might be the case. Taken together, loss of H19 with age is sufficient to reduce the angiogenic capacity of endothelial cells and this can be rescued by exogenous human H19.

As mentioned before, pharmacological inhibition of H19 in aortic rings likely did not only target endothelial cells, but also other cells of the aorta. To exclude that H19 mediates its effects through other cell type than ECs and to further confirm the *ex vivo* findings, inducible endothelial-specific H19 knockout mice were subjected to different experiments. The mouse H19 gene is flanked by *loxP* sites and those mice were mated with an inducible VE-Cadherin promoter driven Cre-line to obtain an inducible EC-specific H19 knockout mouse (H19<sup>IEC-KO</sup>). Isolation of lung ECs upon H19 KO revealed a strong, but not significant downregulation of H19 and a slight upregulation of p21 (Figure 29A&B). One would expect a total absence of H19 RNA in the lung ECs of the H19<sup>IEC-KO</sup> animals, but first, lung EC isolation hardly results in a homogenous EC culture but is rather contaminated with fibroblast, that still express H19. Second, the inducible knockout will never be 100% efficient in all cells and therefore some H19 RNA might still be detectable. The same is true for p21 expression: a trend towards an upregulation is visible, which would resemble the *in vitro* results, but again due to the aforementioned reasons, this effect is not significant. Interestingly, analysis of H19 levels in total hearts revealed a strong downregulation and H19 was hardly detectable after EC-specific knockout (Figure 29C). This confirms our own observations that H19 is mainly expressed in ECs in hearts. Nevertheless, we assumed that the knockout strategy resulted in the EC-specific reduction of H19 and continued with further experiments using this model.

Hind limb ischemia was induced by occluding the femoral artery in one hind limb. After induction of ischemia, blood flow is restored within some weeks by angiogenesis and arteriogenesis in healthy, young mice. Perfusion of the operated hind limb was analyzed after 14 and 21 days and at both time points perfusion tended to be increased in H19<sup>IEC-KO</sup> mice, which was in contrast to our expectations, as H19 depletion *ex vivo* led to less angiogenesis (Figure 30A). Staining for capillary density in the ischemic hind limb revealed a reduced capillary density upon EC-specific H19 depletion, which is in line with the results from the *ex vivo* aortic ring assay and the *in vitro* proliferation and senescence data, but is in contrast to the increased perfusion (Figure 30B). H19 depletion activated STAT3 *in vitro*

and cardiomyocyte-specific STAT3 deletion was shown to reduce myocardial capillary density before<sup>126</sup>. Furthermore, STAT3 was shown to promote tumor angiogenesis by upregulating VEGF<sup>283</sup>. The effect of STAT3 activation in endothelial cells has not been studied before, so it is unclear if endothelial STAT3 induction has oppositional effects to genetic STAT3 deletion. Nevertheless, we did not measure STAT3 and pSTAT3 levels in mouse endothelium.

An increase in perfusion despite reduced capillary density indicates differences in collateral numbers and size and indeed, analysis of smooth muscle cell covered blood vessels revealed an increased number of arteries in the ischemic hind limbs of EC-specific H19 KO mice (Figure 30C). Interestingly, when looking at the collaterals sorted by size, there is a significant increase of arteries with a small diameter (Figure 30E). Arteries with a larger diameter were only detectable in few control animals, while in H19<sup>iEC.KO</sup> animals, larger arteries are abundant (Figure 30F&G). Arteries are usually formed by enlargement of existing blood vessels. This process is stimulated mechanistically by increased blood pressure and thus increased radial wall stress and increased flow, which leads to endothelial surface stress. Both processes do play a role here, as the femoral artery is occluded and blood has to bypass this. Mechanistically, endothelial surface stress leads to cytokine production and adhesion molecule expression, two processes that are common during inflammatory signaling. A stronger inflammatory response upon increased endothelial surface stress would lead to increased arteriogenesis. To analyze if H19 inhibits inflammatory activation of ECs and if therefore its loss contributes to arteriogenesis, the number of leukocytes infiltrating the ischemic tissue was analyzed. In line with this hypothesis, significantly more leukocytes infiltrated the tissue of H19<sup>iEC-KO</sup> mice compared to control littermates (Figure 30D). This observation is striking, as aging does not only lead to impaired angiogenic capacity, but also to an increase in EC inflammatory activation<sup>48</sup>. EC-specific STAT3 deletion was shown to lead to increased leukocyte infiltration and increased inflammatory cytokine production *in vivo* upon stress stimuli<sup>284</sup>. Interestingly, H19 depletion led to increased adhesion molecule expression in a STAT3-dependent manner *in vitro*, again highlighting the inconsistent effects of genetic STAT3 deletion and STAT3 induction in endothelial cells.

To further characterize the phenotype of the EC-specific H19 KO mice, blood pressure was analyzed. Aging usually leads to endothelial dysfunction and stiffening of blood vessels, two processes that lead to increase in arterial blood pressure. Upon EC-specific deletion of H19, mice show a significant increase in systolic blood pressure and a nonsignificant increase in diastolic pressure (Figure 31A & B). Deposition of hyaluronan (HA) in the artery wall was already shown to promote vascular stiffening<sup>285</sup> and our experiments showed that hyaluronan synthase 2 (HAS2) was upregulated upon H19 depletion. Upregulation of HAS2 upon H19 depletion and increased secretion of HA might explain the change in systolic blood pressure in the H19<sup>iEC-KO</sup> animals. In line with our expectations, pulse was not affected by EC-specific H19 knockout (Figure 31C). The increased systolic blood

pressure could potentially also contribute to the increase in arteriogenesis upon EC-specific H19 depletion.

Taken together, the EC-specific deletion of H19 resulted in a reduction in capillary density and an increase in collateral growth and therefore an increase in perfusion of the ischemic hind limb upon hind limb ischemia surgery in mice. Analysis of leukocyte abundance in the ischemic legs revealed an increase in leukocyte infiltration upon EC-specific H19 depletion. Furthermore, systolic blood pressure was increased upon EC-specific H19 depletion, highlighting the detrimental effects of the loss of H19.

#### **5.4 Loss of H19 promotes inflammatory activation of endothelial cells**

As H19 depletion led to increased leukocyte infiltration *in vivo* and HAS2 expression was shown to be increased in inflammatory activated endothelial cells, the exon array from HUVECs upon H19 depletion was reanalyzed for inflammation-related pathways. Indeed, depletion of H19 led to an upregulation of several inflammatory pathways, most notably IL-6 signaling. IL-6 and its receptor IL-6R $\alpha$  were both upregulated on mRNA level upon H19 depletion and IL-6 also on protein level, indicating an inflammatory activation of ECs upon H19 depletion (Figure 32). Inflammatory activation of ECs usually increases expression of cell surface adhesion molecules, an important process in the development of atherosclerosis<sup>30</sup>. ICAM-1 and VCAM-1 adhesion molecules were both upregulated upon H19 depletion on the mRNA levels and their abundance on the cell surface was increased as well (Figure 33A&B). Cell surface adhesion molecule expression facilitates leukocyte adhesion and subsequent transmigration, and indeed, more monocytes attached to HUVECs upon H19 depletion (Figure 33C). Interestingly, inflammatory activation also repressed H19 expression, indicating that loss of H19 with age may lead to more inflammation in ECs and this further represses H19. In summary, depletion of H19 was associated with an induction of the inflammatory IL-6 pathway. In line with these findings, depletion of H19 upregulated ICAM-1 and VCAM-1 expression, and their presentation on the cell surface. Accordingly, monocyte adhesion to HUVECs was increased upon H19 depletion and H19 itself was repressed upon inflammatory activation of HUVECs.

#### **5.5 H19 does not regulate endothelial cell function *via* previously described mechanisms**

A known feature of H19 is its function as a competitive endogenous RNA (ceRNA) by binding several miRNAs, like let-7 and miR-106<sup>246,247</sup>. To analyze whether this is also the case in HUVECs, publicly



available AGO1-4 high-throughput sequencing of RNA isolated by crosslinking immunoprecipitation (HITS-CLIP) data were analyzed<sup>150</sup>. AGO proteins are important members of the RNA-induced silencing complex (RISC) and therefore miRNA-binding RNA molecules must be identified in a HITS-CLIP screen. H19 was not associated to AGO proteins in HUVECs, suggesting that it might not bind miRNAs (Figure 19A). To further test this hypothesis, the initial microarray in HUVECs upon H19 depletion was analyzed for let-7 target genes. None of the analyzed let7 target genes showed a regulation upon H19 depletion in HUVECs, except for high mobility group AT-hook (HMGA2) (Figure 19B). Why HMGA2 is upregulated upon H19 depletion remains unclear. But given the fact that HMGA2 was the only let-7a target that was regulated upon H19 depletion in HUVECs, and the fact that H19 is in general poorly expressed and harbors only four binding sites for all 7 let-7 family members, and let-7 miRNAs are among the highest expressed miRNAs in general, this approach was not followed. These findings are in line with a study from Denzler *et al.*, where they introduced artificial targets for miR-122 in hepatocytes and analyzed miR-122 target gene expression<sup>286</sup>. Interestingly, miR-122 target expression was not altered till  $1.5 \times 10^5$  artificial miR-122 target sites were introduced per cell<sup>287</sup>. Given this high and unphysiological number of required miR-122 target sites, the authors conclude that modulation of miR target abundance is unlikely to cause significant effects on gene expression through a ceRNA effect<sup>287</sup>.

H19 was furthermore shown to act as a precursor molecule for miR-675<sup>234</sup>. H19 and miR-675 were shown to be regulated together during myoblast differentiation and muscle regeneration<sup>190</sup>. Another coupled regulation of H19 and miR-675 was shown during cardiac hypertrophy<sup>240</sup>. In HUVECs, KLF2 overexpression significantly upregulated H19 expression, but failed to alter miR-675 expression significantly (Figure 15B & Figure 20A). miR-675 5p showed a nonsignificant trend towards repression upon KLF2 overexpression. H19 depletion did not alter miR-675 levels significantly, but led to a nonsignificant increase in miR-675 5p expression (Figure 20C). When H19 acts as a precursor for miR-675 in HUVECs, H19 depletion should alter miR-675 levels. We tested the expression of miR-675 target genes as predicted by microrna.org target gene prediction tool and regulation was not consistent among the predicted target genes. Some were repressed and some were induced upon H19 depletion in HUVECs, indicating that miR-675 levels are likely not changed upon H19 depletion. However, H19 overexpression increased miR-675 expression, but random lentiviral integration into the genome may overcome regulatory factors, that regulate miR-675 processing from H19 in endothelial cells (Figure 20B). Other studies already showed a tight regulation of miR-675 and changes in miR-675 levels without changes in H19 levels and *vice versa*<sup>235</sup>. In summary, knockdown and overexpression of H19 induced miR-675 5p expression, although not statistically significant in the case of H19 depletion. KLF2 overexpression induced H19 expression, but did not change miR-675

levels significantly. Given this inconsistent regulation of miR-675, H19 likely does not act as a miRNA precursor molecule in endothelial cells.

Some lncRNAs were already shown to function *in cis* and regulate their neighboring genes<sup>288</sup>. To test whether H19 affects its nearest neighboring gene IGF2, IGF2 mRNA levels were analyzed upon H19 depletion and overexpression. Interestingly, IGF2 was indeed upregulated upon H19 depletion and showed a nonsignificant trend towards downregulation upon H19 overexpression (Figure 21A&B). Previous studies showed that H19 global knockout mice were larger and heavier than WT littermates and this was supposedly due to the increased expression of IGF2<sup>197,198</sup>. Patients suffering from Beckwith-Wiedemann-Syndrome suffer from hypermethylation of the H19/IGF2 locus and increased IGF2 expression, which also leads to an overgrowth phenotype. The main function of IGF2 is to promote growth during gestation and in general, IGF2 has a growth promoting function. H19 depletion leads to more IGF2 in ECs and this should then promote growth. However, H19 depletion in ECs counteracts proliferation, so an effect of IGF2 is not likely. Furthermore, if H19 would have an effect on IGF2 *in cis*, this would take place in the nucleus. We do see effects of H19 depletion on IGF2 when we inhibit H19 with siRNAs, which should not alter nuclear H19 levels. IGF2 was previously shown to promote angiogenesis through upregulation of VEGF<sup>289</sup>. VEGFA was not regulated upon H19 depletion on mRNA level (Figure 21C). If IGF2 would regulate angiogenesis in ECs, VEGFA should be induced upon induction of IGF2 expression and we should see more angiogenesis upon H19 depletion. As this is not the case, these findings further support our hypothesis that the change in IGF2 expression upon H19 depletion does not play a role in ECs.

In summary, H19 does likely not sponge miRNAs in endothelial cells and its precursor-function for miR-675 is negligible. Furthermore, H19 likely does not act *in cis* in ECs, given the fact that its neighboring gene IGF2 is regulated upon H19 depletion, but targets of IGF2 are not.

## **5.6 H19 mainly exerts its functions *via* regulation of STAT3 activation**

Mechanistically, H19 depletion led to increased activity of STAT3 transcription factor, whereas H19 overexpression had the opposite effect (Figure 34B). STAT3 mRNA and protein levels were slightly increased, but STAT3 phosphorylation at tyrosine residue 705 was highly induced. Phosphorylation at TYR705 is required for STAT3 activation, indicating an induction of STAT3 activity upon H19 depletion. Phosphorylation at serine 727 was shown to enhance STAT3 transcriptional activity, but was not necessary for its function. STAT3 phosphorylation is mediated by janus kinase 2 (JAK2), but JAK2 protein expression was not altered upon H19 depletion, indicating another mechanism for the regulation of STAT3 activity (Figure 35). In order to prove that H19 exerts its function *via* STAT3 regulation, we used a small compound inhibitor for STAT3 activation to rescue the effects of H19.

Cryptotanshinone (CPT) binds directly to the phosphorylation site of STAT3 and thus blocks its activation. We hypothesize that when we block STAT3 activation and deplete H19 in HUVECs, the effect of H19 depletion should be abolished. CPT blocks the H19-depletion-induced phosphorylation of STAT3 (Figure 36A). Accordingly, the upregulation of p21, ICAM-1, VCAM-1, and HAS2 mRNA was abolished upon addition of CPT, which clearly indicates that the effect of H19 in ECs is dependent on STAT3 (Figure 36B, C&D). Furthermore, the anti-proliferative effect of H19 depletion was also abolished upon inhibition of STAT3 activation, further supporting the abovementioned hypothesis (Figure 37). Interestingly, the effect of H19 depletion on p16<sup>ink4A</sup> expression was not abolished upon inhibition of STAT3 activation, indicating that p16<sup>ink4A</sup> might not play a major role in loss of H19-induced premature senescence and that p21 upregulation is sufficient to induce senescence in ECs. This further supports the aforementioned hypothesis that p16<sup>ink4A</sup> upregulation upon H19 depletion is a secondary effect of the p21 induction.

STAT3 was previously shown to play a role in the cardiovascular system. Cardiomyocyte-specific deletion of STAT3 led to decreased myocardial capillary density and increased fibrosis in the adult heart of aging mice<sup>126</sup>. The authors did not identify single genes that were responsible for this effect, but microarray analysis revealed differentially regulated gene pathways, leading to a profibrotic and antiangiogenic state in STAT3 deficient cardiomyocytes<sup>126</sup>. Consistently, cardiomyocyte-specific STAT3 overexpression resulted in increased myocardial capillary density, most likely due to an increase in VEGF expression and secretion<sup>127</sup>. In regards to endothelium, conditioned medium from STAT3 deficient cardiomyocytes promoted endothelial cell apoptosis *in vitro*, indicating that STAT3 deletion results in the secretion of paracrine factors<sup>126</sup>. Mice with endothelial-specific STAT3 deletion did not show obvious vascular defects and *in vitro* tube formation was not affected<sup>284</sup>. However, upon lipopolysaccharide-induced shock, these mice showed increased inflammatory activation and leukocyte infiltration, and an increased and prolonged production of inflammatory cytokines, indicating a protective effect of endothelial STAT3 upon stress<sup>284</sup>. EC-specific STAT3 deletion did worsen lesion size and functional outcome in a model of cerebral ischemia, and the authors found an association of STAT3 deletion with antiangiogenic pathways<sup>290</sup>. The authors report an upregulation of the antiangiogenic factor Adamts9 upon STAT3 deletion, indicating a pro-angiogenic role for STAT3 in brain endothelium<sup>290</sup>. Upon H19 depletion, Adamts9 expression was significantly induced by 1.3-fold in HUVECs (data not shown), indicating that loss of H19-induced STAT3 activation might exert effects that are not in line with genetic STAT3 deletion. A study by Yahata *et al.* showed that mutated, and thus not active STAT3, inhibited migration and abolished VEGF-induced tube formation in human dermal microvascular endothelial cells, indicating that STAT3 is at least in parts a downstream target of VEGF<sup>290</sup>. In diverse human cancer cell lines, active STAT3 promoted tumor angiogenesis by upregulation of VEGF<sup>290</sup>.

These data in general indicate a protective and pro-angiogenic effect of STAT3. These data are in contrast to our findings that H19 depletion activates STAT3 and that this is responsible for upregulation of the cell cycle inhibitor p21 and adhesion molecules, which then has detrimental effects on the endothelium. The reason for these oppositional finding is unclear, but one can speculate that loss of H19-induced STAT3 activation functions different than for example virus-mediated STAT3 overexpression. Nearly all of the positive effects of STAT3 are due to upregulation of VEGF. As mentioned before, IGF2 was also shown to promote VEGF expression. But as H19 depletion failed to upregulate VEGF, one can speculate that depletion of H19 regulates VEGF independently of STAT3 or IGF2 through a yet to be identified pathway. However, a study that supports our theory that loss of H19-mediated STAT3 activation has detrimental effects on hallmarks of aging is by Tierney *et al.*, where they show that transient STAT3 inhibition enhanced tissue repair and promoted satellite cell expansion and therefore had positive effects in aged mice <sup>128</sup>. However, these data indicate that STAT3 might have different functions in different cell types.

How H19 regulates STAT3 expression and activation is currently unclear. LncRNAs were shown to directly bind proteins before. For example, TDP-43 was shown to be bound by NEAT1 and MALAT1 lncRNAs <sup>291</sup>. MALAT1 was furthermore shown to bind SR proteins and thereby influenced the localization and abundance of SR proteins in nuclear speckles <sup>292</sup>. Another study showed that the lncRNA Meg3 regulated PRC2 recruitment to the chromatin *via* direct interaction with JARID2 <sup>293</sup>. One can speculate that H19 also binds proteins directly. For example, H19 could potentially directly bind to the phosphorylation site of STAT3 and its depletion could therefore potentially be responsible for the increase in STAT3 phosphorylation. H19 could also block the STAT3 binding site at the gp130 receptor. The lncRNA NKILA was shown to directly block phosphorylation sites of NFκB and thereby inhibited NFκB activation <sup>286</sup>. And the finding that HULC lncRNA directly bound YB-1 and modulated YB-1 phosphorylation shows that lncRNAs can directly influence protein phosphorylation <sup>286</sup>. H19 not only influences pSTAT3 levels, but also total STAT3, so H19 might furthermore also control STAT3 transcriptional activation. A direct interaction between H19 and the STAT3 phosphorylating phosphokinase JAK2 also seems possible. JAK2 levels were not changed upon H19 depletion on protein levels, but this does not give evidence about direct interaction. H19 depletion upregulated IL-6 production in HUVECs and as STAT3 is a downstream-effector of IL-6 signaling, it is possible that STAT3 activation is increased due to the increase in IL-6 signaling. However, IL-6 is also a transcriptional target of STAT3, creating a feedback-loop for the whole pathway. LncRNAs were shown to possess multiple functions in cells and various mechanisms are possible behind the effects of H19 function in endothelial cells. RNA pulldown followed by mass spectrometry analysis would be the method of choice for identifying binding partners of H19 and to unravel the mechanism behind the H19-dependent modulation of STAT3 activation.

Taken together, our data show that loss of H19 promotes STAT3 activation. Loss of STAT3 in endothelial cells was shown to have detrimental effects *in vivo* before, but our results identify a different effect of activated STAT3. Inhibition of STAT3 activation abolished the effects of H19 depletion, clearly indicating that H19 functions through modulation of STAT3 activation in endothelial cells.

## 5.7 H19 overexpression partially confirms loss-of-function studies

Interestingly, lentivirus-mediated H19 overexpression failed to show the opposite effects of H19 depletion in some cases. Proliferation and expression of p16<sup>ink4A</sup> and p21 was not influenced upon overexpression of H19 (Figure 23C & Figure 26C). On the other hand, overexpression of human H19 was sufficient to rescue the impaired angiogenic capacity of aged endothelial cells in the aortic ring assay (Figure 28). The reasons for the lack of consistency with the loss of function studies is unclear. One can speculate that increasing H19 levels do not enhance proliferation because the cells already proliferate maximally. We analyzed H19 overexpression in HUVECs, which are neonatal cells that proliferate at high rates. Maybe overexpressing H19 in adult endothelial cells would have showed an effect. We furthermore used a lentivirus plasmid designed for protein overexpression because of the lack of other options. One may speculate that this plasmid might not be suitable for usage with noncoding RNAs. The plasmid adds a V5-tag to the transcript and usually the sequence is transcribed until the 3' long terminal repeat, meaning that the resulting transcript is much longer than the desired noncoding RNA sequence. For protein-coding genes this is not a problem, as there is a stop codon located immediately downstream of the V5-tag. However, for a lncRNA, elongation of the transcript may lead to a disturbed secondary and tertiary structure. Why H19 overexpression showed effects in some cases while it did not in others remains unclear. A possible explanation is that some H19 effects might depend on its primary sequence, which is unaltered upon lentiviral-mediated overexpression, while other effects might be dependent on H19 secondary or tertiary structure, which is supposedly disturbed. Another possible explanation for the partially functional overexpression of H19 is that lentiviral-mediated overexpression results in partially functional transcripts and that some processes are more sensitive to subtle changes in H19 abundance. Interestingly, in the case of the aortic ring experiment, lentiviral-mediated overexpression of human H19 was sufficient to rescue the impaired angiogenic capacity of aged mouse aortic rings, even though human and mouse H19 are not fully conserved on the primary sequence. Sequence conservation is poor with consistent similarities below 50%, but exon distribution and length are similar between humans and mice and H19 is also conserved in its locus. This indicates that lncRNAs

might be conserved on the secondary and tertiary structure level despite lacking primary sequence conservation.

## 5.8 Therapeutic perspectives of H19

From a therapeutic perspective, H19 might be beneficial for endothelial cells, as its loss has many detrimental effects. Although we did not analyze the effects of H19 overexpression *in vivo*, one can speculate that this might induce angiogenesis, reduce inflammatory activation and lower blood pressure. At the moment it is still complicated, if not impossible to overexpress transcripts in human patients. A study published by Cutler and colleagues showed cardiomyocyte-specific gene delivery in pigs using AAV9 virus and a catheter-based delivery<sup>286</sup>. Another study showed endothelial targeting *in vivo* by lentiviruses and functional gene expression under the control of a Tie2 promoter in mice<sup>286</sup>. A more recent study showed efficient targeting of brain microvasculature endothelial cells with a AAV2 virus in mice, indicating that endothelial cells can be targeted by viruses to induce gene overexpression<sup>286</sup>. If the problems with gene delivery *in vivo* are overcome, the induction of H19 expression would require a tight control mechanism and tissue specificity, as H19 was shown to promote the progression of many different cancers. Furthermore, STAT3 inhibition had detrimental effects in cardiomyocytes and endothelial cells, while, on the basis of this study, inhibition of STAT3 activation is expected to have positive effects in endothelial cells. It is unclear if H19 also regulates STAT3 activation in other cells than endothelial cells, but if this is the case, this would further support the need for a tight control of therapeutic H19 expression. Another drawback of the possible therapeutic use of H19 would be its effect on arteriogenesis. Endothelial-specific depletion of H19 enhanced collateral growth and its overexpression might have the opposite effect. Tissue-specific overexpression of genes *in vivo* can be achieved by different techniques at the moment. Virus-mediated targeted delivery and random integration into the genome or targeted integration by CRISPR/Cas are two examples. Both techniques are done in animal models, but are far from applications in humans. In summary, H19 might be a promising target for therapeutic approaches in specific diseases in the future, but researchers have to overcome many technological barriers before targeting H19 might be applicable.

## 5.9 Conclusion

Taken together, the loss of H19 has detrimental effects in the endothelium and affects two different hallmarks of aging. Loss of H19 leads to more senescence and thus reduced proliferation in human

primary endothelial cells from two different vascular beds. These findings are replicated *ex vivo* and *in vivo*, where depletion or knockout of H19 resulted in reduced angiogenic capacity. These effects are most likely mediated by upregulation of p21 and subsequent induction of p16<sup>ink4A</sup> upon H19 depletion, two cell cycle inhibitors that were shown to promote senescence. Loss of H19 also promotes endothelial inflammatory activation, where depletion of H19 leads to an increase in the expression of cell surface adhesion molecules. Subsequently, the adhesion of monocytes to endothelial cells was enhanced upon H19 depletion *in vitro* and the transmigration of leukocytes into subendothelial tissue was increased upon EC-specific H19 knockout *in vivo*. Furthermore, inflammatory activation of ECs repressed H19 expression, indicating that the loss of H19 favors a pro-inflammatory environment and this further represses H19 expression, leading to a constant low level inflammation, a condition that can be observed in elderly patients. Interestingly, EC-specific H19 knockout also increased the blood pressure in mice already 2 weeks after H19 knockout and elevated blood pressure is again a known feature of vascular aging. The effects of H19 are most likely mediated *via* suppression of STAT3 activation, as inhibition of STAT3 activation abolished the effects of H19 depletion. STAT3 overexpression was shown to have positive effects on the cardiovascular system before, but in the present study, the loss of H19-mediated activation of STAT3 had detrimental effects on the endothelium. These oppositional results are striking and the most likely explanation is that H19-mediated STAT3 activation has other effects than STAT3 overexpression due to yet to be identified mechanisms. These results show that H19 is an aging regulated lncRNA that regulates key endothelial functions *in vitro* and *in vivo*.

## 6. Summary

Cardiovascular disease is the leading cause of death worldwide. Aging is among the greatest risk factors for cardiovascular disease. Cardiovascular disease comprises several diseases, for example myocardial infarction, elevated blood pressure and stroke. Many processes are known to promote or worsen cardiovascular disease and in the present study, cellular senescence and inflammatory activation were of special interest, as they have a strong association to aging and can be seen as hallmarks of cellular aging.

Long noncoding RNAs (lncRNAs) are noncoding RNAs with a length of more than 200 nucleotides. In recent years, numerous regulatory functions were shown for these transcripts and lncRNAs were shown to directly interact with DNA, RNA and proteins. The long noncoding RNA H19 was among the first described noncoding RNAs and was initially shown to act as a tumor suppressor. More recently, several studies showed oncogenic roles for H19. In regards to the cardiovascular system, H19 was not analyzed before.

We show that H19 is the most profoundly downregulated lncRNA in endothelial cells of aged mice compared to young littermates. Microarray analysis of human primary endothelial cells upon pharmacological H19 depletion revealed an involvement of H19 in cell cycle regulation. Loss of H19 in human endothelial cells *in vitro* led to reduced proliferation and to increased senescence. H19 depletion was shown to counteract proliferation before, but none of the described mechanisms applied to endothelial cells. We show that the reduction in proliferative capacity and the pro-senescent function of H19 is most probably mediated by an upregulation of p16<sup>ink4A</sup> and p21 upon H19 depletion.

When we compared the angiogenic capacity of aortic endothelial cells from young and aged mice in an aortic ring assay, rings from aged mice showed a reduced cumulative sprout length. Interestingly, pharmacological inhibition of H19 in aortic rings of young animals, where H19 is highly expressed, was sufficient to reduce the cumulative sprout length to levels we observed from aged animals. Furthermore, overexpression of human H19 in aortic rings of aged mice, where H19 is poorly expressed, rescued the impaired angiogenic capacity of aged endothelial cells.

We generated inducible endothelial-specific H19 knockout mice (H19<sup>IEC-KO</sup>) and subjected these animals to hind limb ischemia surgery followed by perfusion analysis in the hind limbs by laser-doppler velocimetry and histological analysis. Perfusion in the operated hind limb was increased in H19<sup>IEC-KO</sup> compared to Ctrl littermates, which was in contrast to a reduction in capillary density in the operated hind limbs of H19<sup>IEC-KO</sup> animals compared to Ctrl littermates and to our previous results. Analysis of arteriogenesis revealed an increase in collateral growth upon EC-specific H19 depletion in the ischemic hind limbs, which explains the increase in perfusion despite the reduction in capillary



density. Further characterization of the animals revealed an increase in leukocyte infiltration into the tissue in the ischemic hind limbs upon endothelial-specific H19 depletion, indicating a potential role of H19 in inflammatory tissue activation.

Reanalysis of the microarray data from human primary endothelial cells upon H19 depletion revealed an association of H19 with inflammatory signaling and more specifically with IL-6/JAK2/STAT3 signaling. Analysis of cell surface adhesion molecule expression revealed an upregulation of ICAM-1 and VCAM-1 on mRNA level and an increase of the abundance of the two proteins on the cell surface of human primary endothelial cells. Consequently, adhesion of isolated human monocytes to human primary endothelial cells was increased upon H19 depletion *in vitro*. Interestingly, TNF- $\alpha$  mediated inflammatory activation of primary human endothelial cells repressed H19 expression. H19 did not function *via* previously described mechanisms. We excluded a competitive endogenous RNA (ceRNA) function for H19 in endothelial cells and showed that miR-675, which is processed from H19, does not play a role in the endothelium. Furthermore, H19 did not regulate previously described genes or pathways.

Analysis of transcription factor activity upon H19 depletion and overexpression revealed a differential activity of STAT3. STAT3 phosphorylation at TYR705 and thus activation was increased upon H19 depletion. Inhibition of STAT3 activation using a small compound inhibitor abolished the effects of H19 depletion on mRNA expression of p21, ICAM-1 and VCAM-1 and on proliferation, indicating that the effects of H19 are at least partially mediated *via* STAT3. STAT3 was shown to have positive effects on the cardiovascular system before, most likely due to upregulation of VEGF in a STAT3-dependent manner. We were not able to confirm previously described mechanisms for STAT3 in the present study and propose a new mechanism of action for the H19-dependent regulation of STAT3. Taken together, these results identify the long noncoding RNA H19 as a pivotal regulator of endothelial cell function. Figure 38 summarizes the described functions of H19 in endothelial cells.

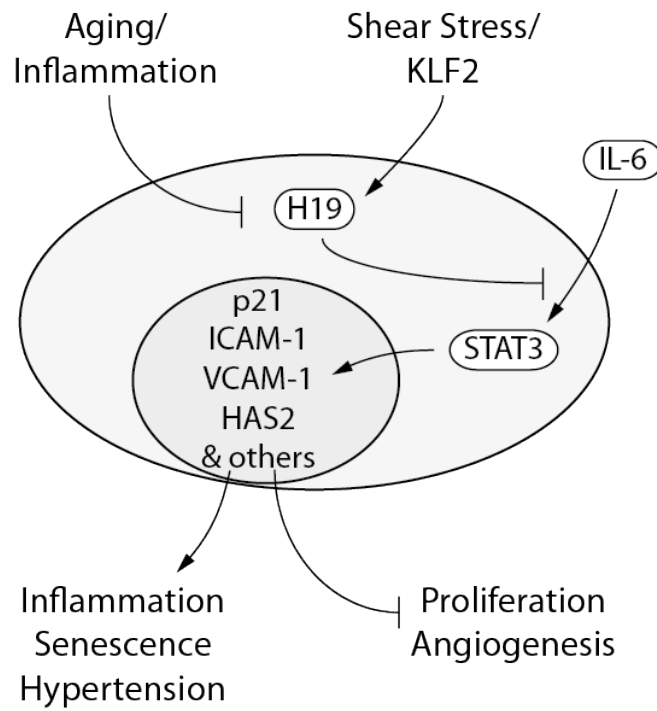


**Figure 38: Summary of the described functions of H19 in endothelial cells. H19 expression is repressed with aging and inflammation and induced with shear stress *via* KLF2. H19 modulates STAT3 activation and regulates several genes in a STAT3-dependent manner. Loss of H19 leads to increased inflammation and cellular senescence, and hypertension. Loss of H19 reduces proliferation and angiogenesis.**

## 7. Zusammenfassung

Das menschliche kardiovaskuläre System besteht aus dem Herz und allen Blutgefäßen des Körpers. Sauerstoffreiches Blut wird aus dem linken Ventrikel über die Aorta in den Körperkreislauf gepumpt. Dort findet in den Kapillaren der Gas- und Nährstoffaustausch statt. Durch Venen fließt das nun sauerstoffarme und CO<sub>2</sub>-reiche Blut zurück zum Herzen und wird über das rechte Atrium und Ventrikel in den Lungenkreislauf gepumpt in welchem erneut ein Gasaustausch stattfindet. Sauerstoffreiches Blut fließt nun zurück über das linke Atrium in das linke Ventrikel, von wo es erneut in den Körperkreislauf gelangt. Endothelzellen bilden die innerste Schicht von Blutgefäßen und sind die einzigen Körperzellen, welche in konstantem Kontakt mit Blut stehen.

Kardiovaskuläre Erkrankungen sind die Haupttodesursache weltweit. Laut statistischem Bundesamt resultierten 2014 39% aller Todesfälle in Deutschland aus Erkrankungen des Herz-Kreislauf-Systems. Neben beeinflussbaren Risikofaktoren wie Diabetes oder Übergewicht zählt fortschreitendes Alter zu den nicht-beeinflussbaren Hauptrisikofaktoren für kardiovaskuläre Erkrankungen. Mit fortschreitendem Alter steigt das Risiko an einer Erkrankung des Herz- Kreislaufsystems zu sterben kontinuierlich. Die Bezeichnung kardiovaskuläre Erkrankung umfasst eine Reihe verschiedener Krankheitsbilder, wie zum Beispiel Hypertonie, Myokardinfarkt oder Apoplex. Der Begriff Altern beschreibt die kontinuierlich schlechter werdende Reaktion eines Organismus auf externe Stressfaktoren und eine generelle Abnahme der Fitness. Während seiner Lebensdauer ist ein Organismus unumgänglich Faktoren ausgesetzt, die Schäden auf verschiedenen Ebenen verursachen. Der menschliche Körper ist mit einer Vielzahl von Reparaturmechanismen ausgestattet um Schäden auf molekularer Ebene zu reparieren. Jeder Reparaturmechanismus ist anfällig für Fehler und dies führt zu einer Ansammlung von Schäden mit zunehmendem Alter eines Organismus. Alterung der Blutgefäße ist durch eine Verdickung der Intima, genereller Dysfunktion des Endothels und chronischer vaskulärer inflammatorischer Aktivierung charakterisiert. Diese Veränderungen der Blutgefäße können in erhöhtem Blutdruck und/oder Atherosklerose resultieren. Verschiedenste Faktoren können kardiovaskuläre Erkrankungen begünstigen oder verschlimmern, in der vorliegenden Arbeit waren vor allem zelluläre Seneszenz und inflammatorische Aktivierung von Interesse, da diese beiden zellulären Prozesse eine wichtige Rolle während des Alterungsprozesses spielen und zusätzlich als Meilensteine zellulärer Alterung angesehen werden.

Durch die Arbeit des humanen Genom Projekts und einer Vielzahl an Verbesserungen der Technik konnte in der vergangenen Dekade nachgewiesen werden, dass circa 80% des humanen Genoms transkribiert, jedoch nur circa 3% des Transkriptoms translatiert werden. Während das nicht-kodierende Transkriptom lange als nicht funktionell angesehen wurde, konnten in den letzten Jahren eine Vielzahl an Funktionen von nicht-kodierenden RNAs nachgewiesen werden. Die sehr heterogene

Bezeichnung nicht-kodierende RNAs umfasst eine Vielzahl von Transkripten, wie zum Beispiel miRNAs, tRNAs, rRNA und lange nicht-kodierende RNAs. Lange nicht-kodierende RNAs sind definiert als nicht-kodierende RNA Moleküle mit einer Länge von mehr als 200 Nukleotiden. In den vergangenen Jahren wurden zahlreiche Funktionen von langen nicht-kodierenden RNAs untersucht und hierbei konnten direkte Interaktionen mit DNA, RNA und Proteinen nachgewiesen werden. Die lange nicht-kodierende RNA H19 war eine der ersten beschriebenen nicht-kodierenden RNAs. H19 liegt im humanen Genom auf Chromosom 15 innerhalb einer Region starker genomischer Prägung. H19 wird nur vom maternalen Allel transkribiert, während das oberhalb gelegene Gen Insulin Growth Factor 2 (IGF2) nur vom paternalen Allel transkribiert wird. H19 und IGF2 sind mit zwei Krankheitsbildern assoziiert, Beckwith-Wiedemann Syndrom (BWS) und Russel-Silver Syndrom (RSS). BWS Patienten leiden an einem verstärkten Wachstum einzelner Körperteile oder des gesamten Körpers. Dies ist auf die Hypermethylierung des IGF2/H19 Locus zurückzuführen, was zur biallelischen Expression von IGF2 führt. RSS Patienten zeigen ein vermindertes Wachstum, was auf dem Fehlen der Methylierung des IGF2/H19 Clusters und dem damit verbundenen Fehlen der Expression von IGF2 beruht.

H19 wurde initial als Tumor-Suppressor beschrieben. In den vergangenen zehn Jahren veröffentlichte Studien deuten jedoch verstärkt auf eine Rolle als Onkogen in verschiedensten Krebsarten hin. Es wurde gezeigt dass die Präsenz von H19 in vielen Krebsarten das Tumorstadium, sowie die Infiltration und Metastasenbildung begünstigt. Eine Rolle von H19 im kardiovaskulären System wurde bisher noch nicht beschrieben.

Das Ziel der vorliegenden Arbeit war einerseits zu zeigen, dass H19 mit dem Alter in Endothelzellen reguliert ist und andererseits den Einfluss von H19 auf das Altern von Endothelzellen zu untersuchen. In der vorliegenden Arbeit wird gezeigt, dass H19 eine der am stärksten herunterregulierte lange nicht-kodierende RNA im Endothel von alten Mäusen ist. Die Analyse von humanen primären Endothelzellen, in welchen H19 pharmakologisch inhibiert wurde, mittels Mikroarray, belegte eine Regulation des Zellzyklus durch H19. Die Inhibition von H19 führte zu einer Herunterregulation vieler an der Proliferation beteiligten Signalwege. In funktionalen Versuchen konnte gezeigt werden, dass die Depletion von H19 in humanen primären Endothelzellen Proliferation verlangsamt und zelluläre Seneszenz begünstigt. In anderen Studien wurde bereits gezeigt, dass die Depletion von H19 Proliferation verlangsamt, jedoch konnten wir keinen der bisher gezeigten Mechanismen im Endothel nachweisen. Wir zeigen, dass der anti-proliferative und pro-seneszenz Effekt der Depletion von H19 höchstwahrscheinlich auf eine Induktion der Expression der Zellzyklus regulierenden Gene p16<sup>ink4A</sup> und p21 zurückzuführen ist. Zelluläre Seneszenz wird durch zwei verschiedene Signalwege aktiviert, durch den p53-p21 und den p16<sup>ink4A</sup>-pRB Signalweg. Beide Signalwege reagieren auf DNA-Schäden. Nach Schädigung der DNA wird p53 aktiviert und stabilisiert. p21 ist im Hinblick auf Seneszenz das

wichtigste transkriptionelle Ziel von p53. p21 inhibiert die Aktivität von allen Mitglieder der Cyclin/CDK Familie <sup>67</sup>. Die Aktivierung von p21 inhibiert die Progression von G1 in die S-Phase während des Zellzyklus <sup>68</sup>. Die Aktivierung von p16<sup>ink4A</sup> inhibiert die Kinasen CDK4 und CDK6. Diese Inhibierung sorgt für eine reduzierte Phosphorylierung von Retinoblastoma Protein (pRB) und dadurch zu einer Inhibierung des Zellzyklus in der G1 Phase <sup>64,65</sup>. Wir zeigen, dass die Depletion von H19 beide Seneszenz-aktivierenden Signalwege durch die Steigerung der Expression von p16<sup>ink4A</sup> und p21 aktiviert. Es wurde bereits gezeigt, dass die Hochregulation von p21 ausreicht, um Seneszenz zu aktivieren und dass dies zu einer Hochregulation von p16<sup>ink4A</sup> führt. Die verstärkte Expression von p16<sup>ink4A</sup> könnte daher potentiell ein sekundärer Effekt der verstärkten Expression von p21 sein.

Die weitere Analyse der Ergebnisse des Microarrays zeigte eine Hochregulation der beiden Proteine Lysozym (LYZ) und Hyaluron Synthase 2 (HAS2). Lysozym ist Teil der Immunantwort auf bakterielle Infektionen und hydrolysiert  $\beta$ -1,4-glycosidische Bindungen in bakteriellen Zellmembranen. Lysozym wurde allerdings auch beschrieben den Abbau von *advanced glycation end products* (AGEs) in diabetischer Nephropathie zu begünstigen und dabei die Ausschüttung von AGE-induziertem Interleukin-6 zu reduzieren <sup>265</sup>. Des Weiteren wurde gezeigt, dass Lysozym eine Rolle bei der Calcifizierung von Knorpelgewebe spielt, am wahrscheinlichsten durch eine Interaktion mit Hyaluronsäure <sup>267</sup>. Interessanterweise war Hyaluronsäure-Synthase 2 (HAS2) das am zweitstärksten hochregulierte Gen nach H19 Depletion. HAS2 produziert die in der extrazellulären Matrix vorkommende Hyaluronsäure. Eine verstärkte Ansammlung von Hyaluronsäure wurde in atherosklerotischen Plaques beschrieben und es wurde gezeigt, dass Hyaluronsäure während der Entstehung von atherosklerotischen Plaques vor allem von glatten Muskelzellen produziert wird <sup>268,269</sup>. Es wurde gezeigt, dass Endothelzellen unter inflammatorischer Aktivierung Hyaluronsäure produzieren und dass dies die Rekrutierung von Immunzellen verstärkt <sup>272,273</sup>. HAS2 überexprimierende Mäuse zeigten eine erhöhte Gefäßsteifheit und, gekreuzt mit ApoE Tieren, eine erhöhte Bildung von atherosklerotischen Plaques in der Aorta <sup>274</sup>. Im humanen kardiovaskulären System zeigten Blutgefäße von gealterten Patienten einen erhöhten Anteil an Hyaluronsäure in der extrazellulären Matrix <sup>276–280</sup>. Wir konnten des Weiteren zeigen, dass die Regulation von HAS2 durch H19 abhängig von STAT3 ist. Diese Ergebnisse deuten darauf hin, dass H19 potentiell am Umbau der extrazellulären Matrix beteiligt ist.

Um weiter zu analysieren welche physiologische Rolle H19 spielt, untersuchten wir die Rolle von H19 in einem *ex vivo* Modell. Mittels eines *ex vivo* Versuchs mit aortischen Ringen von jungen und alten Mäusen konnten wir zeigen, dass die angiogene Kapazität von Endothelzellen aus gealterten Tieren im Vergleich zu jungen Tieren reduziert ist. Die pharmakologische Inhibierung von H19 in aortischen Ringen aus jungen Mäusen, in welchen H19 hoch exprimiert ist, reichte aus um deren Gesamtaussprosslänge auf ein Niveau zu reduzieren, welches wir bei aortischen Ringen aus

gealterten Tieren beobachten konnten. Die lentivirale Überexpression des humanen H19 Transkripts in aortischen Ringen von gealterten Tieren war ausreichend, um die Gesamtausprosslänge nahezu auf das Niveau von jungen Tieren anzuheben.

Wir generierten induzierbare endothelspezifische H19 knockout Mäuse (H19<sup>IEC-KO</sup>) und unterzogen diese Tiere einem Hinterlaufischämie-Experiment. Die Durchblutung der Hinterläufe wurde mittels Laser-Doppler Velozitätsmessung untersucht und das Gewebe anschließend histologisch charakterisiert. Die Durchblutung der operierten Hinterläufe war in den H19<sup>IEC-KO</sup> Tieren im Vergleich zu Kontrolltieren erhöht. Im Gegensatz dazu zeigte sich in der histologischen Untersuchung eine Verminderung der Kapillardichte in den operierten Beinen der H19<sup>IEC-KO</sup> Tiere. Weitere histologische Untersuchungen zeigten, dass im Vergleich zu Kontrolltieren in den ischämischen Hinterläufen der H19<sup>IEC-KO</sup> Tieren vermehrt große, mit glatten Muskelzellen ummantelte Blutgefäße vorkamen. Dies erklärt die verstärkte Durchblutung der Hinterläufe bei gleichzeitiger Verminderung der Kapillardichte der H19<sup>IEC-KO</sup> Tiere. Des Weiteren zeigte sich eine verstärkte Infiltration von Leukozyten in das Gewebe der operierten Beine der H19<sup>IEC-KO</sup> Tiere, was auf die Zunahme von inflammatorischer Aktivierung des Gewebes hinweist. Bei weiteren Untersuchungen stellten wir außerdem eine signifikante Erhöhung des systolischen Blutdrucks der H19<sup>IEC-KO</sup> Tiere fest. Wie bereits vorher beschrieben führte die Depletion von H19 zu einer Zunahme der Expression von HAS2. Die erhöhte Präsenz der Hyaluronsäure in der extrazellulären Matrix von Blutgefäßen in Mäusen führte zu einer erhöhten Steifheit der Blutgefäße<sup>274</sup>. Potenziell könnte die Abwesenheit von H19 im Endothel dazu führen, dass mehr Hyaluronsäure gebildet und in die extrazelluläre Matrix transportiert wird. Dies könnte zu einer erhöhten Steifheit der Blutgefäße führen und demnach den gesteigerten Blutdruck erklären. Der exakte Mechanismus bedarf allerdings noch weiterer Experimente.

Die erneute Analyse des Microarrays aus humanen primären Endothelzellen nach H19 Depletion zeigte eine Assoziation von H19 mit inflammatorischen Signalwegen und mehr detailliert mit dem IL-6/JAK2/STAT3 Signalweg. Weitere Experimente belegten eine Zunahme der mRNA Expression der Adhäsionsmoleküle ICAM-1 und VCAM-1, sowie eine verstärkte Präsentation der beiden Proteine auf der Zelloberfläche von humanen primären Endothelzellen. Adhäsionsmoleküle auf der Oberfläche von Endothelzellen binden im Blut zirkulierende Leukozyten. Gebundene Leukozyten migrieren durch die Endothelzellschicht in das darunter befindliche Gewebe. Dieser Mechanismus spielt zum Beispiel bei der Entstehung von Atherosklerose eine wichtige Rolle. Die Adhäsion von isolierten humanen Monozyten auf primären humanen Endothelzellen war nach H19 Inhibition ebenfalls erhöht. Interessanterweise verminderte die inflammatorische Aktivierung von Endothelzellen mittels TNF- $\alpha$  die Expression von H19. Hypothetisch führt die Herunterregulation von H19 im Alter zur verstärkten inflammatorischen Aktivierung des Gewebes. Die verstärkte inflammatorische Aktivierung inhibiert wiederum die Expression von H19, was zu einer Verstärkung des Effekts beiträgt und theoretisch zur

dauerhaften geringfügigen inflammatorischen Aktivierung des Gewebes sorgt. Eine geringfügige inflammatorische Aktivierung des Endothels lässt sich üblicherweise in älteren Patienten beobachten.

Ein Reporter-Assay für die Aktivität von Transkriptionsfaktoren zeigte eine gesteigerte Aktivität des Transkriptionsfaktor Signal Transducer and Activator of Transcription 3 (STAT3) nach H19 Inhibierung und eine verminderte Aktivität nach H19 Überexpression. Die pharmakologische Inhibierung von H19 in primären humanen Endothelzellen führte zur Zunahme der Phosphorylierung von STAT3 an Tyrosin 705 und so zu einer gesteigerten Aktivität des Transkriptionsfaktors. STAT3 wird von der Phosphokinase Janus Kinase 2 (JAK2) an Tyrosin 705 phosphoryliert. Die Aktivierung dieses Signalweges erfolgt über extrazelluläres Interleukin-6 (IL-6), welches an den zellmembranständigen Interleukin-6 Rezeptor (IL-6R) bindet. Die Bindung von IL-6 an IL-6R induziert die Homodimerisierung von gp130 Rezeptormolekülen in der Zellmembran. Dies führt zur Phosphorylierung von JAK2, welche wiederum das gp130 Homodimer phosphoryliert. Die Phosphorylierung von gp130 führt zur Rekrutierung von monomerem STAT3 an den gp130 Rezeptor. Gebundenes STAT3 wird durch JAK2 an Tyrosin 705 phosphoryliert. Dies führt zur Dimerisierung von STAT3 und zur Translokation in den Nukleus, in welchem STAT3 als Transkriptionsfaktor für verschiedene Gene fungiert. Es wurde bereits gezeigt, dass STAT3 positive Effekte auf das kardiovaskuläre System hat. Kardiomyozyten-spezifische STAT3 Überexpression führte zur Zunahme der Kapillarisation des Myokards in Mäusen <sup>126</sup>. Die endothel-spezifische Deletion von STAT3 führte zu keinem Effekt in Bezug auf Angiogenese, führte jedoch unter Stressbedingungen zu einer deutlich erhöhten und verlängerten inflammatorischen Aktivierung des Endothels <sup>284</sup>. Um zu zeigen, dass die Effekte von H19 im Endothel durch die Modulation der STAT3 Aktivierung hervorgerufen wird, benutzten wir einen chemischen Inhibitor für die Aktivierung von STAT3. Cryptothanshinone (CPT) blockiert die Phosphorylierungsstelle an Tyrosin 705 und verhindert damit die Aktivierung von STAT3. Wir konnten zeigen, dass die Inhibition der Aktivierung von STAT3 mittels CPT den Effekt der Inhibition von H19 auf die mRNA Expression von p21, ICAM-1 und VCAM-1 aufhob. Ebenso zeigte sich unter Inhibition der STAT3 Aktivierung und Depletion von H19 kein Effekt in der Proliferation von Endothelzellen. Diese Daten zeigen, dass H19 im Endothel über die Modulation der Aktivierung von STAT3 funktioniert.

Zusammenfassend zeigen diese Daten, dass die lange nicht-kodierende RNA H19 wichtige Funktionen von Endothelzellen reguliert. Die pharmakologische Inhibition von H19 in Endothelzellen führte zu einer Verringerung der Proliferation und zu mehr Seneszenz. Diese beiden Effekte wurden höchstwahrscheinlich durch die Hochregulation der beiden den Zellzyklus inhibierenden Proteine p16<sup>ink4A</sup> und p21 hervorgerufen. Des Weiteren resultierte die Depletion von H19 in der Induktion der Expression der Hyaluron Synthase 2, welche potentiell eine Rolle in der Umgestaltung der extrazellulären Matrix spielt. Die Inhibition von H19 führte außerdem zu einer verstärkten

inflammatorischen Aktivierung von Endothelzellen und zur verstärkten Adhäsion von Monozyten an Endothelzellen. *In vivo* resultierte der Endothelspezifische Verlust von H19 in einer verringerten Kapillardichte im Hinterlauf von Mäusen nach Hinterlauf Ischämie Experiment. Im gleichen Experiment konnten wir eine verstärkte Infiltration von Leukozyten in das Gewebe der endothelspezifischen H19 KO Mäuse beobachten. Des Weiteren führte der endothelspezifische H19 Knockout zu einem gesteigerten systolischen Blutdruck. Diese Daten zeigen, dass H19 einen interessanten Beitrag zur Pathophysiologie von Herz- Kreislauferkrankungen leistet.



## 8. References

1. Adams, R. H. & Alitalo, K. Molecular regulation of angiogenesis and lymphangiogenesis. *Nat. Rev. Mol. Cell Biol.* **8**, 464–478 (2007).
2. Jussila, L. & Alitalo, K. Vascular Growth Factors and Lymphangiogenesis. *Physiol. Rev.* **82**, 673–700 (2002).
3. Jain, R. K. Molecular regulation of vessel maturation. *Nat. Med.* **9**, 685–693 (2003).
4. Potente, M., Gerhardt, H. & Carmeliet, P. Basic and Therapeutic Aspects of Angiogenesis. *Cell* **146**, 873–887 (2011).
5. Carmeliet, P. Angiogenesis in health and disease. *Nat. Med.* **9**, 653–660 (2003).
6. Carmeliet, P. Manipulating angiogenesis in medicine. *J. Intern. Med.* **255**, 538–561 (2004).
7. Gerhardt, H. & Betsholtz, C. Endothelial-pericyte interactions in angiogenesis. *Cell Tissue Res.* **314**, 15–23 (2003).
8. Phng, L.-K. & Gerhardt, H. Angiogenesis: A Team Effort Coordinated by Notch. *Dev. Cell* **16**, 196–208 (2009).
9. Doddaballapur, A. *et al.* Laminar Shear Stress Inhibits Endothelial Cell Metabolism via KLF2-Mediated Repression of PFKFB3. *Arterioscler. Thromb. Vasc. Biol.* **35**, 137–145 (2015).
10. Geudens, I. & Gerhardt, H. Coordinating cell behaviour during blood vessel formation. *Development* **138**, (2011).
11. De Bock, K. *et al.* Role of PFKFB3-Driven Glycolysis in Vessel Sprouting. *Cell* **154**, 651–663 (2013).
12. Dekker, R. J. *et al.* Prolonged fluid shear stress induces a distinct set of endothelial cell genes, most specifically lung Krüppel-like factor (KLF2). *Blood* **100**, 1689–98 (2002).
13. Chistiakov, D. A., Orekhov, A. N. & Bobryshev, Y. V. Effects of shear stress on endothelial cells: go with the flow. *Acta Physiol.* (2016). doi:10.1111/apha.12725
14. Dekker, R. J. *et al.* Endothelial KLF2 links local arterial shear stress levels to the expression of vascular tone-regulating genes. *Am. J. Pathol.* **167**, 609–18 (2005).

15. SenBanerjee, S. *et al.* KLF2 Is a novel transcriptional regulator of endothelial proinflammatory activation. *J. Exp. Med.* **199**, 1305–15 (2004).
16. Bhattacharya, R. *et al.* Inhibition of Vascular Permeability Factor/Vascular Endothelial Growth Factor-mediated Angiogenesis by the Kruppel-like Factor KLF2. *J. Biol. Chem.* **280**, 28848–28851 (2005).
17. Armulik, A., Abramsson, A. & Betsholtz, C. Endothelial/Pericyte Interactions. *Circ. Res.* **97**, 512–523 (2005).
18. Francavilla, C., Maddaluno, L. & Cavallaro, U. The functional role of cell adhesion molecules in tumor angiogenesis. *Semin. Cancer Biol.* **19**, 298–309 (2009).
19. Nigro, P., Abe, J.-I. & Berk, B. C. Flow shear stress and atherosclerosis: a matter of site specificity. *Antioxid. Redox Signal.* **15**, 1405–14 (2011).
20. Malek, A. M., Alper, S. L. & Izumo, S. Hemodynamic shear stress and its role in atherosclerosis. *JAMA* **282**, 2035–42 (1999).
21. Zhou, J., Li, Y.-S. & Chien, S. Shear stress-initiated signaling and its regulation of endothelial function. *Arterioscler. Thromb. Vasc. Biol.* **34**, 2191–8 (2014).
22. Cunningham, K. S. & Gotlieb, A. I. The role of shear stress in the pathogenesis of atherosclerosis. *Lab. Investig.* **85**, 9–23 (2005).
23. Dekker, R. J. *et al.* Prolonged fluid shear stress induces a distinct set of endothelial cell genes, most specifically lung Kruppel-like factor (KLF2). *Blood* **100**, 1689–1698 (2002).
24. Huddleson, J. P., Ahmad, N., Srinivasan, S. & Lingrel, J. B. Induction of KLF2 by Fluid Shear Stress Requires a Novel Promoter Element Activated by a Phosphatidylinositol 3-Kinase-dependent Chromatin-remodeling Pathway. *J. Biol. Chem.* **280**, 23371–23379 (2005).
25. Parmar, K. M. *et al.* Integration of flow-dependent endothelial phenotypes by Kruppel-like factor 2. *J. Clin. Invest.* **116**, 49–58 (2006).
26. Lin, Z. *et al.* Kruppel-Like Factor 2 (KLF2) Regulates Endothelial Thrombotic Function. *Circ. Res.* **96**, e48–e57 (2005).
27. Dekker, R. J. *et al.* KLF2 provokes a gene expression pattern that establishes functional quiescent differentiation of the endothelium. *Blood* **107**, 4354–4363 (2006).

28. Lin, Z., Hamik, A., Jain, R., Kumar, A. & Jain, M. K. Kruppel-like factor 2 inhibits protease activated receptor-1 expression and thrombin-mediated endothelial activation. *Arterioscler. Thromb. Vasc. Biol.* **26**, 1185–9 (2006).
29. Hahn, C. & Schwartz, M. A. Mechanotransduction in vascular physiology and atherogenesis. *Nat. Rev. Mol. Cell Biol.* **10**, 53–62 (2009).
30. Epstein, F. H. & Ross, R. Atherosclerosis — An Inflammatory Disease. *N. Engl. J. Med.* **340**, 115–126 (1999).
31. Moore, K. J. & Tabas, I. Macrophages in the Pathogenesis of Atherosclerosis. *Cell* **145**, 341–355 (2011).
32. Kwon, G. P., Schroeder, J. L., Amar, M. J., Remaley, A. T. & Balaban, R. S. Contribution of Macromolecular Structure to the Retention of Low-Density Lipoprotein at Arterial Branch Points. *Circulation* **117**, 2919–2927 (2008).
33. Weber, C. & Noels, H. Atherosclerosis: current pathogenesis and therapeutic options. *Nat. Med.* **17**, 1410–1422 (2011).
34. Ross, R. & Glomset, J. A. The Pathogenesis of Atherosclerosis. *N. Engl. J. Med.* **295**, 369–377 (1976).
35. Hartman, J. & Frishman, W. H. Inflammation and atherosclerosis: a review of the role of interleukin-6 in the development of atherosclerosis and the potential for targeted drug therapy. *Cardiol. Rev.* **22**, 147–51
36. Cybulsky, M. I. *et al.* A major role for VCAM-1, but not ICAM-1, in early atherosclerosis. *J. Clin. Invest.* **107**, 1255–1262 (2001).
37. Ridker, P. M., Hennekens, C. H., Roitman-Johnson, B., Stampfer, M. J. & Allen, J. Plasma concentration of soluble intercellular adhesion molecule 1 and risks of future myocardial infarction in apparently healthy men. *Lancet* **351**, 88–92 (1998).
38. Blankenberg, S. *et al.* Circulating cell adhesion molecules and death in patients with coronary artery disease. *Circulation* **104**, 1336–42 (2001).
39. Hansson, G. K. & Hermansson, A. The immune system in atherosclerosis. *Nat. Immunol.* **12**, 204–212 (2011).

40. Gu, L. *et al.* Absence of monocyte chemoattractant protein-1 reduces atherosclerosis in low density lipoprotein receptor-deficient mice. *Mol. Cell* **2**, 275–81 (1998).
41. Hansson, G. K. Inflammation, Atherosclerosis, and Coronary Artery Disease. *N. Engl. J. Med.* **352**, 1685–1695 (2005).
42. Sun, J. *et al.* Mast cells promote atherosclerosis by releasing proinflammatory cytokines. *Nat. Med.* **13**, 719–724 (2007).
43. Libby, P. *et al.* Requiem for the ‘vulnerable plaque’. *Eur. Heart J.* **6**, ehv349 (2015).
44. Libby, P. Mechanisms of Acute Coronary Syndromes and Their Implications for Therapy. *N. Engl. J. Med.* **368**, 2004–2013 (2013).
45. Libby, P. How does lipid lowering prevent coronary events? New insights from human imaging trials. *Eur. Heart J.* **36**, 472–4 (2015).
46. Underhill, H. R. *et al.* Effect of rosuvastatin therapy on carotid plaque morphology and composition in moderately hypercholesterolemic patients: A high-resolution magnetic resonance imaging trial. *Am. Heart J.* **155**, 584.e1-584.e8 (2008).
47. Fuster, J. J. *et al.* Clonal hematopoiesis associated with TET2 deficiency accelerates atherosclerosis development in mice. *Science* **355**, 842–847 (2017).
48. Lakatta, E. G. & Levy, D. Arterial and cardiac aging: major shareholders in cardiovascular disease enterprises: Part I: aging arteries: a ‘set up’ for vascular disease. *Circulation* **107**, 139–46 (2003).
49. Zuliani, G. *et al.* Insulin resistance and systemic inflammation, but not metabolic syndrome phenotype, predict 9 years mortality in older adults. *Atherosclerosis* **235**, 538–45 (2014).
50. Wang, L. *et al.* Integrin-YAP/TAZ-JNK cascade mediates atheroprotective effect of unidirectional shear flow. *Nature* **540**, 579–582 (2016).
51. Pepine, C. J. The effects of angiotensin-converting enzyme inhibition on endothelial dysfunction: potential role in myocardial ischemia. *Am. J. Cardiol.* **82**, 23S–27S (1998).
52. Dillin, A., Gottschling, D. E. & Nyström, T. The good and the bad of being connected: the integrons of aging. *Curr. Opin. Cell Biol.* **26**, 107–112 (2014).

53. Ren, J.-L., Pan, J.-S., Lu, Y.-P., Sun, P. & Han, J. Inflammatory Signaling and Cellular Senescence. *Cell Signal*. **21**, 378–383 (2009).
54. Baylis, D., Bartlett, D. B., Patel, H. P. & Roberts, H. C. Understanding how we age: insights into inflammaging. *Longev. Heal.* **2**, 8 (2013).
55. Fagiolo, U. *et al.* Increased cytokine production in mononuclear cells of healthy elderly people. *Eur. J. Immunol.* **23**, 2375–2378 (1993).
56. Franceschi, C. *et al.* Inflammaging and anti-inflammaging: A systemic perspective on aging and longevity emerged from studies in humans. *Mech. Ageing Dev.* **128**, 92–105 (2007).
57. De Martinis, M., Franceschi, C., Monti, D. & Ginaldi, L. Inflamm-aging and lifelong antigenic load as major determinants of ageing rate and longevity. *FEBS Lett.* **579**, 2035–2039 (2005).
58. HAYFLICK, L. & MOORHEAD, P. S. The serial cultivation of human diploid cell strains. *Exp. Cell Res.* **25**, 585–621 (1961).
59. Bodnar, A. G. *et al.* Extension of life-span by introduction of telomerase into normal human cells. *Science* **279**, 349–52 (1998).
60. Fagagna, F. d'Adda di *et al.* A DNA damage checkpoint response in telomere-initiated senescence. *Nature* **426**, 194–198 (2003).
61. Herbig, U., Jobling, W. A., Chen, B. P. C., Chen, D. J. & Sedivy, J. M. Telomere shortening triggers senescence of human cells through a pathway involving ATM, p53, and p21(CIP1), but not p16(INK4a). *Mol. Cell* **14**, 501–13 (2004).
62. Alimonti, A. *et al.* A novel type of cellular senescence that can be enhanced in mouse models and human tumor xenografts to suppress prostate tumorigenesis. *J. Clin. Invest.* **120**, 681–693 (2010).
63. Michaloglou, C. *et al.* BRAFE600-associated senescence-like cell cycle arrest of human naevi. *Nature* **436**, 720–4 (2005).
64. Sharpless, N. E. *et al.* Loss of p16Ink4a with retention of p19Arf predisposes mice to tumorigenesis. *Nature* **413**, 86–91 (2001).
65. Kamijo, T., Bodner, S., van de Kamp, E., Randle, D. H. & Sherr, C. J. Tumor spectrum in ARF-deficient mice. *Cancer Res.* **59**, 2217–22 (1999).

66. Childs, B. G., Baker, D. J., Kirkland, J. L., Campisi, J. & van Deursen, J. M. Senescence and apoptosis: dueling or complementary cell fates? *EMBO Rep.* **15**, 1139–53 (2014).
67. Xiong, Y. *et al.* p21 is a universal inhibitor of cyclin kinases. *Nature* **366**, 701–704 (1993).
68. Rodriguez, R. & Meuth, M. Chk1 and p21 cooperate to prevent apoptosis during DNA replication fork stress. *Mol. Biol. Cell* **17**, 402–12 (2006).
69. Stein, G. H., Drullinger, L. F., Soulard, A. & Dulić, V. Differential roles for cyclin-dependent kinase inhibitors p21 and p16 in the mechanisms of senescence and differentiation in human fibroblasts. *Mol. Cell. Biol.* **19**, 2109–17 (1999).
70. Kim, W. Y. & Sharpless, N. E. The Regulation of INK4/ARF in Cancer and Aging. *Cell* **127**, 265–275 (2006).
71. Chicas, A. *et al.* Dissecting the Unique Role of the Retinoblastoma Tumor Suppressor during Cellular Senescence. *Cancer Cell* **17**, 376–387 (2010).
72. Kurz, D. J., Decary, S., Hong, Y. & Erusalimsky, J. D. Senescence-associated (beta)-galactosidase reflects an increase in lysosomal mass during replicative ageing of human endothelial cells. *J. Cell Sci.* 3613–22 (2000). at <<http://www.ncbi.nlm.nih.gov/pubmed/11017877>>
73. Rodier, F. *et al.* Persistent DNA damage signalling triggers senescence-associated inflammatory cytokine secretion. *Nat. Cell Biol.* **11**, 973–979 (2009).
74. Coppé, J.-P. *et al.* Senescence-associated secretory phenotypes reveal cell-nonautonomous functions of oncogenic RAS and the p53 tumor suppressor. *PLoS Biol.* **6**, 2853–68 (2008).
75. Kuilman, T. *et al.* Oncogene-Induced Senescence Relayed by an Interleukin-Dependent Inflammatory Network. *Cell* **133**, 1019–1031 (2008).
76. Acosta, J. C. *et al.* Chemokine Signaling via the CXCR2 Receptor Reinforces Senescence. *Cell* **133**, 1006–1018 (2008).
77. Chien, Y. *et al.* Control of the senescence-associated secretory phenotype by NF-κB promotes senescence and enhances chemosensitivity. *Genes Dev.* **25**, 2125–36 (2011).
78. Lasry, A. & Ben-Neriah, Y. Senescence-associated inflammatory responses: aging and cancer perspectives. *Trends Immunol.* **36**, 217–228 (2015).

79. Gurtner, G. C., Werner, S., Barrandon, Y. & Longaker, M. T. Wound repair and regeneration. *Nature* **453**, 314–321 (2008).
80. Krizhanovsky, V. *et al.* Senescence of Activated Stellate Cells Limits Liver Fibrosis. *Cell* **134**, 657–667 (2008).
81. Jun, J.-I. & Lau, L. F. The matricellular protein CCN1 induces fibroblast senescence and restricts fibrosis in cutaneous wound healing. *Nat. Cell Biol.* **12**, 676–685 (2010).
82. Campisi, J. Aging, cellular senescence, and cancer. *Annu. Rev. Physiol.* **75**, 685–705 (2013).
83. Nouredine, H. *et al.* Pulmonary Artery Smooth Muscle Cell Senescence Is a Pathogenic Mechanism for Pulmonary Hypertension in Chronic Lung Disease. *Circ. Res.* **109**, 543–553 (2011).
84. Repin, V. S. *et al.* Heterogeneity of endothelium in human aorta. A quantitative analysis by scanning electron microscopy. *Atherosclerosis* **50**, 35–52 (1984).
85. Bürrig, K. F. The endothelium of advanced arteriosclerotic plaques in humans. *Arterioscler. Thromb. a J. Vasc. Biol.* **11**, 1678–89
86. Minamino, T. *et al.* Endothelial cell senescence in human atherosclerosis: role of telomere in endothelial dysfunction. *Circulation* **105**, 1541–4 (2002).
87. Wang, J. *et al.* Vascular Smooth Muscle Cell Senescence Promotes Atherosclerosis and Features of Plaque Vulnerability. *Circulation* **132**, 1909–19 (2015).
88. Matthews, C. *et al.* Vascular smooth muscle cells undergo telomere-based senescence in human atherosclerosis: effects of telomerase and oxidative stress. *Circ. Res.* **99**, 156–64 (2006).
89. Holdt, L. M. *et al.* Expression of Chr9p21 genes CDKN2B (p15(INK4b)), CDKN2A (p16(INK4a), p14(ARF)) and MTAP in human atherosclerotic plaque. *Atherosclerosis* **214**, 264–70 (2011).
90. Childs, B. G. *et al.* Senescent intimal foam cells are deleterious at all stages of atherosclerosis. *Science (80-. ).* **354**, 472–477 (2016).
91. Muñoz-Espín, D. & Serrano, M. Cellular senescence: from physiology to pathology. *Nat. Rev. Mol. Cell Biol.* **15**, 482–96 (2014).

92. Khanna, A. K. Enhanced susceptibility of cyclin kinase inhibitor p21 knockout mice to high fat diet induced atherosclerosis. *J. Biomed. Sci.* **16**, 66 (2009).
93. Mercer, J., Figg, N., Stoneman, V., Braganza, D. & Bennett, M. R. Endogenous p53 protects vascular smooth muscle cells from apoptosis and reduces atherosclerosis in ApoE knockout mice. *Circ. Res.* **96**, 667–74 (2005).
94. González-Navarro, H. *et al.* p19(ARF) deficiency reduces macrophage and vascular smooth muscle cell apoptosis and aggravates atherosclerosis. *J. Am. Coll. Cardiol.* **55**, 2258–68 (2010).
95. Go, A. S. *et al.* Heart disease and stroke statistics--2013 update: a report from the American Heart Association. *Circulation* **127**, e6–e245 (2013).
96. North, B. J. & Sinclair, D. A. The intersection between aging and cardiovascular disease. *Circ. Res.* **110**, 1097–108 (2012).
97. Collins, C. & Tzima, E. Hemodynamic forces in endothelial dysfunction and vascular aging. *Exp. Gerontol.* **46**, 185–8
98. Heffernan, K. S., Fahs, C. A., Ranadive, S. M. & Patvardhan, E. A. L-arginine as a nutritional prophylaxis against vascular endothelial dysfunction with aging. *J. Cardiovasc. Pharmacol. Ther.* **15**, 17–23 (2010).
99. Vasa, M., Breitschopf, K., Zeiher, A. M. & Dimmeler, S. Nitric oxide activates telomerase and delays endothelial cell senescence. *Circ. Res.* **87**, 540–2 (2000).
100. Bazan, J. F. *et al.* A new class of membrane-bound chemokine with a CX3C motif. *Nature* **385**, 640–644 (1997).
101. Sadeghi, H. M., Schnelle, J. F., Thoma, J. K., Nishanian, P. & Fahey, J. L. Phenotypic and functional characteristics of circulating monocytes of elderly persons. *Exp. Gerontol.* **34**, 959–70 (1999).
102. Belge, K.-U. *et al.* The proinflammatory CD14+CD16+DR++ monocytes are a major source of TNF. *J. Immunol.* **168**, 3536–42 (2002).
103. Stolla, M. *et al.* Fractalkine Is Expressed in Early and Advanced Atherosclerotic Lesions and Supports Monocyte Recruitment via CX3CR1. *PLoS One* **7**, e43572 (2012).
104. Boengler, K., Hilfiker-Kleiner, D., Drexler, H., Heusch, G. & Schulz, R. The myocardial JAK/STAT



- pathway: From protection to failure. *Pharmacol. Ther.* **120**, 172–185 (2008).
105. Mülberg, J. *et al.* The soluble interleukin-6 receptor is generated by shedding. *Eur. J. Immunol.* **23**, 473–480 (1993).
  106. Lust, J. A. *et al.* Isolation of an mRNA encoding a soluble form of the human interleukin-6 receptor. *Cytokine* **4**, 96–100 (1992).
  107. Fischer, P. & Hilfiker-Kleiner, D. Survival pathways in hypertrophy and heart failure: the gp130-STAT axis. *Basic Res. Cardiol.* **102**, 393–411 (2007).
  108. Runhua Liu<sup>1</sup>, Lizhong Wang, Guoyun Chen, Hiroto Katoh, Chong Chen, Y. & Liu, and P. Z. FOXP3 Up-regulates p21 Expression by Site-specific Inhibition of Histone Deacetylase 2/4 Association to the Locus. **69**, 2252–2259 (2009).
  109. Zorn, E. *et al.* IL-2 regulates FOXP3 expression in human CD4+CD25+ regulatory T cells through a STAT-dependent mechanism and induces the expansion of these cells in vivo. *Blood* **108**, 1571–9 (2006).
  110. Schuringa, J. J., Timmer, H., Luttickhuizen, D., Vellenga, E. & Kruijer, W. c-Jun and c-Fos cooperate with STAT3 in IL-6-induced transactivation of the IL-6 response element (IRE). *Cytokine* **14**, 78–87 (2001).
  111. Wung, B. S., Ni, C. W. & Wang, D. L. ICAM-1 induction by TNF $\alpha$  and IL-6 is mediated by distinct pathways via Rac in endothelial cells. *J. Biomed. Sci.* **12**, 91–101 (2005).
  112. Durant, L. *et al.* Diverse targets of the transcription factor STAT3 contribute to T cell pathogenicity and homeostasis. *Immunity* **32**, 605–15 (2010).
  113. Yoon, S. *et al.* NF- $\kappa$ B and STAT3 cooperatively induce IL6 in starved cancer cells. *Oncogene* **31**, 3467–81 (2012).
  114. Kuller, L. H., Tracy, R. P., Shaten, J. & Meilahn, E. N. Relation of C-reactive protein and coronary heart disease in the MRFIT nested case-control study. Multiple Risk Factor Intervention Trial. *Am. J. Epidemiol.* **144**, 537–47 (1996).
  115. Emerging Risk Factors Collaboration *et al.* C-reactive protein concentration and risk of coronary heart disease, stroke, and mortality: an individual participant meta-analysis. *Lancet* **375**, 132–140 (2010).

116. Fibrinogen Studies Collaboration *et al.* Plasma Fibrinogen Level and the Risk of Major Cardiovascular Diseases and Nonvascular Mortality. *JAMA* **294**, 1799–809 (2005).
117. Ridker, P. M., Hennekens, C. H., Buring, J. E. & Rifai, N. C-Reactive Protein and Other Markers of Inflammation in the Prediction of Cardiovascular Disease in Women. *N. Engl. J. Med.* **342**, 836–843 (2000).
118. Yudkin, J. S., Kumari, M., Humphries, S. E. & Mohamed-Ali, V. Inflammation, obesity, stress and coronary heart disease: is interleukin-6 the link? *Atherosclerosis* **148**, 209–14 (2000).
119. Harris, T. B. *et al.* Associations of elevated interleukin-6 and C-reactive protein levels with mortality in the elderly. *Am. J. Med.* **106**, 506–12 (1999).
120. Hurme, M., Lehtimäki, T., Jylhä, M., Karhunen, P. J. & Hervonen, A. Interleukin-6 -174G/C polymorphism and longevity: a follow-up study. *Mech. Ageing Dev.* **126**, 417–8 (2005).
121. Pilling, L. C. *et al.* Gene expression markers of age-related inflammation in two human cohorts. *Exp. Gerontol.* **70**, 37–45 (2015).
122. Mohamed-Ali, V. *et al.* Subcutaneous Adipose Tissue Releases Interleukin-6, But Not Tumor Necrosis Factor- $\alpha$ , *in Vivo*<sup>1</sup>. *J. Clin. Endocrinol. Metab.* **82**, 4196–4200 (1997).
123. Kishimoto, T. Interleukin-6: discovery of a pleiotropic cytokine. *Arthritis Res. Ther.* **8 Suppl 2**, S2 (2006).
124. Huber, S. A., Sakkinen, P., Conze, D., Hardin, N. & Tracy, R. Interleukin-6 exacerbates early atherosclerosis in mice. *Arterioscler. Thromb. Vasc. Biol.* **19**, 2364–7 (1999).
125. Takeda, K. *et al.* Targeted disruption of the mouse Stat3 gene leads to early embryonic lethality. *Proc. Natl. Acad. Sci. U. S. A.* **94**, 3801–4 (1997).
126. Hilfiker-Kleiner, D. *et al.* Signal Transducer and Activator of Transcription 3 Is Required for Myocardial Capillary Growth, Control of Interstitial Matrix Deposition, and Heart Protection From Ischemic Injury. *Circ. Res.* **95**, 187–195 (2004).
127. Osugi, T. *et al.* Cardiac-specific Activation of Signal Transducer and Activator of Transcription 3 Promotes Vascular Formation in the Heart. *J. Biol. Chem.* **277**, 6676–6681 (2002).
128. Tierney, M. T. *et al.* STAT3 signaling controls satellite cell expansion and skeletal muscle repair. *Nat. Med.* **20**, 1182–6 (2014).

129. Bartoli, M. *et al.* Vascular endothelial growth factor activates STAT proteins in aortic endothelial cells. *J. Biol. Chem.* **275**, 33189–33192 (2000).
130. Dunham, I. *et al.* An integrated encyclopedia of DNA elements in the human genome. *Nature* **489**, 57–74 (2012).
131. Bartel, D. P. MicroRNAs: genomics, biogenesis, mechanism, and function. *Cell* **116**, 281–97 (2004).
132. Lee, R. C., Feinbaum, R. L. & Ambros, V. The *C. elegans* heterochronic gene *lin-4* encodes small RNAs with antisense complementarity to *lin-14*. *Cell* **75**, 843–54 (1993).
133. Wightman, B., Ha, I. & Ruvkun, G. Posttranscriptional regulation of the heterochronic gene *lin-14* by *lin-4* mediates temporal pattern formation in *C. elegans*. *Cell* **75**, 855–62 (1993).
134. Ruvkun, G. *et al.* The 21-nucleotide *let-7* RNA regulates developmental timing in *Caenorhabditis elegans*. *Nature* **403**, 901–906 (2000).
135. Lagos-Quintana, M., Rauhut, R., Lendeckel, W. & Tuschl, T. Identification of Novel Genes Coding for Small Expressed RNAs. *Science (80-. )*. **294**, 853–858 (2001).
136. Lau, N. C., Lim, L. P., Weinstein, E. G. & Bartel, D. P. An Abundant Class of Tiny RNAs with Probable Regulatory Roles in *Caenorhabditis elegans*. *Science (80-. )*. **294**, 858–862 (2001).
137. Lee, R. C. & Ambros, V. An Extensive Class of Small RNAs in *Caenorhabditis elegans*. *Science (80-. )*. **294**, 862–864 (2001).
138. Musilova, K. & Mraz, M. MicroRNAs in B-cell lymphomas: how a complex biology gets more complex. *Leukemia* **29**, 1004–1017 (2015).
139. Inui, M., Martello, G. & Piccolo, S. MicroRNA control of signal transduction. *Nat. Rev. Mol. Cell Biol.* **11**, 264–275 (2010).
140. Winter, J., Jung, S., Keller, S., Gregory, R. I. & Diederichs, S. Many roads to maturity: microRNA biogenesis pathways and their regulation. *Nat. Cell Biol.* **11**, 228–234 (2009).
141. Lee, Y. *et al.* MicroRNA genes are transcribed by RNA polymerase II. *EMBO J.* **23**, 4051–60 (2004).
142. CAI, X., Hagedorn, C. H. & Cullen, B. R. Human microRNAs are processed from capped,

- polyadenylated transcripts that can also function as mRNAs. *RNA* **10**, 1957–1966 (2004).
143. Han, J. *et al.* The Drosha-DGCR8 complex in primary microRNA processing. *Genes Dev.* **18**, 3016–3027 (2004).
  144. Han, J. *et al.* Molecular Basis for the Recognition of Primary microRNAs by the Drosha-DGCR8 Complex. *Cell* **125**, 887–901 (2006).
  145. LUND, E. & DAHLBERG, J. E. Substrate Selectivity of Exportin 5 and Dicer in the Biogenesis of MicroRNAs. *Cold Spring Harb. Symp. Quant. Biol.* **71**, 59–66 (2006).
  146. Bang, C. *et al.* Cardiac fibroblast-derived microRNA passenger strand-enriched exosomes mediate cardiomyocyte hypertrophy. *J. Clin. Invest.* **124**, 2136–2146 (2014).
  147. Barwari, T., Joshi, A. & Mayr, M. MicroRNAs in Cardiovascular Disease. *J. Am. Coll. Cardiol.* **68**, 2577–2584 (2016).
  148. Filipowicz, W., Bhattacharyya, S. N. & Sonenberg, N. Mechanisms of post-transcriptional regulation by microRNAs: are the answers in sight? *Nat. Rev. Genet.* **2008**, 102–114 (2008).
  149. Small, E. M. & Olson, E. N. Pervasive roles of microRNAs in cardiovascular biology. *Nature* **469**, 336–342 (2011).
  150. Olson, E. N. MicroRNAs as Therapeutic Targets and Biomarkers of Cardiovascular Disease. *Sci. Transl. Med.* **6**, (2014).
  151. Carè, A. *et al.* MicroRNA-133 controls cardiac hypertrophy. *Nat. Med.* **13**, 613–618 (2007).
  152. Castaldi, A. *et al.* MicroRNA-133 Modulates the  $\beta$ 1-Adrenergic Receptor Transduction Cascade Novelty and Significance. *Circ. Res.* **115**, (2014).
  153. Yang, B. *et al.* The muscle-specific microRNA miR-1 regulates cardiac arrhythmogenic potential by targeting GJA1 and KCNJ2. *Nat. Med.* **13**, 486–491 (2007).
  154. Elia, L. *et al.* Reciprocal Regulation of MicroRNA-1 and Insulin-Like Growth Factor-1 Signal Transduction Cascade in Cardiac and Skeletal Muscle in Physiological and Pathological Conditions. *Circulation* **120**, (2009).
  155. Thum, T. *et al.* MicroRNA-21 contributes to myocardial disease by stimulating MAP kinase signalling in fibroblasts. *Nature* **456**, 980–984 (2008).

156. Roy, S. *et al.* MicroRNA expression in response to murine myocardial infarction: miR-21 regulates fibroblast metalloprotease-2 via phosphatase and tensin homologue. *Cardiovasc. Res.* **82**, (2009).
157. Ji, R. *et al.* MicroRNA Expression Signature and Antisense-Mediated Depletion Reveal an Essential Role of MicroRNA in Vascular Neointimal Lesion Formation. *Circ. Res.* **100**, (2007).
158. Bonauer, A. *et al.* MicroRNA-92a controls angiogenesis and functional recovery of ischemic tissues in mice. *Science* **324**, 1710–3 (2009).
159. Loyer, X. *et al.* Inhibition of MicroRNA-92a Prevents Endothelial Dysfunction and Atherosclerosis in Mice. *Circ. Res.* **114**, 434–443 (2014).
160. Boon, R. a *et al.* MicroRNA-34a regulates cardiac ageing and function. *Nature* **495**, 107–10 (2013).
161. Uchida, S. & Dimmeler, S. Long noncoding RNAs in cardiovascular diseases. *Circ. Res.* **116**, 737–50 (2015).
162. Kino, T., Hurt, D. E., Ichijo, T., Nader, N. & Chrousos, G. P. Noncoding RNA Gas5 Is a Growth Arrest- and Starvation-Associated Repressor of the Glucocorticoid Receptor. *Sci. Signal.* **3**, ra8-ra8 (2010).
163. Tsai, M.-C. *et al.* Long Noncoding RNA as Modular Scaffold of Histone Modification Complexes. *Science (80-. ).* **329**, 689–693 (2010).
164. Wang, K. C. *et al.* A long noncoding RNA maintains active chromatin to coordinate homeotic gene expression. *Nature* **472**, 120–124 (2011).
165. Rinn, J. L. *et al.* Functional demarcation of active and silent chromatin domains in human HOX loci by noncoding RNAs. *Cell* **129**, 1311–23 (2007).
166. Tripathi, V. *et al.* The nuclear-retained noncoding RNA MALAT1 regulates alternative splicing by modulating SR splicing factor phosphorylation. *Mol. Cell* **39**, 925–38 (2010).
167. Yoon, J.-H. *et al.* LincRNA-p21 Suppresses Target mRNA Translation. *Mol. Cell* **47**, 648–655 (2012).
168. Gong, C. & Maquat, L. E. lncRNAs transactivate STAU1-mediated mRNA decay by duplexing with 3' UTRs via Alu elements. *Nature* **470**, 284–288 (2011).

169. Karreth, F. A. *et al.* In Vivo Identification of Tumor- Suppressive PTEN ceRNAs in an Oncogenic BRAF-Induced Mouse Model of Melanoma. *Cell* **147**, 382–395 (2011).
170. Hu, W., Alvarez-Dominguez, J. R. & Lodish, H. F. Regulation of mammalian cell differentiation by long non-coding RNAs. *EMBO Rep.* **13**, 971–83 (2012).
171. Holdt, L. M. *et al.* ANRIL Expression Is Associated With Atherosclerosis Risk at Chromosome 9p21. *Arterioscler. Thromb. Vasc. Biol.* **30**, 620–627 (2010).
172. Congrains, A. *et al.* Genetic variants at the 9p21 locus contribute to atherosclerosis through modulation of ANRIL and CDKN2A/B. *Atherosclerosis* **220**, 449–455 (2012).
173. Ishii, N. *et al.* Identification of a novel non-coding RNA, MIAT, that confers risk of myocardial infarction. *J. Hum. Genet.* **51**, 1087–1099 (2006).
174. Zhu, X.-H., Yuan, Y.-X., Rao, S.-L. & Wang, P. LncRNA MIAT enhances cardiac hypertrophy partly through sponging miR-150. *Eur. Rev. Med. Pharmacol. Sci.* **20**, 3653–60 (2016).
175. Kumarswamy, R. *et al.* Circulating Long Noncoding RNA, LIPCAR, Predicts Survival in Patients With Heart Failure. *Circ. Res.* **114**, 1569–1575 (2014).
176. Vausort, M., Wagner, D. R. & Devaux, Y. Long Noncoding RNAs in Patients With Acute Myocardial Infarction. *Circ. Res.* **115**, 668–677 (2014).
177. Ji, P. *et al.* MALAT-1, a novel noncoding RNA, and thymosin  $\beta$ 4 predict metastasis and survival in early-stage non-small cell lung cancer. *Oncogene* **22**, 8031–8041 (2003).
178. Michalik, K. M. *et al.* Long noncoding RNA MALAT1 regulates endothelial cell function and vessel growth. *Circ. Res.* **114**, 1389–97 (2014).
179. Bell, R. D. *et al.* Identification and initial functional characterization of a human vascular cell-enriched long noncoding RNA. *Arterioscler. Thromb. Vasc. Biol.* **34**, 1249–59 (2014).
180. Huarte, M. *et al.* A Large Intergenic Noncoding RNA Induced by p53 Mediates Global Gene Repression in the p53 Response. *Cell* **142**, 409–419 (2010).
181. Wu, G. *et al.* LincRNA-p21 Regulates Neointima Formation, Vascular Smooth Muscle Cell Proliferation, Apoptosis, and Atherosclerosis by Enhancing p53 Activity. *Circulation* **130**, 1452–1465 (2014).

182. Boon, R. A. *et al.* Long Noncoding RNA Meg3 Controls Endothelial Cell Aging and Function. *J. Am. Coll. Cardiol.* **68**, 2589–2591 (2016).
183. Leisegang, M. S. *et al.* Long Noncoding RNA MANTIS Facilitates Endothelial Angiogenic Function. *Circulation* CIRCULATIONAHA.116.026991 (2017).  
doi:10.1161/CIRCULATIONAHA.116.026991
184. Lee, J.-H. *et al.* Analysis of Transcriptome Complexity Through RNA Sequencing in Normal and Failing Murine Hearts. *Circ. Res.* **109**, 1332–1341 (2011).
185. Matkovich, S. J., Edwards, J. R., Grossenheider, T. C., de Guzman Strong, C. & Dorn, G. W. Epigenetic coordination of embryonic heart transcription by dynamically regulated long noncoding RNAs. *Proc. Natl. Acad. Sci.* **111**, 12264–12269 (2014).
186. Pachnis, V., Belayew, A. & Tilghman, S. M. Locus unlinked to alpha-fetoprotein under the control of the murine raf and Rif genes. *Proc. Natl. Acad. Sci. U. S. A.* **81**, 5523–7 (1984).
187. Pachnis, V., Brannan, C. I. & Tilghman, S. M. The structure and expression of a novel gene activated in early mouse embryogenesis. *EMBO J.* **7**, 673–81 (1988).
188. Poirier, F. *et al.* The murine H19 gene is activated during embryonic stem cell differentiation in vitro and at the time of implantation in the developing embryo. *Development* **113**, 1105–14 (1991).
189. Ayesh, S. *et al.* Possible physiological role of H19 RNA. *Mol. Carcinog.* **35**, 63–74 (2002).
190. Dey, B. K., Pfeifer, K. & Dutta, A. The H19 long noncoding RNA gives rise to microRNAs miR-675-3p and miR-675-5p to promote skeletal muscle differentiation and regeneration. *Genes Dev.* **28**, 491–501 (2014).
191. Brannan, C. I., Dees, E. C., Ingram, R. S. & Tilghman, S. M. The product of the H19 gene may function as an RNA. *Mol. Cell. Biol.* **10**, 28–36 (1990).
192. Leibovitch, M. P. *et al.* The human ASM (adult skeletal muscle) gene: expression and chromosomal assignment to 11p15. *Biochem. Biophys. Res. Commun.* **180**, 1241–50 (1991).
193. Ratajczak, M. Z. Igf2-H19, an imprinted tandem gene, is an important regulator of embryonic development, a guardian of proliferation of adult pluripotent stem cells, a regulator of longevity, and a ‘passkey’ to cancerogenesis. *Folia Histochem. Cytobiol.* **50**, 171–179 (2012).

194. Engel, N., Thorvaldsen, J. L. & Bartolomei, M. S. CTCF binding sites promote transcription initiation and prevent DNA methylation on the maternal allele at the imprinted H19/Igf2 locus. *Hum. Mol. Genet.* **15**, 2945–54 (2006).
195. Bergström, R., Whitehead, J., Kurukuti, S. & Ohlsson, R. CTCF Regulates Asynchronous Replication of the Imprinted H19/Igf2 Domain. *Cell Cycle* **6**, 450–454 (2007).
196. DeBaun, M. R. *et al.* Epigenetic alterations of H19 and LIT1 distinguish patients with Beckwith-Wiedemann syndrome with cancer and birth defects. *Am. J. Hum. Genet.* **70**, 604–11 (2002).
197. Leighton, P. A., Ingram, R. S., Eggenschwiler, J., Efstratiadis, A. & Tilghman, S. M. Disruption of imprinting caused by deletion of the H19 gene region in mice. *Nature* **375**, 34–39 (1995).
198. Ripoche, M.-A., Kress, C., Poirier, F. & Dandolo, L. Deletion of the H19 transcription unit reveals the existence of a putative imprinting control element.
199. Gabory, A. *et al.* H19 acts as a trans regulator of the imprinted gene network controlling growth in mice. *Development* **136**, 3413–21 (2009).
200. Brunkow, M. E. & Tilghman, S. M. Ectopic expression of the H19 gene in mice causes prenatal lethality. *Genes Dev.* **5**, 1092–101 (1991).
201. Hao, Y., Crenshaw, T., Moulton, T., Newcomb, E. & Tycko, B. Tumour-suppressor activity of H19 RNA. *Nature* **365**, 764–7 (1993).
202. Matouk, I. J. *et al.* The oncofetal H19 RNA connection: hypoxia, p53 and cancer. *Biochim. Biophys. Acta* **1803**, 443–51 (2010).
203. Luo, M. *et al.* Long non-coding RNA H19 increases bladder cancer metastasis by associating with EZH2 and inhibiting E-cadherin expression. *Cancer Lett.* **333**, 213–21 (2013).
204. Deng, Y. *et al.* Prostacyclin-producing human mesenchymal cells target H19 lncRNA to augment endogenous progenitor function in hindlimb ischaemia. *Nat. Commun.* **7**, 11276 (2016).
205. Sun, H. *et al.* H19 lncRNA mediates 17 $\beta$ -estradiol-induced cell proliferation in MCF-7 breast cancer cells. *Oncol. Rep.* (2015). doi:10.3892/or.2015.3899
206. Han, D. *et al.* Long noncoding RNA H19 indicates a poor prognosis of colorectal cancer and promotes tumor growth by recruiting and binding to eIF4A3. *Oncotarget* **7**, 22159–73 (2016).



207. Ohtsuka, M. *et al.* H19 Noncoding RNA, an Independent Prognostic Factor, Regulates Essential Rb-E2F and CDK8- $\beta$ -Catenin Signaling in Colorectal Cancer. *EBioMedicine* (2016).  
doi:10.1016/j.ebiom.2016.10.026
208. Huang, C. *et al.* Upregulation of H19 promotes invasion and induces epithelial-to-mesenchymal transition in esophageal cancer. *Oncol. Lett.* **10**, 291–296 (2015).
209. Jia, P. *et al.* Long non-coding RNA H19 regulates glioma angiogenesis and the biological behavior of glioma-associated endothelial cells by inhibiting microRNA-29a. *Cancer Lett.* **381**, 359–69 (2016).
210. Jiang, X. *et al.* Increased level of H19 long noncoding RNA promotes invasion, angiogenesis, and stemness of glioblastoma cells. *J. Neurosurg.* **124**, 129–136 (2016).
211. Lv, J., Yu, Y.-Q., Li, S.-Q., Luo, L. & Wang, Q. Aflatoxin B1 promotes cell growth and invasion in hepatocellular carcinoma HepG2 cells through H19 and E2F1. *Asian Pac. J. Cancer Prev.* **15**, 2565–2570 (2014).
212. Li, S. *et al.* The YAP1 oncogene contributes to bladder cancer cell proliferation and migration by regulating the H19 long noncoding RNA. *Urol. Oncol. Semin. Orig. Investig.* **33**, 427.e1-427.e10 (2015).
213. Ma, L. *et al.* The long noncoding RNA H19 promotes cell proliferation via E2F-1 in pancreatic ductal adenocarcinoma. *Cancer Biol. Ther.* **17**, 1051–1061 (2016).
214. Monnier, P. *et al.* H19 lncRNA controls gene expression of the Imprinted Gene Network by recruiting MBD1. *Proc. Natl. Acad. Sci. U. S. A.* **110**, 20693–8 (2013).
215. Varrault, A. *et al.* Zac1 Regulates an Imprinted Gene Network Critically Involved in the Control of Embryonic Growth. *Dev. Cell* **11**, 711–722 (2006).
216. Wang, S.-H. *et al.* Long non-coding RNA H19 regulates FOXM1 expression by competitively binding endogenous miR-342-3p in gallbladder cancer. *J. Exp. Clin. Cancer Res.* **35**, 160 (2016).
217. Matouk, I. J. *et al.* The H19 non-coding RNA is essential for human tumor growth. *PLoS One* **2**, (2007).
218. Voellenkle, C. *et al.* Implication of Long noncoding RNAs in the endothelial cell response to hypoxia revealed by RNA-sequencing. *Sci. Rep.* **6**, 24141 (2016).

219. Matouk, I. J. *et al.* The oncofetal H19 RNA connection: Hypoxia, p53 and cancer. *Biochim. Biophys. Acta - Mol. Cell Res.* **1803**, 443–451 (2010).
220. Dugimont, T. *et al.* The H19 TATA-less promoter is efficiently repressed by wild-type tumor suppressor gene product p53. *Oncogene* **16**, 2395–401 (1998).
221. Berteaux, N. *et al.* H19 mRNA-LIKE NON-CODING RNA PROMOTES BREAST CANCER CELL PROLIFERATION THROUGH POSITIVE CONTROL BY E2F1 \* The last two authors made an equal contribution to this work Running title : H19 promotes cell proliferation. (2005).
222. Klein, R. H. *et al.* Cofactors of LIM Domains Associate with Estrogen Receptor  $\alpha$  to Regulate the Expression of Noncoding RNA H19 and Corneal Epithelial Progenitor Cell Function. *J. Biol. Chem.* **291**, 13271–13285 (2016).
223. Han, D. K., Khaing, Z. Z., Pollock, R. A., Haudenschild, C. C. & Liao, G. H19, a marker of developmental transition, is reexpressed in human atherosclerotic plaques and is regulated by the insulin family of growth factors in cultured rabbit smooth muscle cells. *J. Clin. Invest.* **97**, 1276–85 (1996).
224. Kim, D. K., Zhang, L., Dzau, V. J. & Pratt, R. E. H19, a developmentally regulated gene, is reexpressed in rat vascular smooth muscle cells after injury. *J. Clin. Invest.* **93**, 355–60 (1994).
225. Devlin, A. M., Bottiglieri, T., Domann, F. E. & Lentz, S. R. Tissue-specific changes in H19 methylation and expression in mice with hyperhomocysteinemia. *J. Biol. Chem.* **280**, 25506–11 (2005).
226. Li, L., Xie, J., Zhang, M. & Wang, S. Homocysteine harasses the imprinting expression of IGF2 and H19 by demethylation of differentially methylated region between IGF2/H19 genes. *Acta Biochim. Biophys. Sin. (Shanghai)*. **41**, 464–71 (2009).
227. Hernández-Valero, M. A. *et al.* Interplay between polymorphisms and methylation in the H19/IGF2 gene region may contribute to obesity in Mexican-American children. *J. Dev. Orig. Health Dis.* **4**, 499–506 (2013).
228. Adkins, R. M. *et al.* Association of birth weight with polymorphisms in the IGF2, H19, and IGF2R genes. *Pediatr. Res.* **68**, 429–34 (2010).
229. Tragante, V. *et al.* Gene-centric Meta-analysis in 87,736 Individuals of European Ancestry Identifies Multiple Blood-Pressure-Related Loci. *Am. J. Hum. Genet.* **94**, 349–360 (2014).

230. Gao, W. *et al.* Association of polymorphisms in long non-coding RNA H19 with coronary artery disease risk in a Chinese population. *Mutat. Res.* **772**, 15–22 (2015).
231. Greco, S. *et al.* Long noncoding RNA dysregulation in ischemic heart failure. *J. Transl. Med.* **14**, 183 (2016).
232. Hadji, F. *et al.* Altered DNA Methylation of Long Non-coding RNA H19 in Calcific Aortic Valve Disease Promotes Mineralization by Silencing NOTCH1. *Circulation* (2016).  
doi:10.1161/CIRCULATIONAHA.116.023116
233. Tao, H. *et al.* Long noncoding RNA H19 controls DUSP5/ERK1/2 axis in cardiac fibroblast proliferation and fibrosis. *Cardiovasc. Pathol.* **25**, 381–389 (2016).
234. Cai, X. & Cullen, B. R. The imprinted H19 noncoding RNA is a primary microRNA precursor. *RNA* **13**, 313–6 (2007).
235. Keniry, A. *et al.* The H19 lincRNA is a developmental reservoir of miR-675 that suppresses growth and Igf1r. *Nat. Cell Biol.* **14**, 659–65 (2012).
236. Mineno, J. *et al.* The expression profile of microRNAs in mouse embryos. *Nucleic Acids Res.* **34**, 1765–71 (2006).
237. Chiang, H. R. *et al.* Mammalian microRNAs: experimental evaluation of novel and previously annotated genes. *Genes Dev.* **24**, 992–1009 (2010).
238. Lim, L. P. *et al.* The microRNAs of *Caenorhabditis elegans*. *Genes Dev.* **17**, 991–1008 (2003).
239. Lee, Y. S. & Dutta, A. The tumor suppressor microRNA let-7 represses the HMGA2 oncogene. *Genes Dev.* **21**, 1025–30 (2007).
240. Liu, G., Xiang, T., Wu, Q.-F. & Wang, W.-X. Long Noncoding RNA H19-Derived miR-675 Enhances Proliferation and Invasion via RUNX1 in Gastric Cancer Cells. *Oncol. Res. Featur. Preclin. Clin. Cancer Ther.* **23**, 99–107 (2016).
241. Li, X. *et al.* lncRNA H19/miR-675 axis regulates cardiomyocyte apoptosis by targeting VDAC1 in diabetic cardiomyopathy. *Sci. Rep.* **6**, 36340 (2016).
242. Tsang, W. P. *et al.* Oncofetal H19-derived miR-675 regulates tumor suppressor RB in human colorectal cancer. *Carcinogenesis* **31**, 350–8 (2010).

243. Zhou, Y.-W. *et al.* miR-675-5p enhances tumorigenesis and metastasis of esophageal squamous cell carcinoma by targeting REPS2. *Oncotarget* **7**, 30730–47 (2016).
244. Vennin, C. *et al.* H19 non coding RNA-derived miR-675 enhances tumorigenesis and metastasis of breast cancer cells by downregulating c-Cbl and Cbl-b. *Oncotarget* **6**, 29209–23 (2015).
245. Liu, L. *et al.* The H19 long noncoding RNA is a novel negative regulator of cardiomyocyte hypertrophy. *Cardiovasc. Res.* (2016).
246. Kallen, A. N. *et al.* The Imprinted H19 LncRNA Antagonizes Let-7 MicroRNAs. *Mol. Cell* **52**, 101–12 (2013).
247. Imig, J. *et al.* miR-CLIP capture of a miRNA targetome uncovers a lincRNA H19–miR-106a interaction. *Nat. Chem. Biol.* **11**, 1–10 (2014).
248. Gao, Y. *et al.* The H19/let-7 double-negative feedback loop contributes to glucose metabolism in muscle cells. *Nucleic Acids Res.* **42**, 13799–13811 (2014).
249. Giovarelli, M. *et al.* H19 long noncoding RNA controls the mRNA decay promoting function of KSRP. *Proc. Natl. Acad. Sci.* **111**, E5023-8 (2014).
250. Liang, W. *et al.* The lncRNA H19 promotes epithelial to mesenchymal transition by functioning as miRNA sponges in colorectal cancer. *Oncotarget* **6**, 22513–25 (2015).
251. Li, M., Chen, H., Zhao, Y., Gao, S. & Cheng, C. H19 Functions as a ceRNA in Promoting Metastasis Through Decreasing miR-200s Activity in Osteosarcoma. *DNA Cell Biol.* **35**, 235–240 (2016).
252. Wang, W.-T. *et al.* LncRNAs H19 and HULC, activated by oxidative stress, promote cell migration and invasion in cholangiocarcinoma through a ceRNA manner. *J. Hematol. Oncol.* **9**, 117 (2016).
253. Dekker, R. J. *et al.* Endothelial KLF2 links local arterial shear stress levels to the expression of vascular tone-regulating genes. *Am. J. Pathol.* **167**, 609–18 (2005).
254. Huang, D. W., Sherman, B. T. & Lempicki, R. A. Bioinformatics enrichment tools: paths toward the comprehensive functional analysis of large gene lists. *Nucleic Acids Res.* **37**, 1–13 (2009).
255. Huang, D. W., Sherman, B. T. & Lempicki, R. A. Systematic and integrative analysis of large

- gene lists using DAVID bioinformatics resources. *Nat. Protoc.* **4**, 44–57 (2009).
256. Baker, M. *et al.* Use of the mouse aortic ring assay to study angiogenesis. *Nat. Protoc.* **7**, 89–104 (2012).
257. Boon, R. A. *et al.* MicroRNA-29 in aortic dilation: implications for aneurysm formation. *Circ. Res.* **109**, 1115–9 (2011).
258. Loots, G. G. & Ovcharenko, I. rVISTA 2.0: evolutionary analysis of transcription factor binding sites. *Nucleic Acids Res.* **32**, W217–21 (2004).
259. Kim, K. W. *et al.* Insulin-like growth factor II induced by hypoxia may contribute to angiogenesis of human hepatocellular carcinoma. *Cancer Res.* **58**, 348–51 (1998).
260. Michalik, K. M. *et al.* Long Noncoding RNA MALAT1 Regulates Endothelial Cell Function and Vessel Growth Novelty and Significance. *Circ. Res.* **114**, 1389–1397 (2014).
261. Betel, D., Wilson, M., Gabow, A., Marks, D. S. & Sander, C. The microRNA.org resource: targets and expression. *Nucleic Acids Res.* **36**, D149–D153 (2007).
262. Ahluwalia, A., Jones, M. K., Szabo, S. & Tarnawski, A. S. Aging impairs transcriptional regulation of vascular endothelial growth factor in human microvascular endothelial cells: implications for angiogenesis and cell survival. *J. Physiol. Pharmacol.* **65**, 209–15 (2014).
263. Shin, D.-S. *et al.* Cryptotanshinone inhibits constitutive signal transducer and activator of transcription 3 function through blocking the dimerization in DU145 prostate cancer cells. *Cancer Res.* **69**, 193–202 (2009).
264. Boon, R. A. *et al.* Kruppel-like factor 2 improves neovascularization capacity of aged proangiogenic cells. *Eur. Heart J.* **32**, 371–7 (2011).
265. Gallo, D. *et al.* Human recombinant lysozyme downregulates advanced glycation endproduct-induced interleukin-6 production and release in an in-vitro model of human proximal tubular epithelial cells. *Exp. Biol. Med. (Maywood)*. **239**, 337–346 (2014).
266. Gallo, D. *et al.* Human recombinant lysozyme downregulates advanced glycation endproduct-induced interleukin-6 production and release in an *in-vitro* model of human proximal tubular epithelial cells. *Exp. Biol. Med.* **239**, 337–346 (2014).
267. Kuettner, K. E., Eisenstein, R. & Sorgente, N. Lysozyme in calcifying tissues. *Clin. Orthop. Relat.*

Res. 316–39 (1975). at <<http://www.ncbi.nlm.nih.gov/pubmed/1192645>>

268. Kolodgie, F. D., Burke, A. P., Wight, T. N. & Virmani, R. The accumulation of specific types of proteoglycans in eroded plaques: a role in coronary thrombosis in the absence of rupture. *Curr. Opin. Lipidol.* **15**, 575–82 (2004).
269. Kolodgie, F. D. *et al.* Differential accumulation of proteoglycans and hyaluronan in culprit lesions: insights into plaque erosion. *Arterioscler. Thromb. Vasc. Biol.* **22**, 1642–8 (2002).
270. Wight, T. N. Arterial remodeling in vascular disease: a key role for hyaluronan and versican. *Front. Biosci.* **13**, 4933–7 (2008).
271. Viola, M. *et al.* Regulated Hyaluronan Synthesis by Vascular Cells. *Int. J. Cell Biol.* **2015**, 1–8 (2015).
272. Genasetti, A. *et al.* Hyaluronan and Human Endothelial Cell Behavior. *Connect. Tissue Res.* **49**, 120–123 (2008).
273. Vigetti, D. *et al.* Proinflammatory Cytokines Induce Hyaluronan Synthesis and Monocyte Adhesion in Human Endothelial Cells through Hyaluronan Synthase 2 (HAS2) and the Nuclear Factor- $\kappa$ B (NF- $\kappa$ B) Pathway. *J. Biol. Chem.* **285**, 24639–24645 (2010).
274. Chai, S. *et al.* Overexpression of hyaluronan in the tunica media promotes the development of atherosclerosis. *Circ. Res.* **96**, 583–91 (2005).
275. Kashima, Y. *et al.* Crucial role of hyaluronan in neointimal formation after vascular injury. *PLoS One* **8**, e58760 (2013).
276. Stuhlsatz, H. W., Löffler, H., Mohanaradhakrishnan, V., Cosma, S. & Greiling, H. Topographic and age-dependent distribution of the glycosaminoglycans in human aorta. *J. Clin. Chem. Clin. Biochem.* **20**, 713–21 (1982).
277. Murata, K. & Yokoyama, Y. Acidic glycosaminoglycans in human atherosclerotic cerebral arterial tissues. *Atherosclerosis* **78**, 69–79 (1989).
278. Tovar, A. M., Cesar, D. C., Leta, G. C. & Mourão, P. A. Age-related changes in populations of aortic glycosaminoglycans: species with low affinity for plasma low-density lipoproteins, and not species with high affinity, are preferentially affected. *Arterioscler. Thromb. Vasc. Biol.* **18**, 604–14 (1998).

279. Chajara, A. *et al.* Effect of aging on neointima formation and hyaluronan, hyaluronidase and hyaluronectin production in injured rat aorta. *Atherosclerosis* **138**, 53–64 (1998).
280. Varga, R. *et al.* Progressive vascular smooth muscle cell defects in a mouse model of Hutchinson-Gilford progeria syndrome. *Proc. Natl. Acad. Sci. U. S. A.* **103**, 3250–5 (2006).
281. Vigetti, D. *et al.* Hyaluronan-CD44-ERK1/2 Regulate Human Aortic Smooth Muscle Cell Motility during Aging. *J. Biol. Chem.* **283**, 4448–4458 (2008).
282. Jokela, T. A. *et al.* Extracellular UDP-Glucose Activates P2Y<sub>14</sub> Receptor and Induces Signal Transducer and Activator of Transcription 3 (STAT3) Tyr705 Phosphorylation and Binding to Hyaluronan Synthase 2 (HAS2) Promoter, Stimulating Hyaluronan Synthesis of Keratinocytes. *J. Biol. Chem.* **289**, 18569–18581 (2014).
283. Niu, G. *et al.* Constitutive Stat3 activity up-regulates VEGF expression and tumor angiogenesis. *Oncogene* **21**, 2000–2008 (2002).
284. Kano, A. *et al.* Endothelial Cells Require STAT3 for Protection against Endotoxin-induced Inflammation. *J. Exp. Med.* **198**, 1517–1525 (2003).
285. Moretto, P. *et al.* Regulation of hyaluronan synthesis in vascular diseases and diabetes. *J. Diabetes Res.* **2015**, 167283 (2015).
286. Liu, B. *et al.* A Cytoplasmic NF- $\kappa$ B Interacting Long Noncoding RNA Blocks I $\kappa$ B Phosphorylation and Suppresses Breast Cancer Metastasis. *Cancer Cell* **27**, 370–381 (2015).
287. Denzler, R., Agarwal, V., Stefano, J., Bartel, D. P. & Stoffel, M. Assessing the ceRNA Hypothesis with Quantitative Measurements of miRNA and Target Abundance. *Mol. Cell* **54**, 766–776 (2014).
288. Quinn, J. J. & Chang, H. Y. Unique features of long non-coding RNA biogenesis and function. *Nat. Rev. Genet.* **17**, 47–62 (2015).
289. Kim, K. W. *et al.* Insulin-like growth factor II induced by hypoxia may contribute to angiogenesis of human hepatocellular carcinoma. *Cancer Res.* **58**, 348–51 (1998).
290. Hoffmann, C. J. *et al.* Vascular Signal Transducer and Activator of Transcription-3 Promotes Angiogenesis and Neuroplasticity Long-Term After Stroke. *Circulation* **131**, 1772–1782 (2015).
291. Tollervey, J. R. *et al.* Characterizing the RNA targets and position-dependent splicing

- regulation by TDP-43. *Nat. Neurosci.* **14**, 452–458 (2011).
292. Tripathi, V. *et al.* The Nuclear-Retained Noncoding RNA MALAT1 Regulates Alternative Splicing by Modulating SR Splicing Factor Phosphorylation. *Mol. Cell* **39**, 925–938 (2010).
293. Kaneko, S. *et al.* Interactions between JARID2 and Noncoding RNAs Regulate PRC2 Recruitment to Chromatin. *Mol. Cell* **53**, 290–300 (2014).



## Abbreviations

<b>Abbreviation</b>	<b>Meaning</b>
µm	Mikrometer
µM	Mikromolar
7-AAD	7 aminoactinomycin D
Ago2	Argonaute protein 2
αSMA	Alpha smooth muscle actin
ANOVA	Analysis of variance
Ang2	Angiotensin 2
bp	Basepairs
BrdU	Bromodeoxyuridine
BSA	Bovine Serum Albumin
C57Bl6	C57 Black 6
CaCl <sub>2</sub>	Calcium chloride
CD31	Cluster of differentiation 31
Cdh5	Cadherin 5
Cdk	Cyclin dependent kinase
cDNA	complementary deoxyribonucleic acid
CMV	Cytomegalovirus
CO <sub>2</sub>	Carbondioxide
CPT	Cryptothanshinone
Cre	Causes Recombination
Ct	Threshold cycle
Ctrl	Control
DAPI	4', 6'-diamin-2-phenylindol
DMEM	Dulbecco's modified eagle medium
DMSO	Dimethyl sulfoxid
DNA	Desoxyribonucleic acid
dsDNA	double stranded deoxyribonucleic acid
e. g.	(lat.) <i>exempli gratia</i> - for example
EBM	Endothelial basal medium
EC	Endothelial cell
ECGS	Endothelial growth supplement
ECM	Extracellular matrix
EDTA	Ethylene diamine tetra acetic acid
EIF4E	Eucaryotic initiatin factor 4E
ELISA	Enzyme-linked immunosorbent assay
eNOS	endothelial nitric oxide synthase
ERT2	Estrogen receptor 2
EtOH	Ethanol
FACS	Fluorescence activated cell sorting
FBS	Fetal bovine serum
FITC	Fluorescein isothiocyanat
fl/fl	flox/flox
g	gravitational constant (6.67x10 <sup>-11</sup> N (m/kg) <sup>2</sup> )

GAPDH	Glyceraldehyde 3-phosphate dehydrogenase
h	hour
H19iEC-KO	H19 inducible endothelial knockout (H19 <sup>fl/fl</sup> ;Cdh5(PAC)-CreERT2)
HBSS	Hank's balanced salt solution
HCl	Hydrogen chloride
hCoAEC	Human coronary artery endothelial cell
Hek	Human embryonic kidney (cell)
HEPES	4-(2-hydroxyethyl)-1-piperazinethanesulfonic-acid
HIF	Hypoxia inducible factor
HLI	Hind limb ischemia
HRP	Horseradish peroxidase
HUVEC	Human umbilical vein endothelial cell
ICAM-1	Intercellular adhesion molecule 1
IgG	Immunoglobulin G
IL-6	Interleukin 6
IL-6R $\alpha$	Interleukin 6 Receptor $\alpha$
JAK2	Janus kinase 2
KCl	Potassium Chloride
kDa	Kilodalton
KH <sub>2</sub> PO <sub>4</sub>	Potassium Phosphate monobasic
KLF2	Krüppel-like factor 2
KO	Knockout
KSRP	KH-type splicing regulatory protein
LDL	Low density lipoprotein
LNA	Locked nucleic acid
lncRNA	Long noncoding ribonucleic acid
M	Molar
MALAT-1	Metastasis associated lung adenocarcinoma transcript 1
MgCl <sub>2</sub>	Magnesium chloride
min	minute
miR	micro ribonucleic acid
miRNA	micro ribonucleic acid
mLEC	Mouse lung endothelial cell
mM	Millimolar
MMP	Matrix metalloproteinase
mRNA	Messenger ribonucleic acid
Na <sub>2</sub> HPO <sub>4</sub>	Sodium Phosphate dibasic anhydrous
Na <sub>2</sub> HPO <sub>4</sub> -7H <sub>2</sub> O	Sodium Phosphate dibasic
NaCl	Sodium chloride
NaHCO <sub>3</sub>	Sodium Bicarbonate
NaOH	Sodium hydroxide
ncRNA	Noncoding RNA
NF $\kappa$ B	Nuclear factor kappa B
nm	Nanometer
nM	Nanomolar
nt	Nucleotides
O <sub>2</sub>	Oxygen

P0	Ribosomal protein large P0
PAGE	Polyacrylamid gel electrophoresis
PBS	Phosphate buffered saline
PCR	Polymerase chain reaction
PDGF $\beta$	Platelet derive growth factor subunit B
PDGFR $\beta$	Platelet derive growth factor receptor beta
PECAM-1	Platelet endothelial cell adhesion molecule
PFA	Paraformaldehyde
pre-miR	Precursor micro ribonucleic acid
pri-miR	Primary micro ribonucleic acid
qRT-PCR	quantitative real-time polymerase chain reaction
RIP	RNA immunoprecipitation
RIPA	Radio immune precipitation assay
RISC	RNA-induced silencing complex
RNA	Ribonucleic acid
RPLP0	Ribosomal protein large P0
rRNA	Ribosomal ribonucleic acid
s	second
SDS	Sodium dodecyl sulfate
SEM	Standard error of the mean
shRNA	short hairpin ribonucleic acid
sIL-6R $\alpha$	Soluble Interleukin 6 Receptor $\alpha$
siRNA	small interfering ribonucleic acid
SMC	Smooth muscle cell
STAT3	Signal transducer and activator of transcription 3
TNF- $\alpha$	Tumor necrosis factor alpha
UTR	Untranslated region
VCAM-1	Vascular cell adhesion molecule 1
VE-cadherin	Vascular endothelial cadherin
VEGF	Vascular endothelial growth factor
VEGFR	Vascular endothelial growth factor receptor
WT	Wild type

## **Eidesstattliche Erklärung**

Hiermit versichere ich, dass ich die vorliegende Dissertation selbstständig und nur unter zu Hilfenahme der hier angegebenen Quellen und Hilfsmitteln verfasst habe.

Die Dissertation wurde bisher keiner anderen Fakultät vorgelegt. Ich erkläre, dass ich bisher kein Promotionsverfahren erfolglos beendet habe und dass keine Aberkennung eines bereits erworbenen Doktorgrades vorliegt.

Frankfurt am Main, den

Patrick Hofmann

## Acknowledgements

This study would not have been possible without the help of many people, which I'm highly indebted to thank for their contribution. My heartfelt thanks to

- Reinier, for giving me the opportunity to pursue this project. Many thanks for your superb supervision, all your input, your infinite patience, your great ideas and for many laughter!
- Stefanie, for providing a stimulating work environment and for all your support and ideas throughout the years.
- Amparo Acker-Palmer for the revision of my thesis.
- Anne, Anu, Katha, Shemsi and Eva H. for the help and patience during my first months and for the numerous table-soccer rounds.
- Jasmin, Larissa, Nico, Phillip, Tina L. and Yosif for the scientific advice.
- Andrea, Ariane, Astrid, Christina, Denise, Janina, Marion, Nina and Tina R. for the technical support and all your help throughout the years.
- My "Denkzelle"-colleagues Dora, Eva H., Julia, Laura, Nicole, Philipp, Shemsi and Yosif for the good times, discussions and lots of laughter.
- All the colleagues from the institute: Andi, David, Diewertje, Eva R., Luisa, Noelia, Phat, Simone, Tatiana and others for being ever so helpful and creating a pleasant environment.

# Curriculum Vitae

## Personal Data:

---

Name: Patrick Hofmann  
E-Mail: hofmann.pat@googlemail.com  
Date of Birth: 02.10.1986  
Place of Birth: Weinheim (Bergstraße), Germany  
Nationality: German

## Education & Training:

---

07/2013 until present      **PhD Thesis**, Institute of Cardiovascular Regeneration (Director: Prof Dr. Stefanie Dimmeler), Center for Molecular Medicine, Goethe University Frankfurt, Group of Prof. Dr. Reinier Boon

10/2011 to 05/2013      **Master of Science in Technical Biology**, Technical University Darmstadt, Germany  
Final Grade: 1.3  
Specialization courses:  
Technical Genetics, Biochemistry, Cell Biology, Plant Biotechnology

**Master-Thesis:**  
Institute of Microbiology and Genetics, Technical University Darmstadt and Institute of Biochemistry, Jacobs University Bremen  
Group of Prof. Dr. Christian Hammann  
Titel: „RNA FISH in *Dictyostelium discoideum*: Adaptation and application”  
(Final Grade: 1.3)

10/2008 – 08/2011      **Bachelor of Science in Biology**, Technical University Darmstadt, Germany  
Final Grade: 2.4  
Specialization courses:  
Technical Genetics, Cell Biology, Radiation Biology, Biophysics of Ion Channels

**Bachelor-Thesis:**  
Institute of Microbiology and Genetics, Technical University Darmstadt  
Group of Prof. Dr. H. Ulrich Göringer  
Titel: „RNA editing in *Trypanosoma brucei* does not show cell cycle dependence”  
(Final Grade: 1.7)

## Publications:

---

- **Hofmann P**, Domicke J, Fischer A, Li Y, Perisic L, Hedin U, Maegdefessel L, Dimmeler S, Boon RA; Long noncoding RNA H19 regulates endothelial cell aging via inhibition Stat3 signaling; *in revision*
- Leisegang MS, Fork C, Josipovic I, Richter F, Preussner J, Hu J, Miller MJ, Epah JN, **Hofmann P**, Günther S, Moll F, Valasarajan C, Heidler J, Ponomareva Y, Freimann TM, Maegdefessel L, Plate KH, Mittelbronn M, Uchida S, Künne C, Stellos K, Schermuly RT, Weissmann N, Devraj K, Wittig I, Boon RA, Dimmeler S, Pullamsetti SS, Looso M, Miller FJ, Brandes RP; The lncRNA *MANTIS* maintains the angiogenic function of endothelial cells; *Circulation*, 2017 Mar 28; PMID: 28351900
- Boon RA, **Hofmann P**, Michalik KM, Lozano-Vidal N, Berghäuser D, Fischer A, Knau A, Jaé N, Schürmann C, Dimmeler S; Long non-coding RNA Meg3 controls endothelial cell ageing and function: Implications for regenerative angiogenesis; *J Am Coll Cardiol*. 2016 Dec 13; PMID: 27931619
- **Hofmann P**, Boon RA; Non-coding RNA enhances cardiac development; *J Mol Cell Cardiol*. 2014 Sep 18; PMID: 25240640 (Editorial)
- **Hofmann P**, Kruse J, Hammann C; Transcript localization in *D. discoideum* cells by RNA FISH; *Methods Mol Biol*. 2013; PMID: 23494315
- Wiegand S, Meier D, Seehafer C, Malicki M, **Hofmann P**, Schmith A, Winckler T, Földesi B, Boesler B, Nellen W, Reimegård J, Käller M, Hällman J, Emanuelsson O, Avesson L, Söderbom F, Hammann C. *Nucleic Acids Res*. 2014 Mar; PMID: 24369430

## Presentations and Posters (selection):

---

- Annual Meeting of the German Cardiology Society 2016; 21.04.2017; Mannheim, Germany
- Keystone Symposia on Protein-RNA Interactions 06.02.2017; Banff, CA
- NAVBO International Vascular Biology Meeting, 01.11.2016; Boston, MA, USA
- Perspectives in Vascular Biology; 26.09.2016; Frankfurt, Germany
- 2<sup>nd</sup> Cologne Aging Conference; 04.04.2016; Cologne, Germany
- Annual Meeting of the German Cardiology Society 2016; 31.03.2016; Mannheim, Germany
- Meeting of the Dutch German Molecular Cardiology Working Groups 2016, 19.03.2016; Leiden, Netherlands
- Excellence Cluster for Cardiopulmonary Systems Retreat 2015, 18.06.2015; Bad Nauheim, Germany
- Annual Meeting of the German Cardiology Society 2015; 10.04.2015; Mannheim, Germany
- Keystone Symposia Long non-coding RNAs: From evolution to function; 16.03.2015; Keystone, Co, USA
- American Heart Association Scientific Sessions 2014, 19.11.2014, Chicago, IL, USA

## Graduate School:

---

- Integrated research training unit of SFB834 “endothelial signaling and vascular repair”
- Student speaker 2015-2017